creative commons
COMMONS DEED

저작자표시-비영리-변경금지 2.0 대한민국

이용자는 아래의 조건을 따르는 경우에 한하여 자유롭게

- 이 저작물을 복제, 배포, 전송, 전시, 공연 및 방송할 수 있습니다.

다음과 같은 조건을 따라야 합니다:

저작자표시. 귀하는 원저작자를 표시하여야 합니다.

비영리. 귀하는 이 저작물을 영리 목적으로 이용할 수 없습니다.

변경금지. 귀하는 이 저작물을 개작, 변형 또는 가공할 수 없습니다.

- 귀하는, 이 저작물의 재이용이나 배포의 경우, 이 저작물에 적용된 이용허락조건을 명확하게 나타내어야 합니다.
- 저작권자로부터 별도의 허가를 받으면 이러한 조건들은 적용되지 않습니다.

저작권법에 따른 이용자의 권리는 위의 내용에 의하여 영향을 받지 않습니다.

이것은 이용허락규약(Legal Code)을 이해하기 쉽게 요약한 것입니다.

Disclaimer

dCollection

ULSAN NATIONAL INSTITUTE OF
SCIENCE AND TECHNOLOGY

ULSAN NATIONAL INSTITUTE OF SCIENCE AND TECHNOLOGY

Doctoral Thesis

An IoT Edge Gas Sensor Device with Analog Supported Continual Learning Scheme

Hee young Chae

Department of Electrical Engineering

Ulsan National Institute of Science and Technology

2022

ULSAN NATIONAL INSTITUTE OF
SCIENCE AND TECHNOLOGY

An IoT Edge Gas Sensor Device with Analog Supported Continual Learning Scheme

Hee Young Chae

Department of Electrical Engineering

Ulsan National Institute of Science and Technology

ULSAN NATIONAL INSTITUTE OF
SCIENCE AND TECHNOLOGY

An IoT Edge Gas Sensor Device with Analog Supported Continual Learning Scheme

A thesis/dissertation submitted to
Ulsan National Institute of Science and Technology
in partial fulfillment of the
requirements for the degree of
Doctor of Philosophy

Hee Young Chae

06.08.2022 of submission

Approved by

Advisor

Jae Joon Kim

ULSAN NATIONAL INSTITUTE OF
SCIENCE AND TECHNOLOGY

An IoT Edge Gas Sensor Device with Analog Supported Continual Learning Scheme

Hee Young Chae

This certifies that the thesis/dissertation of Hee Young Chae is approved.

06.08.2022 of submission

Signature

Advisor: Jae Joon Kim

Signature

Thesis Committee member #1: Yunsik Lee

Signature

Thesis Committee member #2: Hungsun Son

Signature

Thesis Committee member #3: Hyunhyub Ko

Signature

Thesis Committee member #4: Jeong Min Baik

ULSAN NATIONAL INSTITUTE OF
SCIENCE AND TECHNOLOGY

Abstract

The development of technology is one of the major factors that increase a number of factories in the daily life. Due to its reason, a quantity of harmful gas emission is rising simultaneously, resulting unexpected and critical accidents. To prevent human accidents, the necessity of the gas monitoring system in such dangerous areas is being highlighted. The deployment of an Internet of Things (IoT) gas-sensing systems is widely used to gather various data of different toxic gases in a dangerous area to prevent such accidents. Generally, to design such gas sensing IoT platform a cost and power efficient semiconductor sensor is well suited for large scale IoT deployment. However, there are several challenges to overcome when using a semiconductor type gas sensor such as selectivity of the gas type and reliability of the gas data. This selectivity challenge comes from a physical property of the semiconductor gas sensor which react to numerous gases and the reliability problem comes from the environment effect on the sensor, poisoning and other ageing problem. Thus, processing the semiconductor gas sensor data becomes important to analyze qualitative gas sensor data.

In the classical approach to resolve such problems, most of the existing IoT gas sensor systems or devices only send the obtained data, and these data are processed in the server side. Thus, the server processing burden becomes high. Recently, one recent notable trend is to embed the artificial intelligence like pattern recognition (PR) into the IoT device, providing the edge-computing capability. Therefore, using this edge computing capability, the selectivity can be improved, and the reliability problems can be resolved with a physical calibration of the sensor and the processing burden of the server also can be resolved.

This doctoral thesis aims to design an Intelligent IoT Edge gas sensor platform embedding analog supported continual learning scheme multi-gas pattern recognition device that has an optimized system structure for edge computing in internet of things (IoT) environments. Considering the environment effect on the semiconductor gas sensor device characteristics, a read out integrated circuit (ROIC) is fabricated in a 180 nm CMOS process to calibrate sensor sample variation in real time. Conventional calibration is performed in the processing side. However, in the Edge computing environment, Memory constraint digital signal processing (DSP) device performs pattern recognition to resolve selectivity problem and the processing burden is already high. Thus, using the ROIC and pre-calibrate sensor data relieves much computational burden for the edge IoT device than a classical approach. Then, performing

ULSAN NATIONAL INSTITUTE OF
SCIENCE AND TECHNOLOGY

the pattern recognition through a continual learning-based algorithm allows the IoT gas sensor modules to be adaptable to the environment and learn continuously gas pattern in various environment. Among different continual learning model, a mask-based continual learning considers the memory efficient learning method which can be applied to the memory constraint device. Mask-based continual learning scheme keep the previous learned weights to not forget previous trained pattern and enlarging the network when new pattern arrives can additionally give the opportunity to learn additional pattern. However, classical application of mask-based continual learning can conduct to the serious processing confusion, thus this doctoral thesis also proposes an efficient mask-based continual learning (MBCL) scheme adapted to the gas sensor system. Temperature and humidity are the major factor to make the gas sensor data in contradictory situation. Thus, adopting classical continual learning method can face a contradictory gas sensor data statement situation. Therefore, forgetting previous learned weights connected to the temperature and humidity node makes the learning in new environment robust against temperature and humidity of the environment.

Keywords**:** Readout integrated circuit, analog front-end, gas sensor, temperature humidity robust, continual learning, edge-computing, Internet of things, harmful gases.

ULSAN NATIONAL INSTITUTE OF
SCIENCE AND TECHNOLOGY

ULSAN NATIONAL INSTITUTE OF SCIENCE AND TECHNOLOGY

Contents

ULSAN NATIONAL INSTITUTE OF
SCIENCE AND TECHNOLOGY

ULSAN NATIONAL INSTITUTE OF SCIENCE AND TECHNOLOGY

List of Figures

ULSAN NATIONAL INSTITUTE OF SCIENCE AND TECHNOLOGY

ULSAN NATIONAL INSTITUTE OF
SCIENCE AND TECHNOLOGY

ULSAN NATIONAL INSTITUTE OF
SCIENCE AND TECHNOLOGY

List of Tables

ULSAN NATIONAL INSTITUTE OF
SCIENCE AND TECHNOLOGY

Nomenclature

ROIC	Readout integrated circuit
AFE	Analog front-end
AI	Artificial Intelligence
ANN	Artificial Neural Network
EMG	Electromyogram
SAR	Successive approximation register
ADC	Analog-to-digital converter
SPI	Serial peripheral interface
MCU	Microcontroller unit
DSP	Digital signal processing
HPF	High-pass filter
LPF	Low-pass filter
SNR	Signal-to-noise ratio
MOSFET	Metal oxide semiconductor field effect transistor
CDS	Correlated double sampling
MLP	Multi-Layer perceptron
ML	Machine learning
TL	Transfer learning
CL	Continual learning
MBCL	Mask based continual learning
GAN	Generative adversarial network
EWC	Elastic-weights consolidation

ULSAN NATIONAL INSTITUTE OF
SCIENCE AND TECHNOLOGY

DEN	Dynamic expansion net
CCIA	Capacitor coupled instrumental amplifier.
PGA	programmable gain amplifier
FFT	Fast Fourier transform
MOS	Metal oxide semiconductor
LTE	Long term evolution

ULSAN NATIONAL INSTITUTE OF SCIENCE AND TECHNOLOGY

Chapter I

Motivation and requirement

1.1 Motivation and requirement.

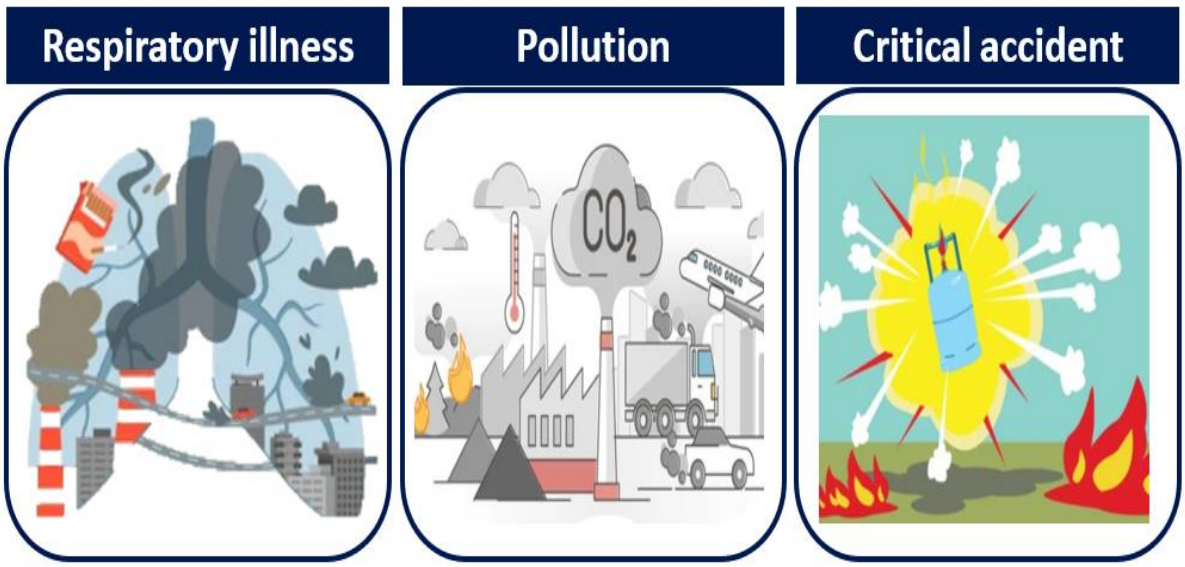

Figure 1.1. Needs of gas sensor system

Gas emission topic becomes a global interested because of critical accidents caused by pollution. Inattentional critical accidents can happens when explosive type gas emission arrives, or harmful gas emission is strongly related with the cause of the human respiratory disease [1], [2], [3]. Thus, the needs of a continuous harmful gas monitoring system have been highlighted. Related with this issue, to prevents a direct contact with harmful gases, internet of thing (IoT) system is efficiently use in the measuring site [4]. For a large scale IoT deployment application, adopting low-cost gas sensor is suitable for the monitoring system. However, several challenges coming from using low-cost gas sensor need to be overcome. Specially, reliability and selectivity problems exist with their sensing mechanisms. To resolve these problems artificial intelligence (AI) based signal processing method give a prospective solution to resolve selectivity problems [5] and calibration method is adopted to stabilize the reliability of low-cost sensor [6].

ULSAN NATIONAL INSTITUTE OF
SCIENCE AND TECHNOLOGY

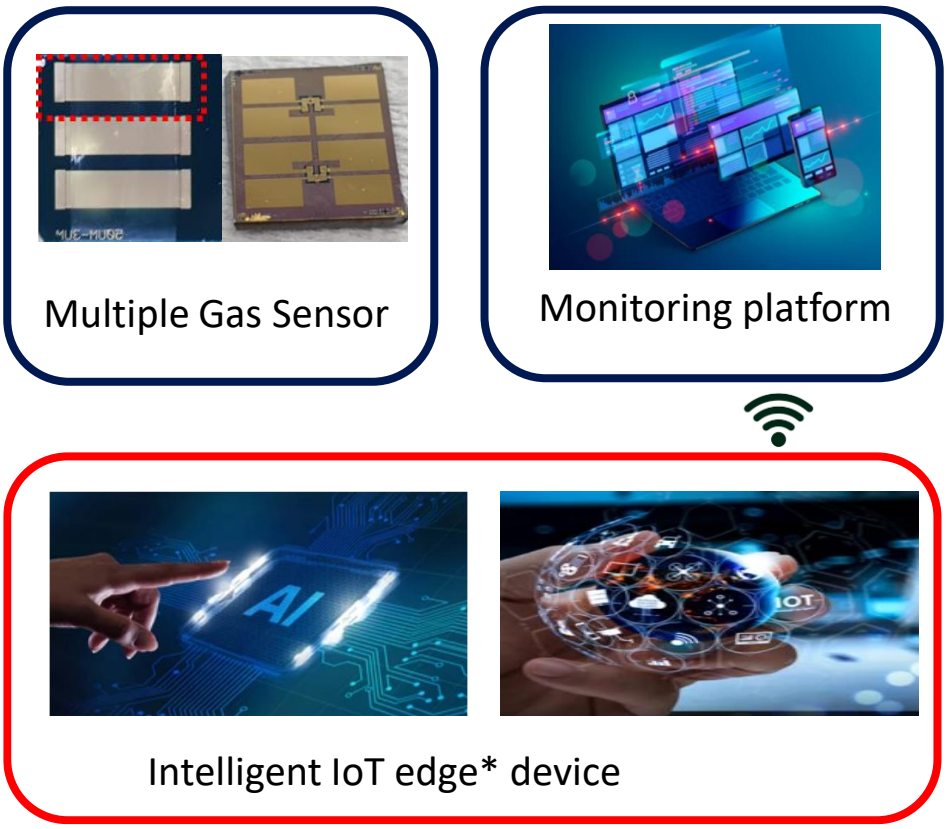

Figure 1.2. Research objective

Figure 1.2 present a general gas sensor monitoring system interface to sense the gas sensor signal and monitor its result. Multiple gas sensor signals are sensed via the sensor and to make the sensor work, the interfacing circuit is designed in the sensing device or in the integrated circuit. The interfacing circuit is generally composed with a front-end circuit which acquire the sensor signal depending its type such as resistance, capacitance and voltage type to read the sensor signal. After acquiring multiple sensor signals, those signals are digitalized via the analog to digital converter (ADC) and it is delivered to the IoT edge device. The edge-device or edge computing means that the sensor signal is processed in the device at the edge of the sensing field. Finally, the processed and acquired data is send to the monitoring platform via the communication module controlled by the micro controller unit (MCU).

The gas sensor system is composed with a combination of numerous research area such as signal processing, circuit design and the combination of the recent technology. Thus, several researches concentrate mainly to analyze the gas type [5] or sensor drift characteristic [7]. Therefore, a system level research is required to design an IoT based complete gas sensor system including the solution to resolve the reliability and selectivity problem. According, to the gas sensor characteristic, a pre-calibration of the gas sensor signal using circuit design and determining in an efficient way the gas type using an AI based algorithm can be combined in a conventional gas sensor system. Furthermore, when designing such a complete gas sensor system embedding an algorithm which can make the system

ULSAN NATIONAL INSTITUTE OF
SCIENCE AND TECHNOLOGY

robust against environmental factor which affect greatly the sensor system, can give an opportunity to bring an advanced gas sensor system.

1.2 Thesis organization

This thesis focuses on the design of the Internet of things (IoT) gas sensor device which can learn gas pattern continuously in different environment. The proposing analogue supported continual learning scheme is implemented in two steps. First, gas front-end circuit is designed to read in a wide range of sensor signal in a read out integrated circuit (ROIC). After reading the sensor signal a calibration is applied to reduce computational burden for the processing side. Then, the second step is the application of signal processing to release selectivity problem. The main, objective is to be robust for the temperature and the humidity effect on the sensor while resolving the selectivity problem. Chapter I discusses the research motivation.

Chapter II introduces a background of sensor characteristic and general architecture of IoT Multi gas sensor device.

Chapter III introduces previous works to resolve selectivity problems based on AI processing technics.

Chapter IV describes the implementation of the Environment adaptable IoT Edge gas sensor device embedding analog supported continual learning scheme for pattern recognition.

In chapter V experimental results of the designed environment adaptable IoT Edge gas sensor device embedding analog supported continual learning scheme will be presented and finally in chapter VI a conclusion on the results of the thesis will be presented.

ULSAN NATIONAL INSTITUTE OF SCIENCE AND TECHNOLOGY

Chapter II

Background

2.1 IoT gas pattern recognition system interfaces

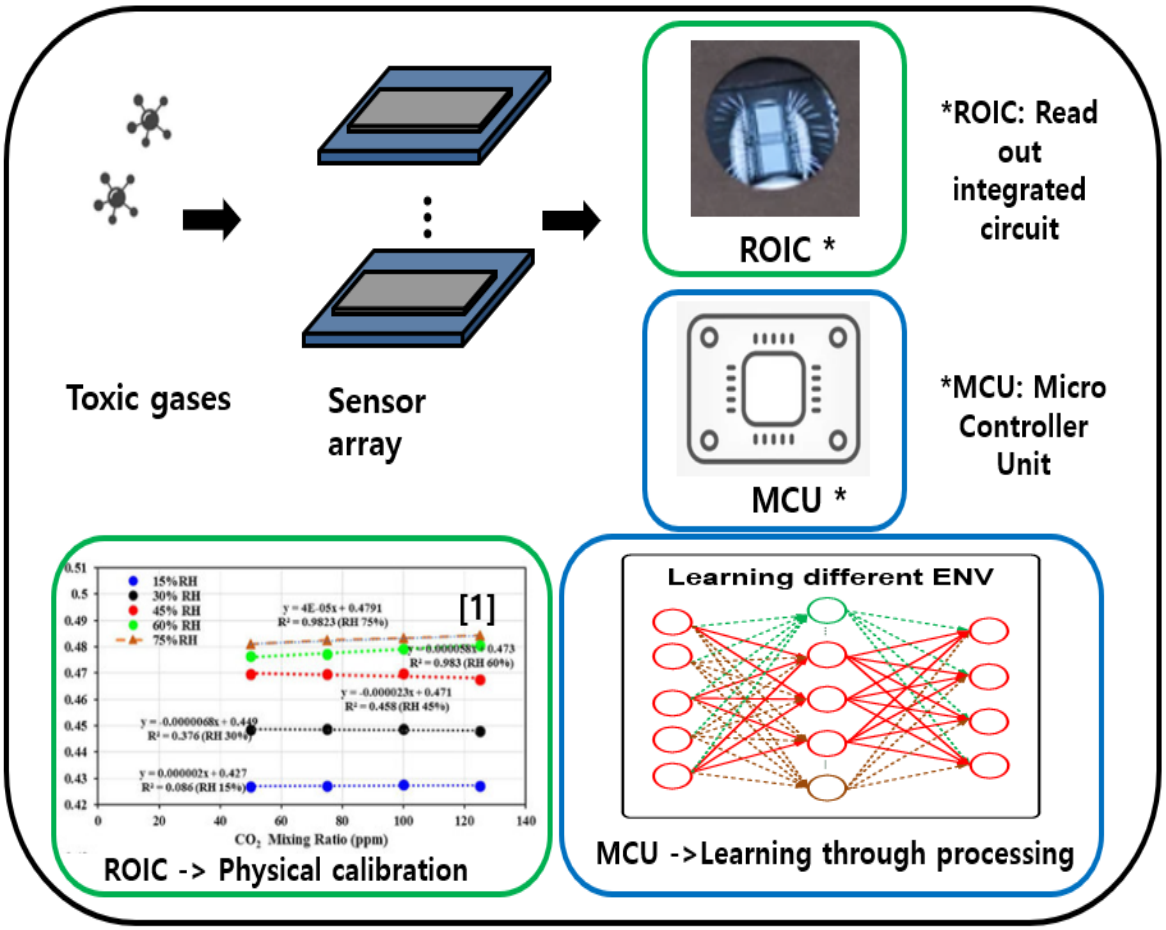

Figure 2.1. System interface of the IoT gas sensor device.

Figure 2.1 shows the general gas sensor system interface structure. According to various target gases, a sensor stage is presents first to sense target gases. Here, because of the selectivity problems, multi gas sensors array is used instead of a single sensor to have in advance more information about the target gas. Next, the analog front-end circuit is presents to interface sensor array signal. In this thesis, the

ULSAN NATIONAL INSTITUTE OF SCIENCE AND TECHNOLOGY

analogue front-end circuit is implemented in the read out integrated circuit (ROIC). After reading the analogue signal of the gas sensor, a calibration process is suggested to reduce the instability of the gas sensor signal. In this thesis, the calibration is applied physically, and it is implemented in the ROIC. Finally, data are converted through an analogue to digital converter (ADC) to be finally processed. The micro controller unit is used to control and to process multi gas sensor data and the data is sent to a server to be monitored. In this thesis, the processing algorithm is based on the continual learning scheme because in the gas sensor system, the instability of the gas sensor signal makes classical artificial neural networks (ANN) to be trained in a narrow condition.

2.2 Type of gas sensor

2.2.1 Basic of gas sensor

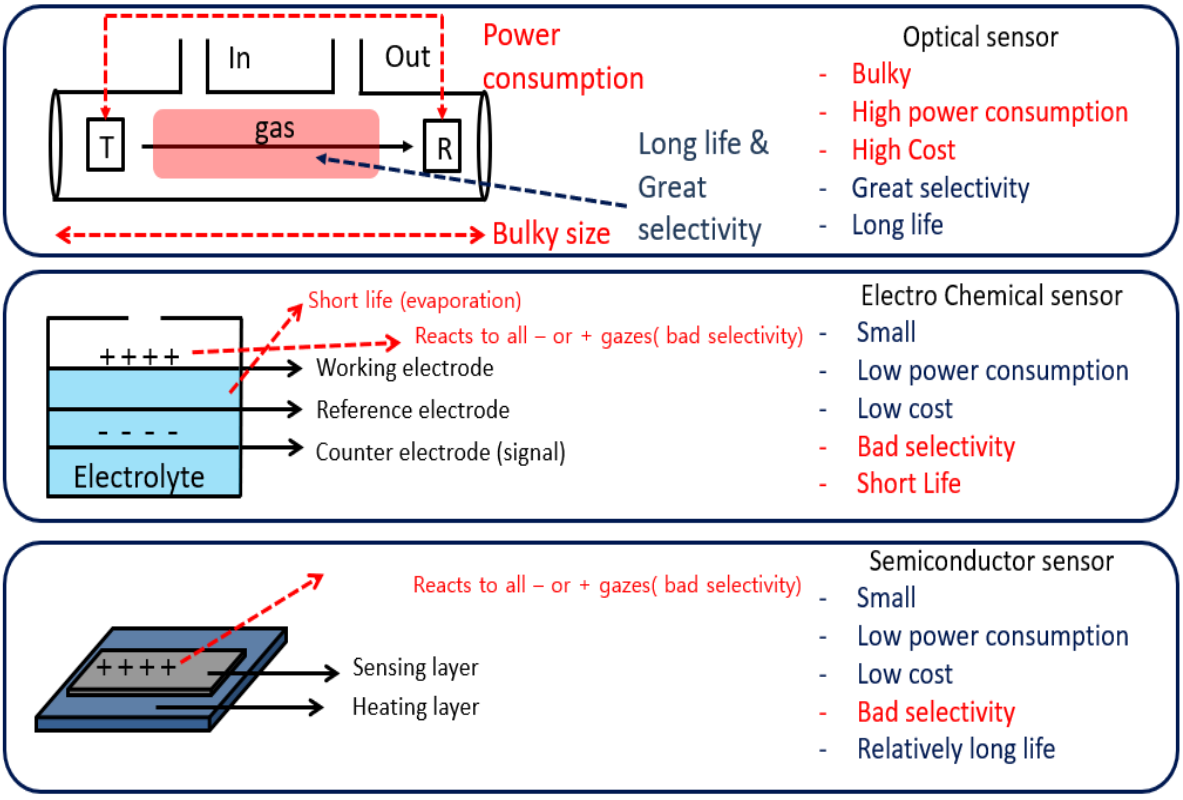

Figure 2.2. Basic of gas sensor.

The most used gas sensor in a IoT gas sensing device are presents in Figure 2.2. Their application possibilities depend on the sensing method, for the optical sensor case [8], the sensing method is based on the emission and absorption of a specific or multiple wavelength light. In this case the gas particle size and quantity of the gas are detected when reacting to the light. Thus, the selectivity

ULSAN NATIONAL INSTITUTE OF SCIENCE AND TECHNOLOGY

determining specific gases are accurate and the reliability of the sensor signal is also high. Compared to other sensor, optical type of gas sensor is more robust in front of environmental effect with its sensing mechanism and has a long life. However, the price and the power consumption of using the optical sensor is high and this sensor is often used to make a reference device measuring gas type and concentration. Thus, for a large-scale deployment objective, using an optical gas sensor is not suitable. In the case of the Electro-chemical [9] gas sensor, the sensing mechanism is based on chemical reactions. As shown in figure 2.2, target gas reacts to the surface of the sensor and the electrical reaction characteristics is expressed as a sensor signal. The cost and size and power consumption of the sensor device is low but, in the selectivity case, because of the sensor reacting with multiple gases, it is hard to determine gas type with its sensing mechanism. Also because of the short life, it is not suited for a large scale IoT deployment objective. Finally, for the semiconductor sensor type of the gas sensor [10], like electro chemical sensor, the reaction is based on the chemical reactions. Thus, the selectivity is low but in the term of price, power, life and size it is well suited for a large-scale IoT deployment.

2.2.2 Requirements for IoT gas sensor monitoring platform.

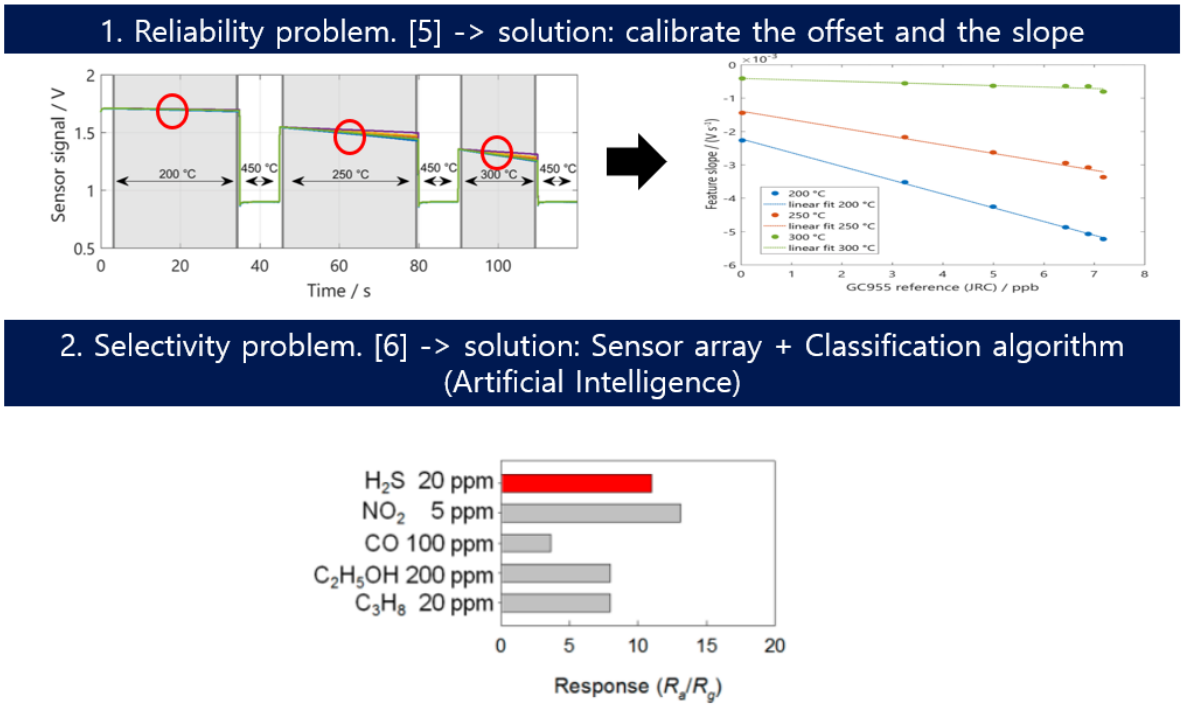

Figure 2.3. Challenges to be resolved in gas sensor system.

As mentioned in the chapter 2.1.1 using a semiconductor type of gas sensor has several challenges to overcome such as the selectivity and the reliability of the sensor. As shown in figure 2.3, for a same

ULSAN NATIONAL INSTITUTE OF SCIENCE AND TECHNOLOGY

experimental condition exposing same type of gas and concentration give different sensor signal depending on the temperature. Gas sensor signal is mostly influenced by environmental effect such as temperature and humidity. When target gas is absent at the air state or when the sensor reacts to the gas, the offset and the slope of the sensor signal depends on the environmental factor and its dependance make difficult to give exact information about the sensed gases. Classical approaches to resolves this reliability problem is to adopt calibration algorithms to stabilize this dependence. On the other hand, this semiconductor type of gas sensor reacts to multiple gases, and it is difficult to recognize the exact type of gas presents in the measuring site. To resolve this problem adopting an array of gas sensor and applying AI based algorithms give a prospective solution to find the gas type for the selectivity.

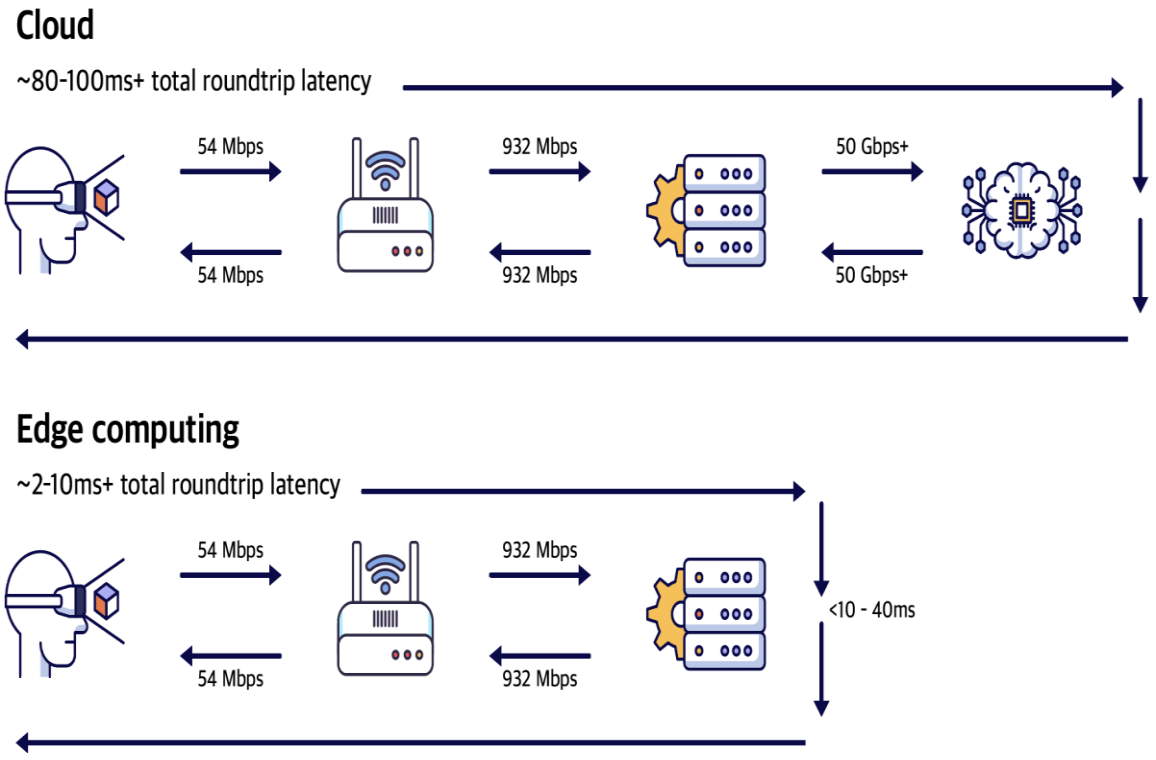

Figure 2.4. Necessity of the edge computing

The edge computing is a rising technology to make efficient the IoT system [11]. The meaning of the edge computing is to distribute processing effect from the server side to the sensing device presents in the field. There are several advantages of using edge computing structure. First, in the processing efficiency, classical approach without using edge computing system, the server is presents to process all the raw data received from the sensor device. Thus, the device communicates their raw data to the

ULSAN NATIONAL INSTITUTE OF
SCIENCE AND TECHNOLOGY

server. In this case, communication time of the data is consumed first to send the data and additional processing time is also consumed in the server side additionally. In this case, the application of the IoT system for a system which need a short-time application becomes difficult. On the other hand, if the edge computing system is used, the processing is distributed in the sensor device. Thus, except to communicate raw data a processed data is communicated to the server and in the server side a partial processing is applied, and the time of the processing is reduced, and its comparison is presented in figure 2.4. The second advantage to use the edge computing structure is to reduce the memory consumption in the server side. If unprocessed raw data is continuously stored to the server side, the memory of the server will be inefficiently handled.

Thus, adopting this edge computing capability to process challenges presented in the previous section, the requirement of designing a gas IoT monitoring platform can be efficient.

2.3 Processing method

2.3.1 Basic of gas sensor calibration

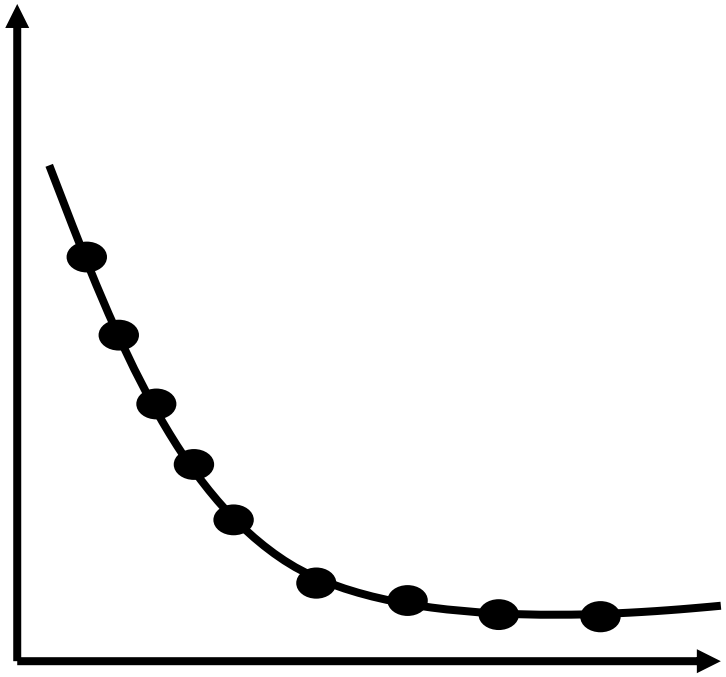

Figure 2.5. Calibration of gas sensor through mathematical relation

As introduced in the section 2.2 gas calibration method are necessary to ensure the reliability of the

ULSAN NATIONAL INSTITUTE OF SCIENCE AND TECHNOLOGY

low-cost semiconductor gas sensor influenced by environmental factor. Previous studies are categorized into using the calibration equation to reduce effect of the environment effect such as temperature and humidity or reduce the effect of the aging on the sensor. There are several approaches to realize this calibration. First, it is to apply mathematically equation where the environmental effect is present in the coefficient of the mathematical equation. Previous study [12] shows that from the basic equation relating temperature and humidity effect on the heater of the sensor, a decorrelation of the temperature and humidity effect can be mathematically modelized. The change of the energy band can be related with the change of the resistance. Equation (1) presents this relation where R_I is the resistance before the exposure of the gas and R_f after the exposure of the gas. $\Delta\Phi$ represents the work function and $\Delta\chi$ represents the electron affinity changes.

$$\ln\left(\frac{R_f}{R_I}\right) = \frac{1}{K_B * T}(\Delta\Phi - \Delta\chi) \quad (1)$$

From this equation, they developed a polynomial equation which rely on temperature and humidity variation parameter to the energy band equation. Equation (2) is the equation where in β_1, β_2 and β_3 coefficient include the environmental effect and they experimentally acquire data to find these parameters value.

$$\ln\left(\frac{R_f}{R_I}\right) = \beta_1 \Delta H + \beta_2(\Delta H^2) + \beta_3 \Delta H \Delta T_E \quad (2)$$

They finally decorrelate temperature and humidity effect and also, they train their parameter for 3 months to handle sensor characteristic variation over time. Several similar study to handle aging, poisoning and other factor also apply a polynomial equation to handle sensor signal variation characteristic. However, the aging factor also influence the sensor characteristic. Therefore, the aging factor is always limited only for the time that the experiment was performed.

ULSAN NATIONAL INSTITUTE OF SCIENCE AND TECHNOLOGY

Other study shows the solution for the calibration over time using network to update calibration equation [13].

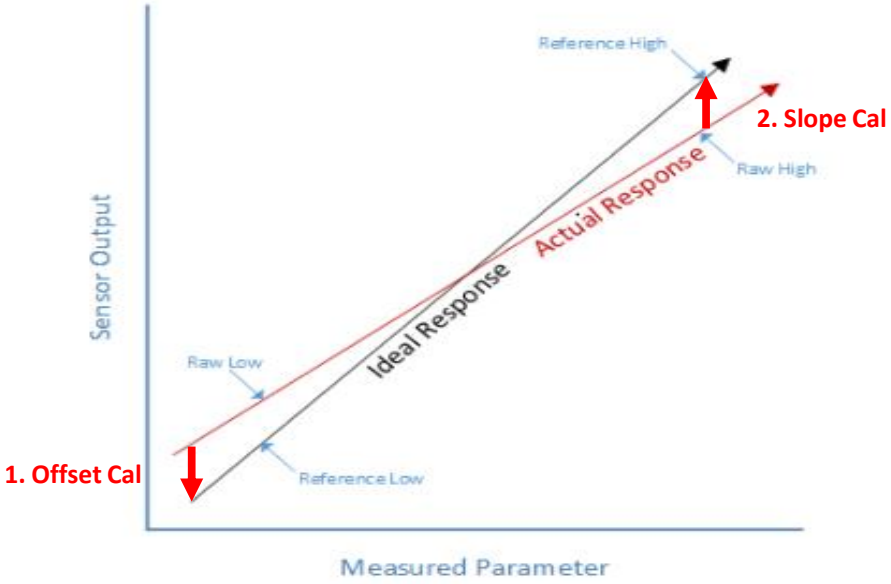

Figure 2.6. Calibration of gas sensor signal adapting offset and slope of sensor

In this study, they install in several fields a reference gas sensor detector to measure gas concentration and a designed low-cost gas sensor device is installed near this reference instrument and calibrated via network continuously. For the qualitative air quality measurement, they calibrated the low-cost sensor characteristic fitting the offset and slope to the reference instrument. Their fitting method is to match the offset of the deployed low-cost gas sensor device to the reference instrument and then fit the slope of the sensor reaction to the gases. Equation (3) and equation (4) represent the slope and offset relating equation where a_1 represents the offset of the low-cost sensor device, (t – td:t) represents the slope coefficient, Zi(t – td: t) denotes the proxy data, Yi(t – td : t) is the low-cost sensor device data and a_0 is the corrected data.

$$a_1 = \sqrt{\frac{var<\text{Zi(t - td: t)}>}{var<\text{Yi(t - td: t)}>}} \quad (3)$$

$$a_0 = E < Zi(t - td: t) > - a_0 \, E < \text{Yi(t - td : t)} > \quad (4)$$

E <> express the arithmetic mean evaluated over time period (t – td : t) and the var <> means the arithmetic variance of the mean. This relation can be used to obtain the sensor signal with the linear equation expressed in equation (5)

$$X = a_0 + a_1 . Y \quad (5)$$

ULSAN NATIONAL INSTITUTE OF SCIENCE AND TECHNOLOGY

With this equation low-cost gas sensor can be calibrated using a reference instrument and the network will update continuous period. This network using calibration changing the offset and gas reaction slope value to fit low-cost gas sensor signal value. However, reference instrument is needed to perform this calibration and to handle the network and updating every low-cost gas sensor for different place becomes an important cost.

Previous studies presented use a mathematical model for the sensor signal calibration. On the other hand, calibration performed in the physical method are also proposed. An implementation of a calibration circuit allows to calibrate sensor physical signal directly and doesn't consume processing power [6].

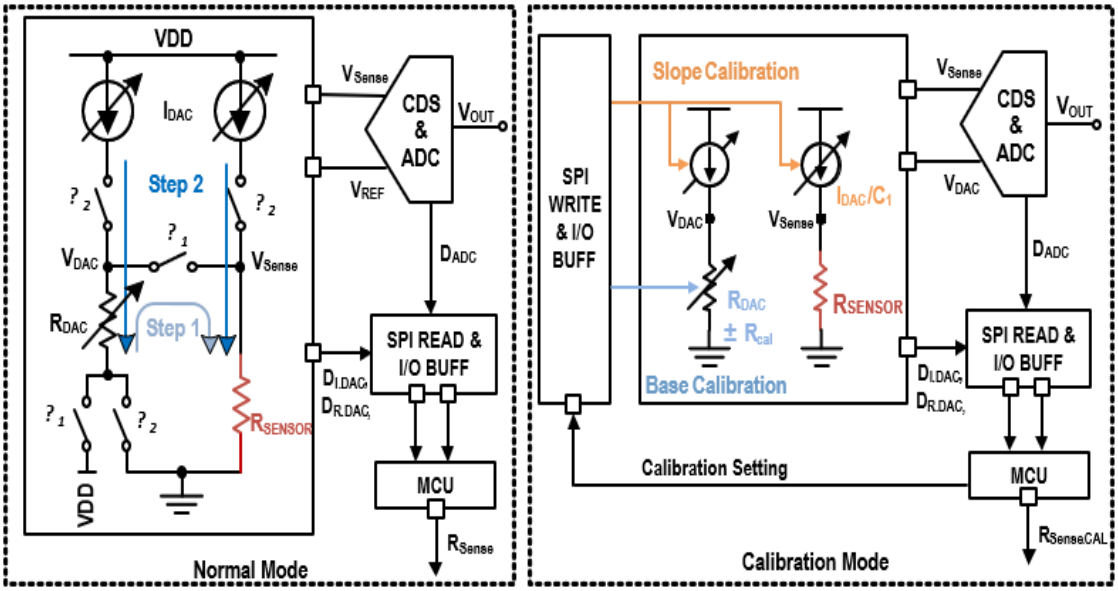

Figure 2.7. Physical calibration with electrical circuit.

Figure 2.7 shows the implementation and the functional operation about the calibration circuit. The calibration is performed through 3 steps. Depending on the gas sensor, electrically, the resistance range is very wide. Thus, the first step consists of finding the resistance of the sensor. It is called initial range or base-resistance detection phase of the sensor. Inside the ROIC at the sensor contact point, a voltage divider circuit is presents and when the first step is performed, the divided voltage value is sent to the resistive SAR operation block. The SAR operation logic compare the divided voltage with the common mode voltage (VCM). In this step like previous study with the network, the offset of the sensor signal can be adjusted. In the second step, for a fine detection, a binary search algorithm is performed with two current sources of 8-bit current digital-to-analog converter to find the one output voltage presented in equation (6) around the common mode voltage.

ULSAN NATIONAL INSTITUTE OF SCIENCE AND TECHNOLOGY

$$I_{DAC} \text{ X } R_{SENSING} \quad (6)$$

After that the difference of the voltage is given by equation (7) where the difference of the resistance is the result of the SAR operation.

$$I_{DAC} \text{ X } \Delta R \quad (7)$$

The calibration of the sensor slope when the reaction with the target gas happens can be performed in this step controlling I_{DAC}. This calibration method is a physical method not consuming computing power. However, several optimizations can be performed and also can be used to resolve selectivity problems of the sensor which is not performed in this study.

2.3.2 Basic of gas pattern recognition

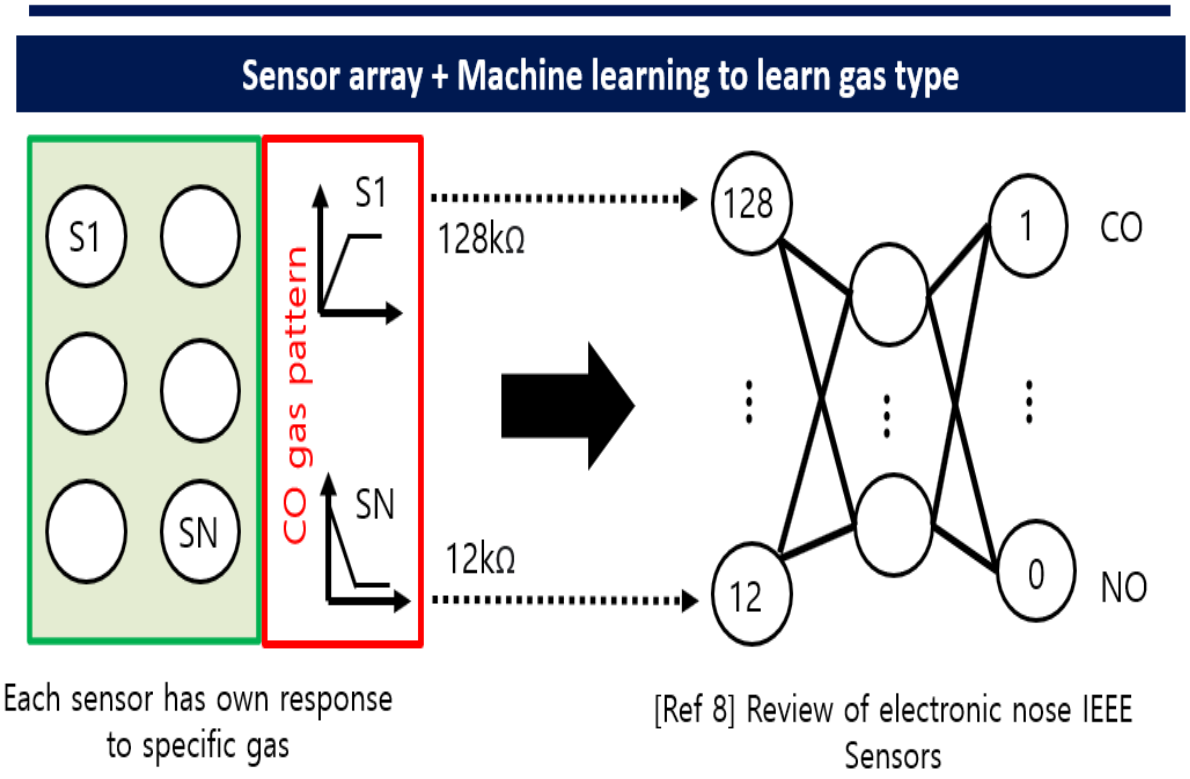

Figure 2.8. Basic structure of artificial neural network and sensor array

As mentioned in the previous section 2.2.1, the selectivity problems exist in a gas sensor monitoring system due to their physical characteristics. To give a solution to the selectivity problems, using a combination of sensors array and machine learning processing method is proposed in previous work [5]. As shown in figure 2.8, the standard procedure is defined with a hardware composed with sensor array and in the algorithm side AI based classification algorithm analyze the sensor data to find the gas

ULSAN NATIONAL INSTITUTE OF SCIENCE AND TECHNOLOGY

type. Before classifying the gas type several additional steps called preprocessing methods exist.

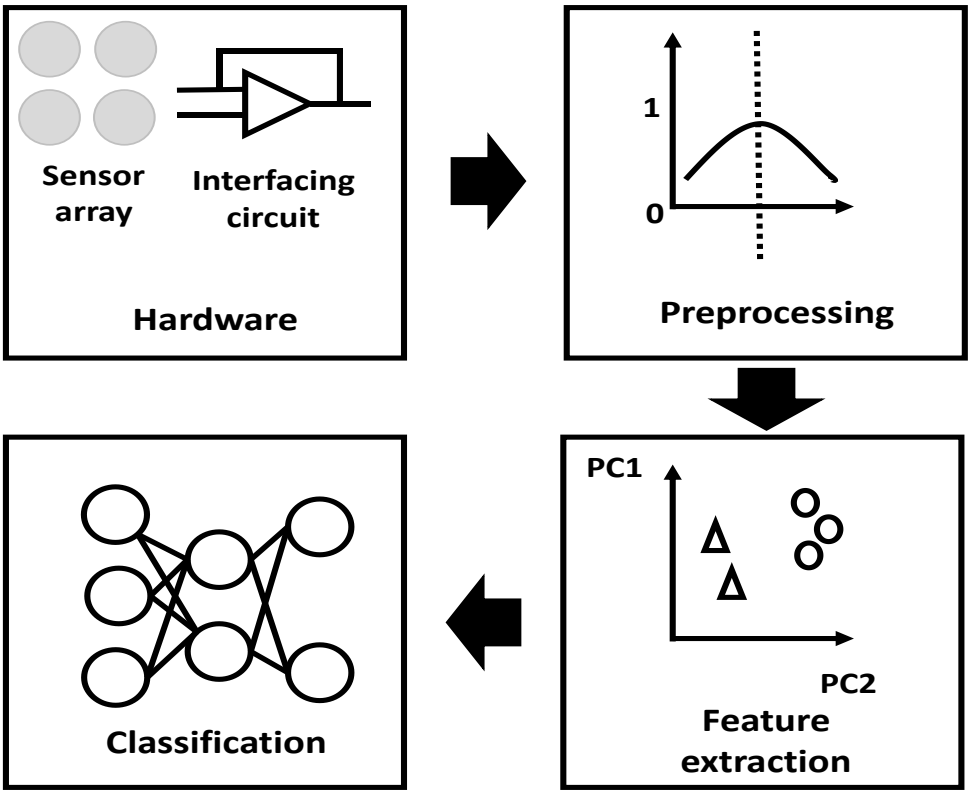

Figure 2.9. Gas sensor data classification block diagram

Figure 2.9 represents multiple steps for gas type classification. Starting from the hardware design, a sensor array is present at the front-end of the system with its interfacing electronic circuit. After acquiring sensor data from the array, preprocessing method such as normalization can reduce sensor data variation. Then, a feature extraction step such as dimension reduction method can be additionally applied to augments the pattern recognition accuracy. The dimension reduction method such as principal component analysis (PCA) is a famous method to reduce the dimension of the gas data complexity. This method is based on changing the coordinate of the high-dimensional data to a new coordinate called principal component. It is useful to simplify and visualize the clustering of high dimensional data projecting in only few principal components coordinate. Finally, after the feature extraction step a classification algorithm such as multi-layer perceptron (MLP), k-nearest neighbor (KNN) or radial basis function (RBF) are widely adopted as classifiers. However, all this method presented in the previous work [5] are only capable to train the data in a narrow condition. The classification can be performed only to the acquired data. In this condition, if new data come, the training process need to be applied including the previous data to learn about the new data without forgetting previous one. In a continuous point of view, the cost of retraining becomes higher, and the learning time also becomes higher.

Thus, to learn continuously new gas data and give an adaptability to the environment, the continual

ULSAN NATIONAL INSTITUTE OF SCIENCE AND TECHNOLOGY

learning becomes a prospective solution.

To prevent such problem, an extended study adopting the transfer learning scheme [7], which is within the family of continual learning, has been proposed. The principle of the transfer learning is to transfer previous trained knowledge to a new dataset to learn additionally new task to the old task. The transfer learning scheme has an additional benefit on the training time.

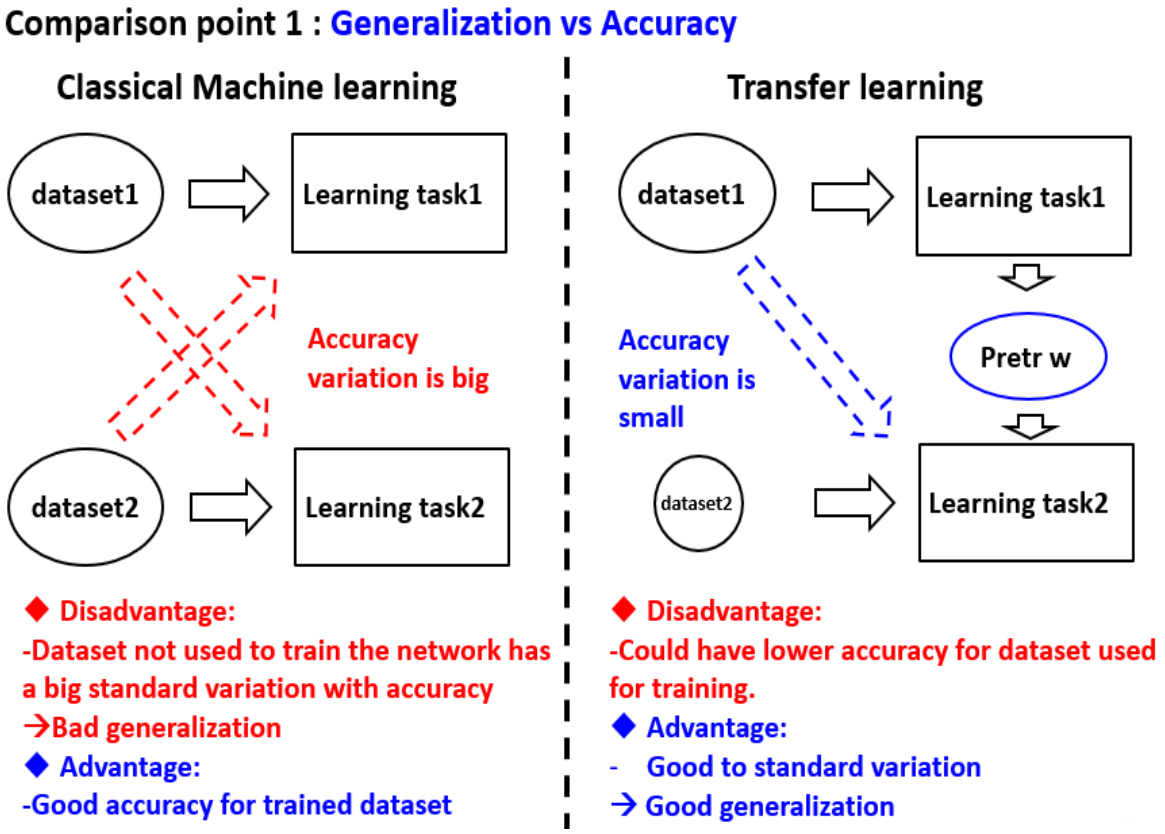

Figure 2.10 Comparison of TL and classical ML for learning method and generalization

Figure 2.10 represents a block diagram comparing the classical ML scheme with TL scheme. As shown in the figure 13, The disadvantage of the classical ML scheme is that 1 dataset used to train 1 network has a big standard deviation used in a second network trained with another dataset even it is similar. In a classical supervised machine learning scheme, before training, weights inside the network are spread randomly and repeating the training steps, weights converge to a specific number. When the training is finished, these weights are converged for the fed input dataset used for training. And if additional data is acquired, to balance this new dataset, we need to totally retrain the network to make in consideration of the new data.

For the TL cases, if one network is trained with a specific dataset and new data need to be in consideration, weights resulting the pretrained network can be transmit and only the pre-trained

ULSAN NATIONAL INSTITUTE OF SCIENCE AND TECHNOLOGY

weights are sufficient to be transmitted to the new network. Then, a training process is applied with a new dataset and the standard deviation with the new data and previous data is very small compared to input data applied to 2 cross trained classical machine learning schemes. The disadvantage compared to the classical learning model is the possibility of the accuracy reduction.

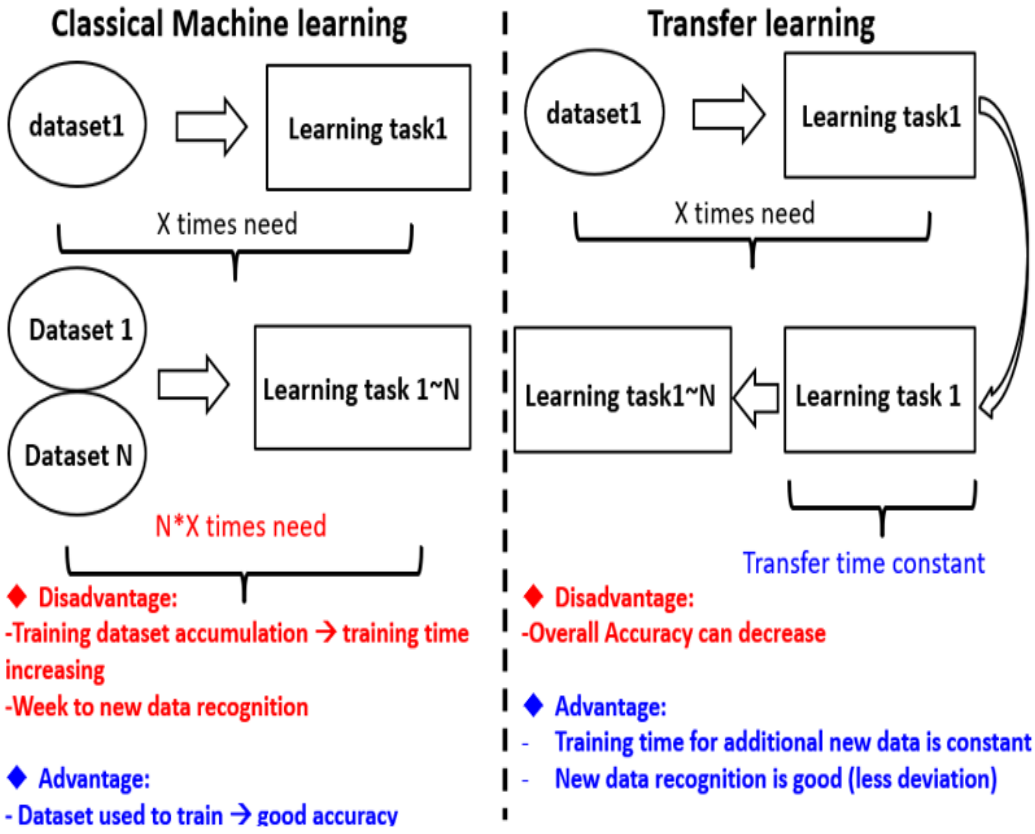

Figure 2.11 Comparison of the training time of TL and classical ML

Figure 2.11 represents the comparison block diagram of the training time of TL and classical ML. As presented in the previous section, the classical ML need to gather first all the data to be considered. Supposing that one batch has a fixed size, and its training time is about Xs increasing linearly the dataset increase the training time together. For example, if we double the dataset the training time 2*X s. On the other hand, for the TL learning scheme only weights are transmitted, and the weights numbers are fixed. Thus, the training time stay constant for the new incoming data and the processing time for training in the continuous situation can be saved. However, this learning method has a critical risk. A catastrophic forgetting can happen any time when retraining the gas data.

2.3.3 Summary

To design an IoT gas sensor platform needs diverse electrical technics. Selecting low-cost gas sensor

ULSAN NATIONAL INSTITUTE OF SCIENCE AND TECHNOLOGY

for the sensor, this type of sensor is influenced critically to the environment effect. In order to calibrate this effect multiple approach was studied before.

From making an equation relating these effects, calibration can be performed to the sensor module and achieve a high performance. However, conventional method concentrating only to one module can not be applied to the general application. Furthermore, if a sensor node covers a wide range including multiple IoT devices, a generalization of the calibration model is difficult. Several AI-based calibration methods were emerged to resolve this problem. However, data quantity used to train the AI model stay still huge to achieve a high accuracy performance and not generalized experimental condition is often used to achieve a high performance.

Another approach to calibrate from a reference sensor was performed. Nevertheless, getting far from the reference node, sensor modules performance was reduced. To calibrate wirelessly each sensor module in the field, data rate needs to be considered and a generalization of the AI model need to be proposed. A TL based learning scheme can resolve these 2 problems.

First, not sending the entire data to train an AI model but sending only the trained finished weights can save communication resource.

Secondly, the learning method about TL is based on retraining the AI model with a pretrained weights and data to be considered. Thus, in place of increasing accumulation of data, only previous trained weights and new dataset is needed to perform a global training. Saving a training time and generalize the model can be achieved with TL based method.

TL based ML calibration model can resolve classical problems such as increasing processing time, data communication amount and not generalized model. However, this TL based method has a risk to forget the previous learned task.

In the next chapter, other continual learning method will be presented. Continual learning has recently been in the spotlight due to its additional learning capability.

2.4 Continual learning for environmental adaptive classification.

2.4.1 Principle of Continual learning

Continual learning has recently been in the spotlight due to its additional learning capability [14]. There are several classes. Transfer learning was presented in the previous section and other method such as Elastic-weights consolidation (EWC), generative adversarial network (GAN), dynamic expansion net (DEN) and mask applicable network structure. Each method has their advantages and disadvantages in this thesis the objective is to implement a memory efficient algorithm in order to implement to a memory constrain MCU units. The assumption of the previous task data is not available is the principle of the continual learning. The principle of the EWC [15] is to limit the weights of the

ULSAN NATIONAL INSTITUTE OF
SCIENCE AND TECHNOLOGY

previous trained model when training an additional task to prevents the catastrophic forgetting effect. Thus, one network model can learn new task additionally to the previous tasks. However, restricting the weights variation make a limitation on the new training process. It means that the learning can maybe not achieved to the target accuracy when training the new task or the training process becomes longer than training the old and new task together to the new network. Figure 2.12 presents the working principle of the EWC.

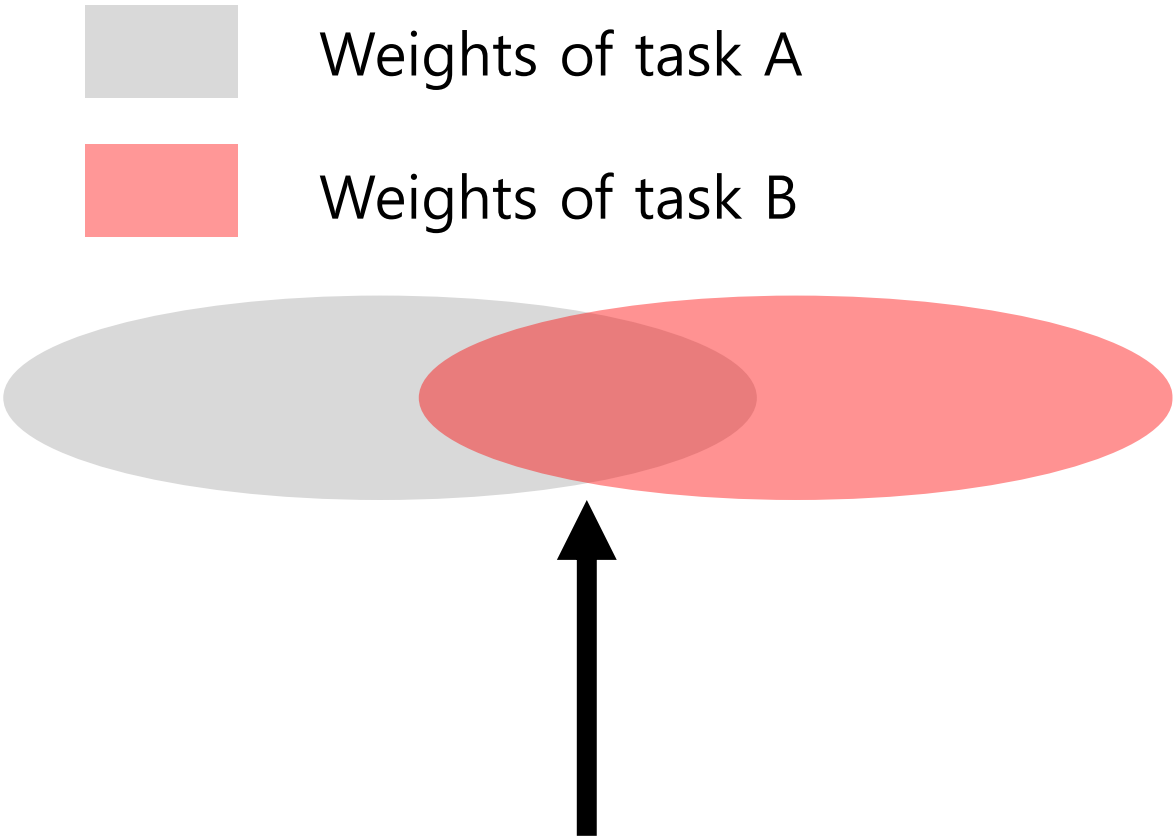

Figure 2.12. EWC working principle when training new B task to the old A task.

Figure 2.13 shows the working principle of the GAN which can be used as a memory replay method. Two network is used to learn continuously incoming new data. Among these two networks, one is used to generate fake data and other is used to discriminate between the fake and the real data. In continual learning method, the fake data produced by the generator is stored in the memory and it is reused to be train together when new task to learn is presents.

ULSAN NATIONAL INSTITUTE OF SCIENCE AND TECHNOLOGY

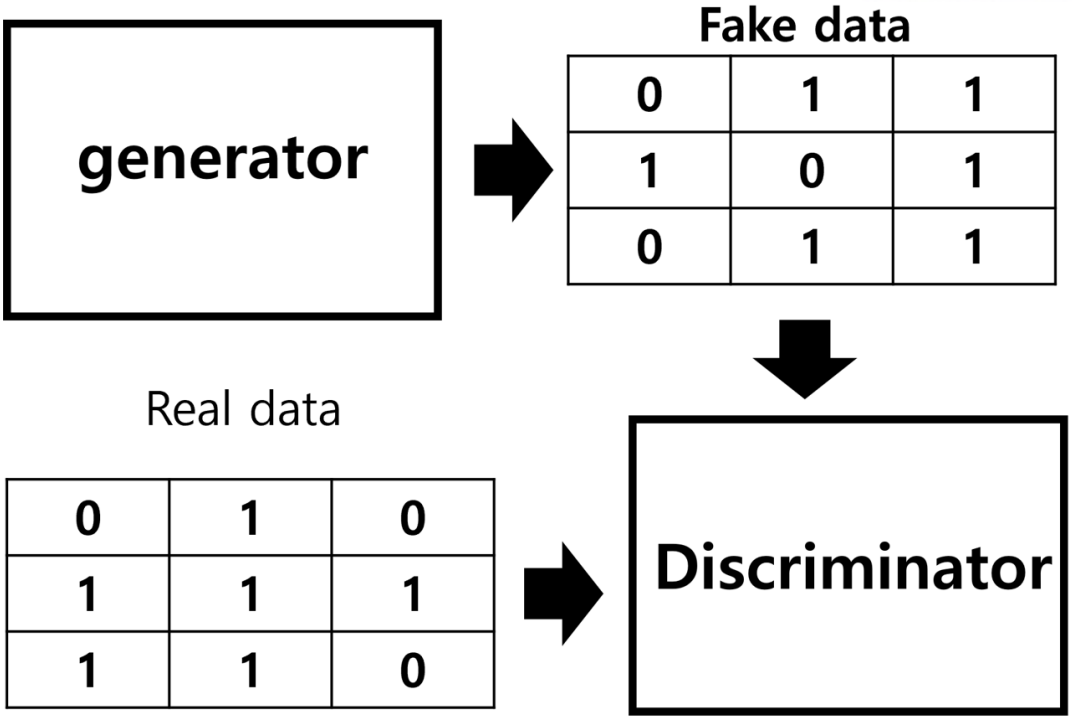

Figure 2.13. GAN working principle.

However, this method requires lots of memory and implementing 2 networks in a memory constraint becomes a challenge. Thus, implementing in the MCU the GAN method will bring a limitation to learn new task.

ULSAN NATIONAL INSTITUTE OF SCIENCE AND TECHNOLOGY

In the case of the DEN method, the structure of the network learns first the task 1 and use the network regularization first the structure of the network grown to create new weights to learn new task the working principle is presented in figure 2.14.

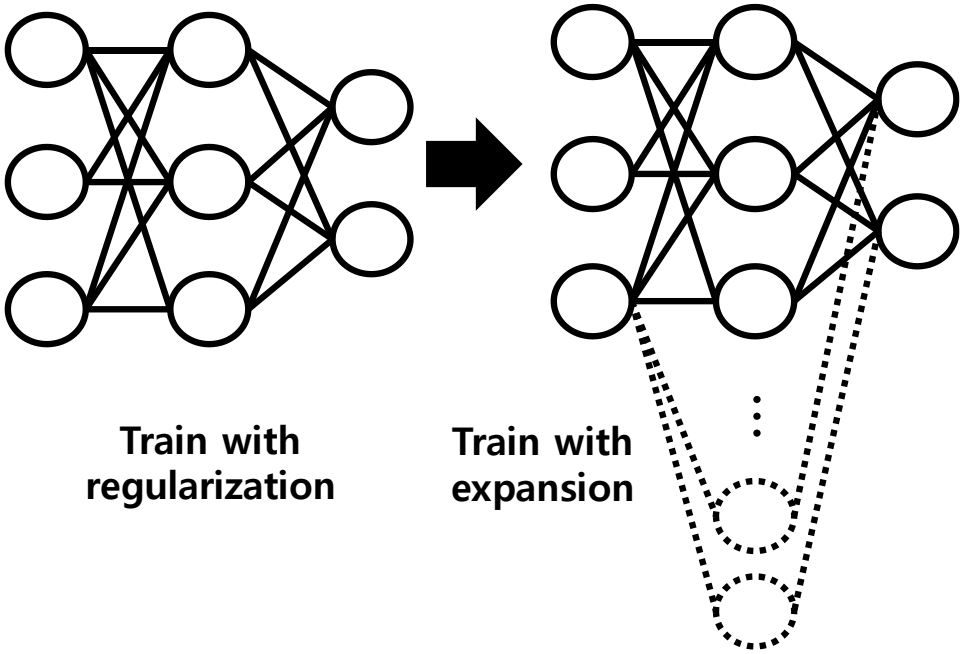

Figure 2.14. DEN working mechanism train with regularization and expend when learning new task.

Lastly the mask applicable network structure is proposed in previous work [16]. The step for the classification here is separated in 3 steps. First, they train a classical MLP structure to train the network to be fitted to the first given task. Then, pruning the network with the thresholding method can suppress unimportant weights in the network and thus make additional memory space. After pruning the network, the classification accuracy drops and relearning only with the remaining weights allows the network to recover the dropped accuracy. The second step is to use the pruned space to train new coming task without touching weights trained for the first task. In this step, untouching weights related to the first task allows the network never to forget the first trained task condition. Thus, catastrophic forgetting does not happen with this learning method. Lastly if the pruned space were not enough sufficient to achieve target accuracy for the new task, the hidden layer node number is increased incrementally to achieve the target accuracy. This method is useful to apply to the memory constraint device and the method is compact handling the memory and can give the adaptability of the network to be trained to a new task or new environment this working principle is presented in figure 2.15. However, this learning method can bring a processing confusion when learning an opposite state of data. For example, in the gas sensor system, sensor signal variation can give opposite data when temperature and humidity are different. Also, other environmental influence makes the sensor data different for the same experimental condition. In this case, using a classical learning method where the hidden layer node number increase

ULSAN NATIONAL INSTITUTE OF SCIENCE AND TECHNOLOGY

simply, the opposite data for the same condition can not achieve the target accuracy for the new task. Furthermore, if it can achieve the target accuracy, the number of hidden layer node number will increase a lot.

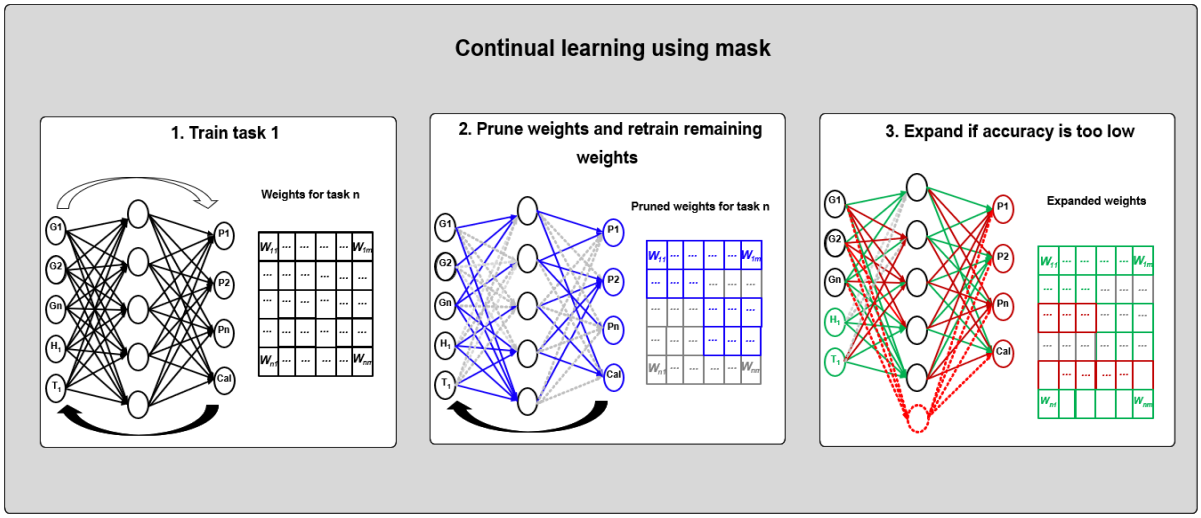

Figure 2.15. Mask applicable continual learning working mechanism.

ULSAN NATIONAL INSTITUTE OF SCIENCE AND TECHNOLOGY

Chapter III

Preliminary research result

3.1 Bio signal acquisition ROIC control and wearable module architecture

This preliminary research result presents a wearable wireless surface electromyogram (sEMG) integrated interface that utilizes a proposed analog wavelet preprocessor (AWP) for signal acquisition and pattern recognition [17]. The AWP is integrated with a readout integrated circuit (ROIC), which is fabricated in a 0.18-μm CMOS process. Based on this ROIC, a wearable device module and its wireless system prototype were implemented to recognize five kinds of real-time hand-gesture motions, where the power consumption was reduced by adopting low-power components. Real-time measurements of sEMG signals and AWP data through this wearable interface are wirelessly transferred to a laptop or a sensor hub and are then further processed to implement the pseudo-wavelet transform under a MATLAB environment. The resulting AWP-augmented pattern-recognition algorithm was experimentally verified as improving accuracy by 6% and processing time by 10%. This system will be adopted to the gas sensor monitoring further.

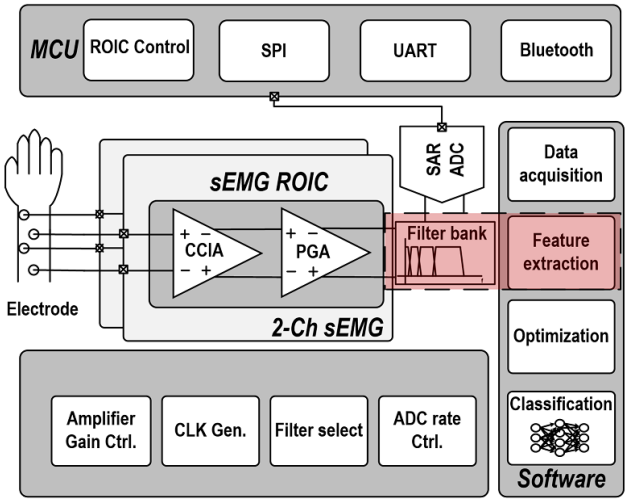

Figure 3.1. Block diagram of the sEMG sensing platform.

© 2021 IEEE. Reprinted, with permission, from Chae, Hee Young, et al. "A wearable sEMG pattern-recognition integrated interface embedding analog pseudo-wavelet preprocessing." IEEE Access 7

ULSAN NATIONAL INSTITUTE OF SCIENCE AND TECHNOLOGY

(2019): 151320-151328.

Figure 3.1 shows how the sEMG sensing platform works. The system is composed of three main parts: a front-end analog circuit, embedded components, and software. The gas sensor monitoring system will also be designed similarly. First, sensing of the sEMG signal starts from the sEMG detection channel which is composed of a capacitor coupled instrumental amplifier (CCIA) and a programmable gain amplifier (PGA). After sensing and amplifying the sEMG analog signal, this signal passes through the AWP and is filtered or can go directly to the SAR ADC to be digitalized. Finally, the digital data is communicated to the low power MCU (STM32L4). In order to augment pattern recognition accuracy, two sEMG channels are included and are switched successively in front of one ADC. After the data is collected in the MCU, the MCU manages the timing to send data wirelessly to the PC via low power Bluetooth. After the MCU sends the data to the PC via Bluetooth, feature extraction in the data is done for the MLP. To compare the performance from data that has passed the AWP and the original data, both were processed and compared for accuracy. Applying the FFT algorithm to the gathered data changes data that has passed the filter pass into a pseudo wavelet transform. This processed data of the EMG will be the data input for the MLP. MLP is chosen because of its efficiency has been proven in past research. After training the neural network, the trained network will be implemented in the receiver software to recognize patterns.

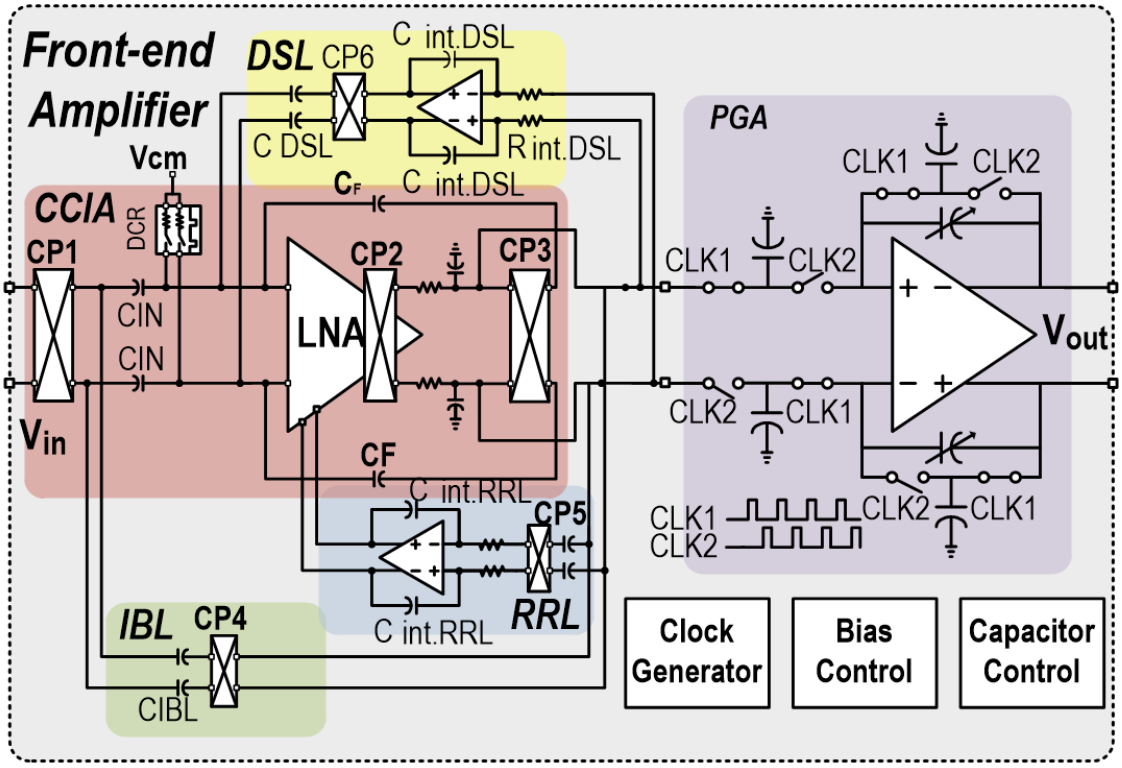

Figure 3.2. sEMG read-out circuit diagram.

ULSAN NATIONAL INSTITUTE OF SCIENCE AND TECHNOLOGY

A detailed implementation of the proposed ROIC circuit is shown in figure3.2. This implementation considers several noise problems when acquiring the sEMG signal. One of the major problems when acquiring an sEMG signal from a wearable module is the condition of the physical contact with the skin. Various physical movements make the contact between the electrode and the skin unstable. This condition modifies the impedance model for the input condition of the circuit. This problem is resolved through an impedance boosting loop (IBL) at the input of the low noise amplifier (LNA). Past study shows that each person has a different sEMG frequency, but the meaningful frequency range is always between 0~500 Hz and the amplitude of the signal is less than 1mV. Therefore, the LNA is designed to cover this frequency band and amplifies the signal to a few hundred mV to make the signal analyzable. The DC servo loop (DSL) reduces the DC offset at the input of the LNA. The DC offset is added because of the distance between two electrodes in contact with the skin. A chopper removes low-frequency noise including 1/f noise. While using the chopper to suppress low-frequency noise, there will be ripple at the output of the LNA due to frequency switching. To resolve this problem, RRL is applied to stabilize this ripple. After these multiple steps to reduce noise and amplify the signal, the Programmable Gain Amplifier (PGA) amplifies the signal coming from the CCIA output one more time. As its name implies, the gain is controllable by the MCU.

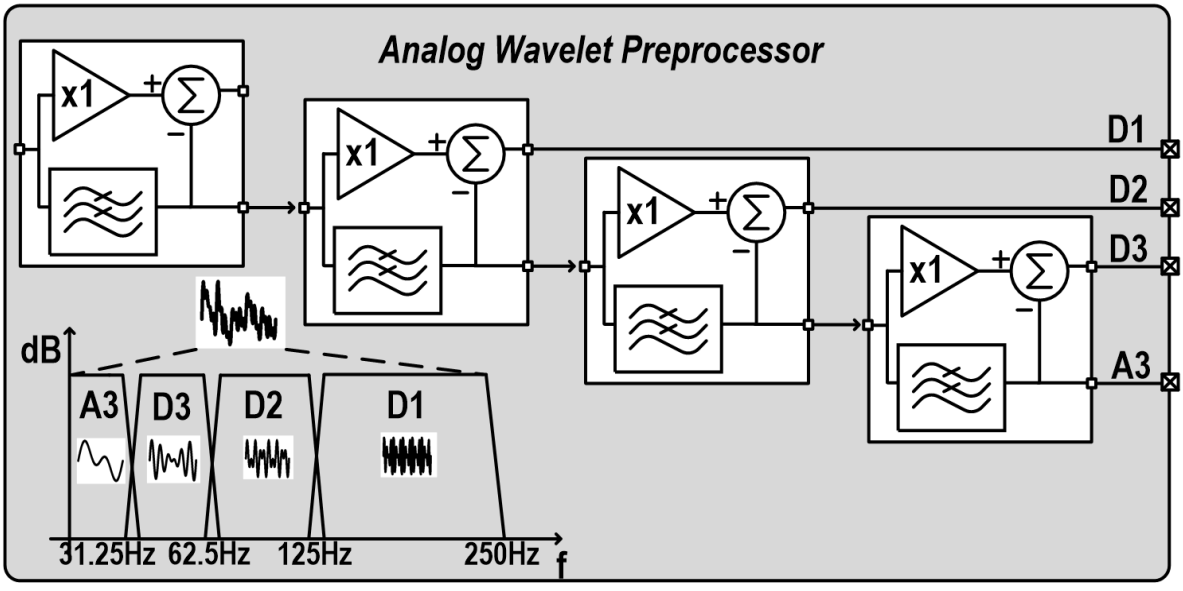

Figure 3.3. Wavelet preprocessor logic diagram.

Wavelet transform is an emerging process to treat various bio signals. The main idea of wavelet transform is to first decompose the input signal into multiple frequency ranges and then perform frequency domain analysis. Implementing half of this wavelet transform, which is a decomposition step with an analog circuit, provides AWP with several advantages. Due to the analog filtering decomposition, the information is digitalized without loss. Then, the selectivity of the bandwidth can

ULSAN NATIONAL INSTITUTE OF SCIENCE AND TECHNOLOGY

remove unwanted noise like motion artifacts, which is a critical noise when treating bio-physiological data. In addition, filtering the signal means that the signal is processed, and it can augment the quality of the signal and can reduce the processing time in the digital signal processor (DSP). Additionally, considering sEMG characteristics, the AWP is designed to support a frequency range of 0~250 Hz.

Figure 3.3 shows how AWP performs the decomposition of the signal. The original signal first passes through the low pass filter (LPF) and the analog buffer. Then an analog subtractor circuit subtracts the LPF signal passed from the original signal to realize a high pass filter. Repeating this activity, four band pass filters are realized. Detailed (D) information in the HPF can be selected from D1 to D3 and the approximation (A) information in the LPF, A3 can be selected. With the digital implementation of wavelet decomposition, a down-sampling procedure is included after decomposing the signal into multiple frequency ranges. However, with an analog circuit, scaling the cut-off frequency of each stage in a wavelet preprocessor by two results in down-sampling with a factor of two.

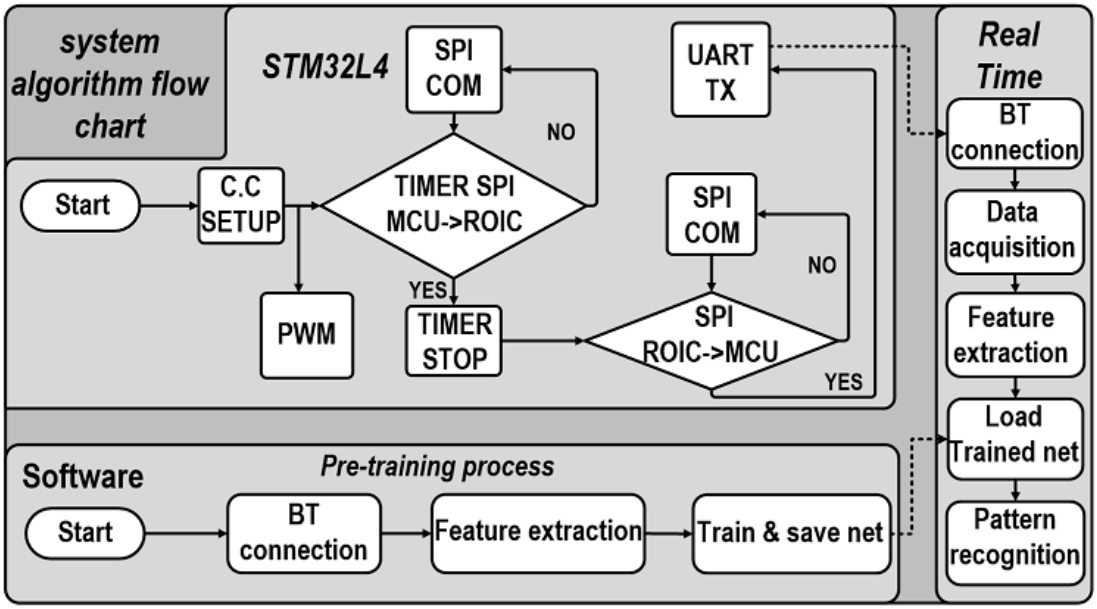

Figure 3.4. Embedded and system algorithm flow chart.

Figure 3.4 shows the detailed implementation of the embedded system and system algorithm. The embedded system that controls the entire module was implemented on a STM32L4 MCU and the communication and pattern recognition was done with MATLAB2016a. For accurate timing control, it is necessary to first set the system core clock (C.C.). Then, from this C.C., a pulse width modulation (PWM) is activated to feed a digital clock for the ROIC chip. This digital clock is used to activate serial peripheral interface (SPI) communication with the MCU, and to activate the ADC and other digital blocks to make the ROIC operational. After the PWM is set-up, SPI communication is enabled and through this chip-to-chip communication interface, two channels of sEMG are selected and switched in

ULSAN NATIONAL INSTITUTE OF SCIENCE AND TECHNOLOGY

front of the integrated ADC. For each channel, the gain, the ADC data rate, and the wavelet filter are adaptively selected. SPI communication needs to be controlled with precise timing. A timer interrupt is used in order to provide control with exact timing. After checking the transmission of data and if there is no problem in the communication, the ADC data coming from the ROIC is collected and sent through a universal asynchronous receiver and transmitter (UART) protocol via Bluetooth to a PC. The sampling frequency for the ADC was selected as 1,000 samples per second for each two independent channels in consideration of the Nyquist rate for data analysis in a frequency domain. MATLAB receives data and first pre-trains the MLP, then after the training step, the trained MLP is implemented in the real-time application environment. This will be similar in gas sensor monitoring system except in the gas monitoring system, the receiver is not only MATLAB but also will be designed to monitor data via internet protocol.

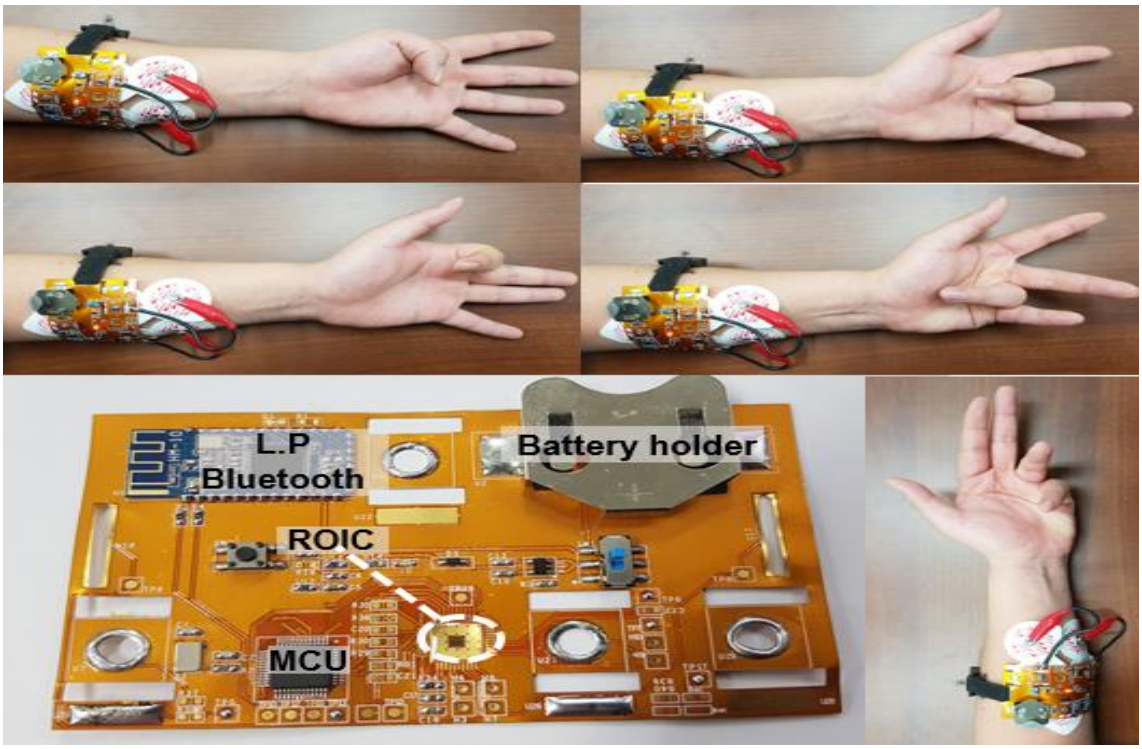

Figure 3.5. Wearable flexible module and finger gestures.

Figure 3.5 shows the designed flexible wearable module including the ROIC and the five target movements to recognize. This module is designed with a low power component, and in order to achieve the objective of being able to wear the module, the printed circuit board (PCB) was designed with a flexible PCB. An elastic band is tied to the module to reduce the skin contact noise problem. Three healthy subjects participated in trials to collect the sEMG signal. Wearing this module, the sEMG signals are collected via Bluetooth communication. In a total of 800 data samples, 400 data for the filter

ULSAN NATIONAL INSTITUTE OF SCIENCE AND TECHNOLOGY

passed signal and 400 data for the original sEMG were prepared.

For the electrode position, the palmaris longus (PL) and flexor carpi ulnaris (FCU) muscles were selected as suitable candidates for pattern recognition. Past studies show that these two muscles are involved in the wrists and different finger movements. The sEMG signal coming from these muscles and associated finger movement gestures can be analyzed. Figure 3.6 shows the experimental results of the wirelessly acquired time domain sEMG signals. figure 3.6 (e) is the original unfiltered signal and from figure 3.6 (a) to figure 3.6 (d) each filter from D1 to A3 was applied. As shown in the figure, the D2 passed signal and D1 passed signal have less noise compared to the original signal. A motion artefact noise, which is a low frequency noise, is not present in the D2 filter passed signal. Meanwhile, in the D1 passed signal, filter passed signal and D1 filter passed signal bands include the meaningful frequency range of the sEMG signal. Therefore, the analysis shows the performance of the AWP by comparing between the accuracy of the pattern recognition of the D2 passed signal, which includes the 62.5~125 Hz frequency range, and the original sEMG signal.

ULSAN NATIONAL INSTITUTE OF
SCIENCE AND TECHNOLOGY

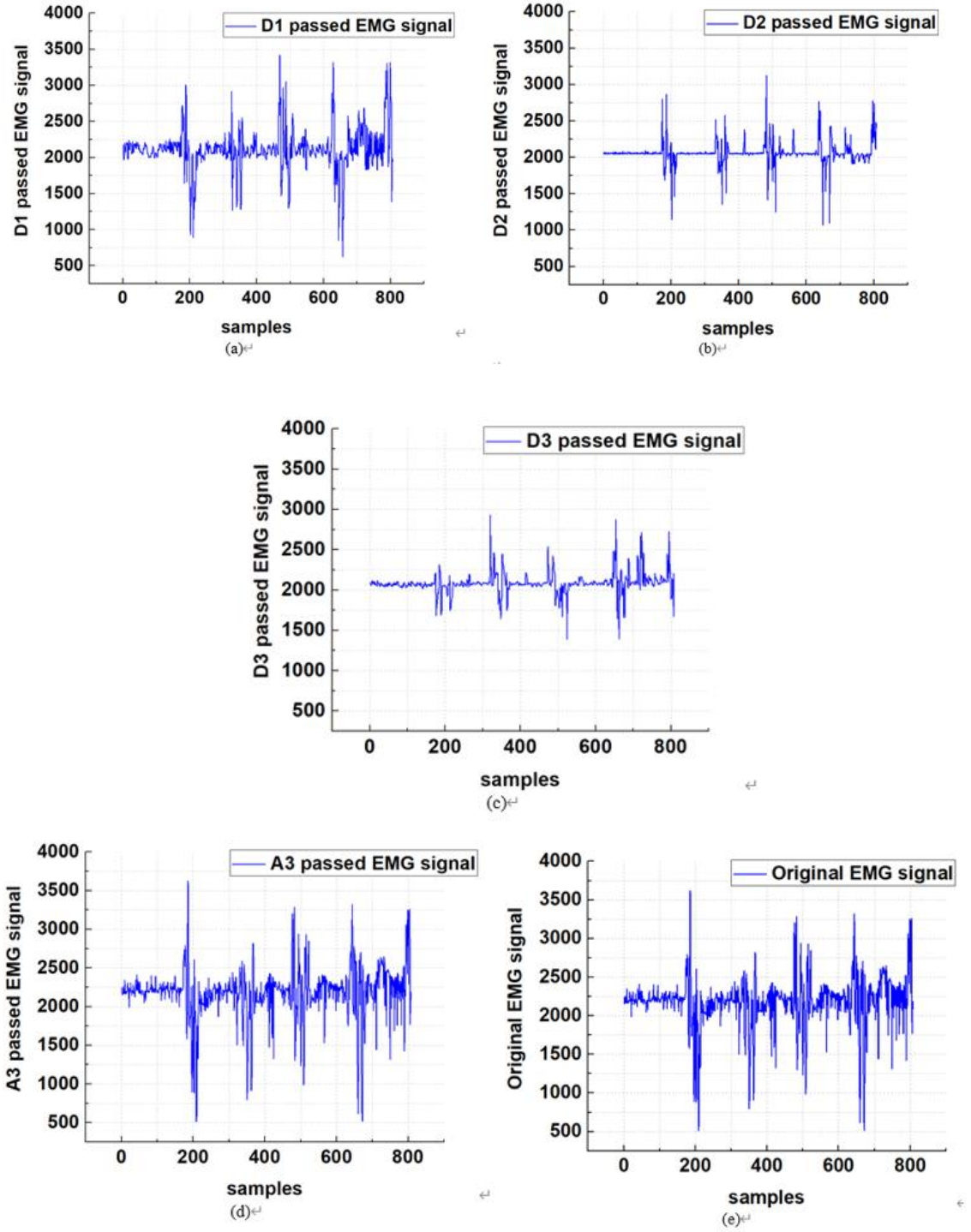

Figure 3.6. Data acquired from wireless communication of: (a) D1 filtered signal, (b) D2 filtered signal, (c) D3 filtered signal, (d) A3 filtered signal, and (e) original sEMG signal.

ULSAN NATIONAL INSTITUTE OF
SCIENCE AND TECHNOLOGY

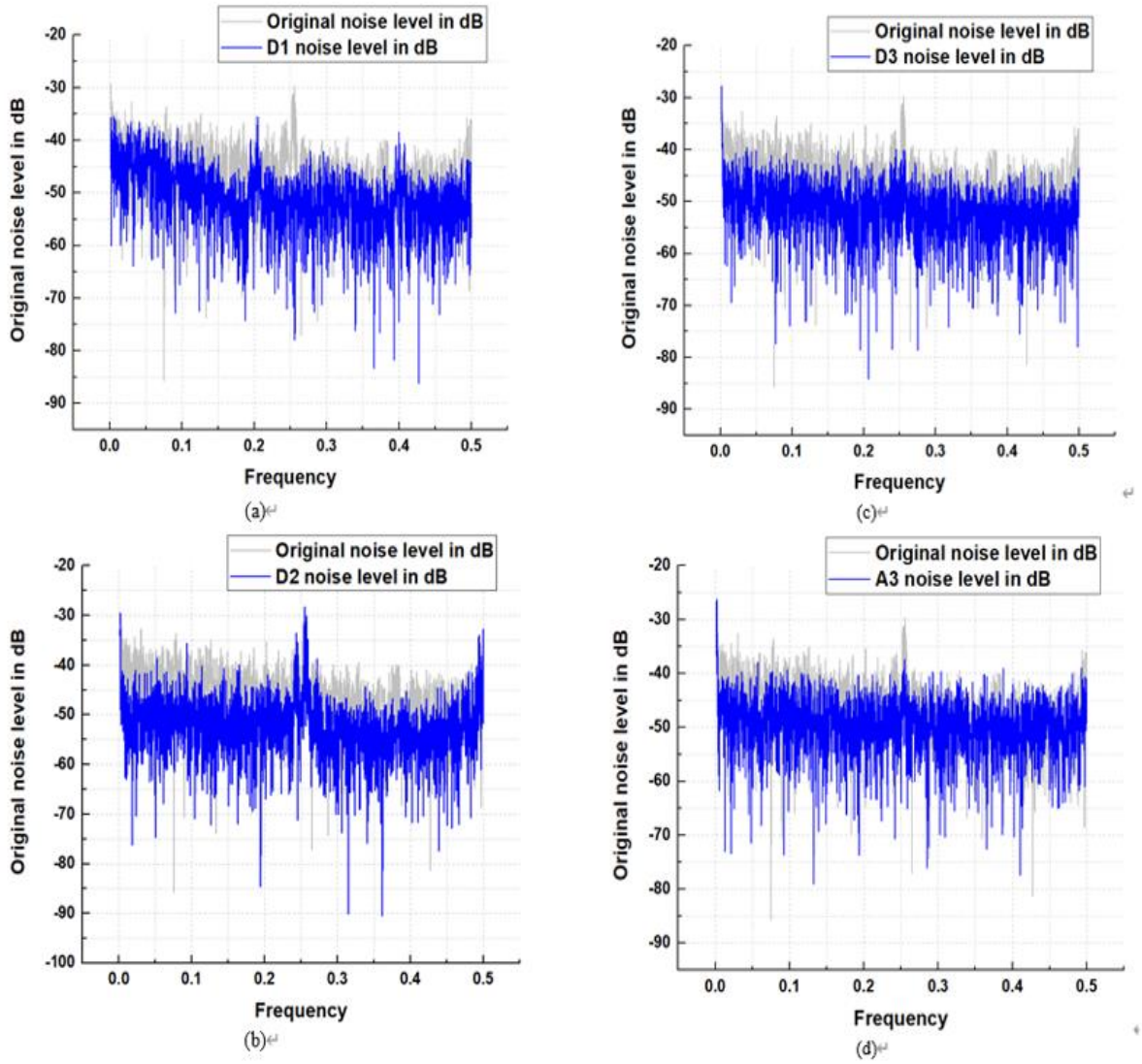

Figure 3.7. Noise level comparison in a frequency domain with the original sEMG signal of: (a) D1 filter passed signal, (b) D2 filter passed signal, (c) D3 filter passed signal, and (d) A3 filter passed signal.

Figure 3.7 shows a noise level comparison in a frequency domain between figure 3.7 (a) D1 and the original sEMG signal, figure 3.7 (b) D2 and original signal, figure 3.7 (c) D3 and original signal, and figure 3.7 (d) A3 and original signal. This frequency domain analysis was done with a sEMG time domain data in a window size of 1,000 samples points and the analysis was done between 0.1~500 Hz. figure 3.7 shows that the D1~D3 filter passed signal has a low noise level in dB compared to the original sEMG signal. sEMG has a low signal-to-noise ratio (SNR) , therefore, a small noise level attenuation can improve pattern recognition accuracy for MLP. Considering this diminution of noise, the Fast Fourier Transform (FFT) is applied to the time domain sEMG data. Meanwhile, to show the processed

ULSAN NATIONAL INSTITUTE OF SCIENCE AND TECHNOLOGY

data performance of the AWP, this feature extraction method is applied especially to the AWP D2 filter passed data and the original sEMG data. Applying the FFT process for the AWP D2 filter passed data, the processing becomes a pseudo-wavelet transform and for the original sEMG data it becomes simple FFT processed data. As mentioned in the previous experimental environment, we collected 400 data samples for each filter passed data and original sEMG data. Finally, after applying the FFT process, taking the two strongest intensities in the frequency spectra of the FFT spectra and its frequency for each channel, eight digital values were chosen for training.

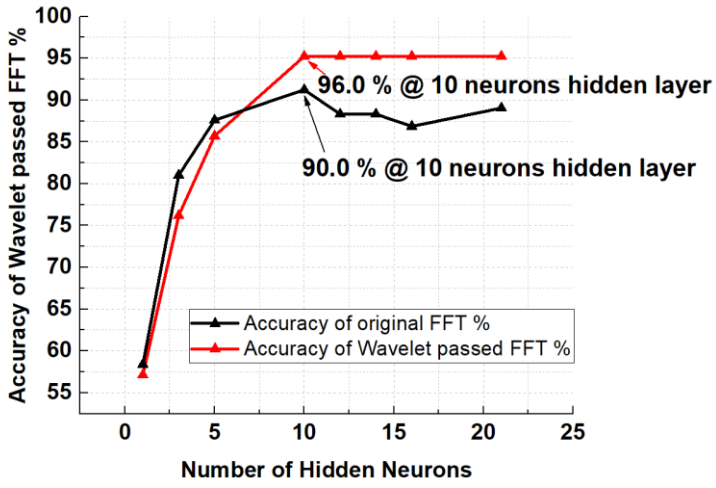

(a)

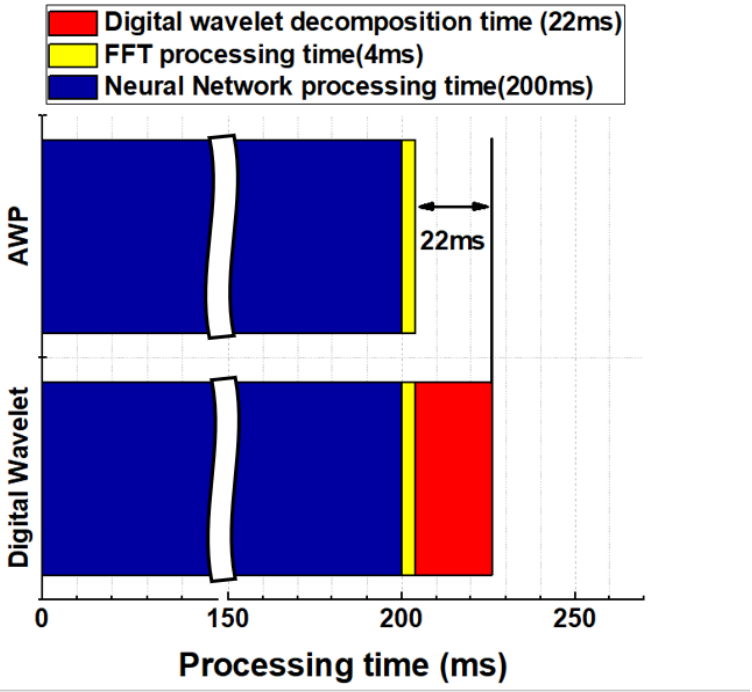

(b)

Figure 3.8. (a) Number of hidden neurons vs. accuracy and (b) saved processing time.

ULSAN NATIONAL INSTITUTE OF SCIENCE AND TECHNOLOGY

After feature extraction, a matrix of the eight digital values for 400 samples are prepared for training. Before training with the MLP, an optimization algorithm to predetermine the size of the MLP is applied to the network design. This optimization selects the optimal number of hidden neurons present in a single hidden layer in order to avoid an overfitting problem coming from noise fitting and diminished processing time. The number of all the neurons present in the MLP is applied together with an undetermined weight before the training state. The weight will be determined after training and from the fixed weight value, and the neural network will do the calculation to find the pattern. Figure 3.8 (a) shows the results of the optimization done for the filter bank passed EMG data analysis and the original EMG data analysis. The results indicate that the optimal number of hidden layer neurons is 10 and if the number of the hidden neurons goes over 10, the accuracy may decrease in the case of the original EMG data because of the noise fitting effect or stay the same in the case of the wavelet passed FFT.

Figure 3.8 8(a) shows that the highest accuracy comes from the AWP D2 passed signal feature. Finally, the structure of the MLP was decided upon through this simulation as 8 inputs, 10 neurons in 1 hidden layer and 5 outputs to determine 5 movements. After choosing the structure of the MLP, the sample number required to resolve all undetermined weights was determined as 400 based on past research proving the upper bound for the hidden neuron number theorem. From the total samples, 60% were used to train MLP, 20% were used to test MLP, and the other 20% was used to test the network.

Figure 3.8 (b) shows the saved processing time with the given profiler function in MATLAB when the MLP structure is composed of 8 inputs, 1 hidden layer with 10 hidden neurons and 5 outputs, and the calculation time was around 200 ms to recognize a pattern. In the case of the wavelet decomposition function given in MATLAB, it takes around 25 ms to decompose the signal of 1000 samples points. For the FFT process, with the same profiler function, the processing time is about 4 ms. Therefore, we experimentally verified that the proposed AWP reduces the decomposing processing steps by about 25 ms, which is around 10% of the processing time and augments accuracy by about 6%.

Figure 3.9 shows the confusion matrix for the pattern recognition of five hand gestures. Figure 3.9 (a) shows the accuracy of the AWP D2 passed signal. This confusion matrix shows that for the average classification, the thumb finger movements for four samples were classified as pinky finger movements with an accuracy of about 95%. For the index finger movement and the middle finger movement, the total number of samples recognized was 100%. For ring finger movement, four samples were recognized as a middle finger movement and the other four samples were recognized as a pinky finger movement. The accuracy for ring finger movements was about 90%. Finally, for pinky finger movements among 80 samples, four samples were recognized as a thumb finger movement, which reflects a pattern recognition accuracy of 95%. On average, finger movement pattern recognition accuracy was 96%. For Figure 3.9 (b), which represents the original sEMG finger movement pattern recognition accuracy, specifically for thumb finger movement, four samples were confused with an

ULSAN NATIONAL INSTITUTE OF SCIENCE AND TECHNOLOGY

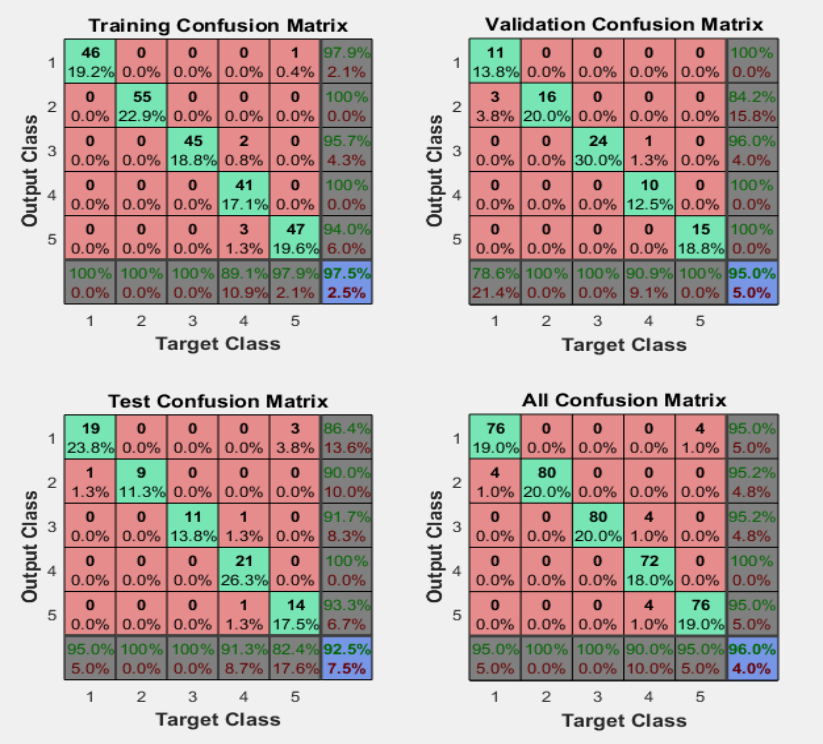

(a)

(b)

Figure 3.9. Accuracy of (a) AWP D2 processed signal and (b) original sEMG signal.

ULSAN NATIONAL INSTITUTE OF SCIENCE AND TECHNOLOGY

index finger movement. Meanwhile, index finger movements and ring movements were recognized with 100% accuracy. Middle finger movement accuracy was relatively low with 12 samples among 80 samples confusing the movement as a ring movement, while another 12 samples confused the movement with a pinky finger movement, and four more samples confused the movement as a thumb movement, which represent an accuracy of about 65%. Finally, pinky finger movements were confused with thumb finger movements in about four samples. The total average accuracy for the original sEMG pattern recognition without the AWP process was 90%.

For a fair comparison, a digital wavelet processed performance is shown in figure 3.10. As shown in figure 3.10 the performance of the digital wavelet decomposition is close to the AWP performance. The accuracy is higher about 0.5% compared to the AWP but the processing time is needed to achieve 96.5%. Therefore, using a AWP can reduce the processing time with a reasonable accuracy.

Figure 3.10. Accuracy of digital wavelet decomposition.

ULSAN NATIONAL INSTITUTE OF SCIENCE AND TECHNOLOGY

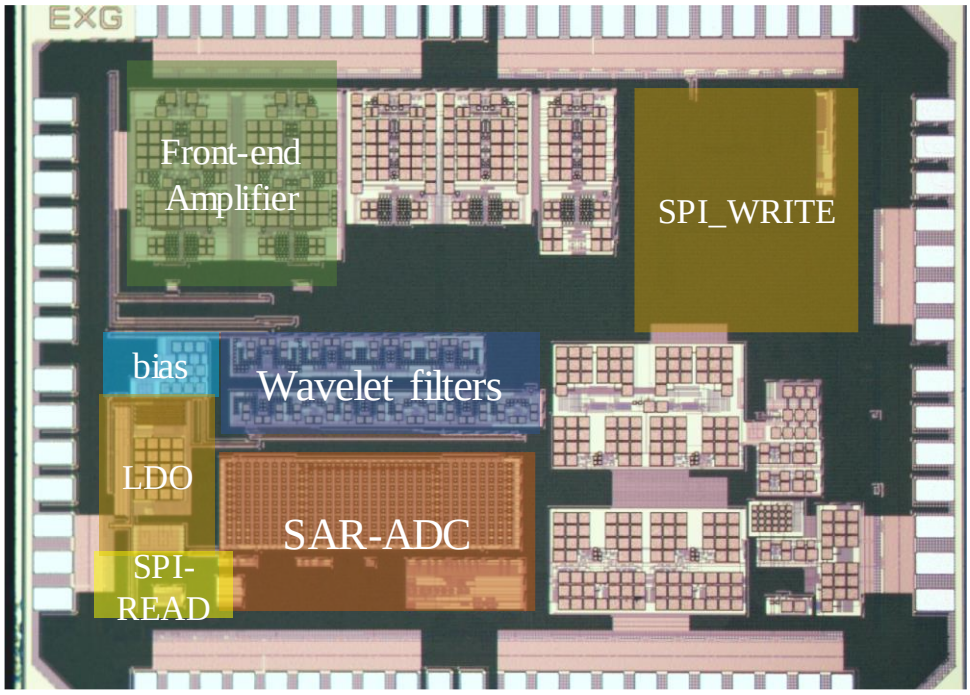

Figure 3.11. Microphotography of the sEMG ROIC circuit.

Figure 3.11 shows a microphotography of the chip prototype of the proposed wavelet preprocessor with the ROIC and the SAR ADC integrated interface. It was fabricated in a 0.18-μm complementary metal oxide-semiconductor (CMOS) process, occupying a silicon area of 2 mm by 2 mm. Table 1 summarizes the overall performance of the proposed wearable sEMG Pattern-Recognition integrated interface embedding AWP which is also compared with previous work on an sEMG pattern recognition system. The proposed wearable sEMG pattern recognition AWP achieved a recognition accuracy of about 96% using the artificial neural network classification, and the power consumption of the wearable prototype is about 66 mW. Additionally, from the AWP the processing time is reduced by about 10% which is comparable to state-of-the-art technologies.

A wearable sEMG Pattern-Recognition Integrated Interface Embedding Analog Wavelet Preprocess was proposed and its accuracy, processing time and low power consumption were experimentally verified with a flexible and wearable prototype module. Tests with three subjects were performed for pattern recognition of five hand gestures in real-time. The saved time was about 10% of the total processing time with a high accuracy of 96% and power consumption was about 66 mW in the prototype. The system was optimized from the circuit level to the neural network application level. The proposed method could contribute to the commercialization of an artificial neural network applied to wearable devices and replace conventional simple non wearable sEMG prototypes or conventional steady state

ULSAN NATIONAL INSTITUTE OF SCIENCE AND TECHNOLOGY

sEMG analysis devices.

Table Ⅰ
PERFORMANCE SUMMARY AND COMPARISON WITH OTHER RECENT WORK

	This work	[14]	[15]	[16]
year	**2019**	2015	2017	2017
Process [nm]	**180**	x	x	x
Application	**EMG**	EMG	EMG	EMG
Supply Voltage [V]	**1.8/3.3**	3.3	3.7	3.7
Power consumption [mW]	**66**	86	100.6	44
# of electrode channel	**2**	4-8	4	2
#of gestures	**5**	4-7	10	16
Gesture set	**Finger**	Hand Gesture	Trackpad	Finger/Trackpad
Accuracy [%]	**96**	90	94	96
Saved processing time [%]	**10%**	x	x	x

ULSAN NATIONAL INSTITUTE OF SCIENCE AND TECHNOLOGY

3.2. Gas sensor interfacing ROIC control and gas pattern recognition architecture

This section presents 2 preliminary research results about multi gas sensor pattern recognition monitoring platform. The first one is a gas sensor pattern recognition platform like the bio signal acquisition wearable model [6]. It is composed with a control of the ROIC which is at the front-end of the gas sensor to acquire gas sensor data and after sending via Bluetooth to the PC, MATLAB receive in real time gas sensor data and recognize the gas type and concentration. Gases used in this work are CO, CH_4, SO_2 and H_2. The second one presents a gas sensor monitoring platform where similarly acquire gas sensor data and process the data in the MCU side it is an edge processing method. The edge computing method process in the device level the pattern and send the data to the server the result of the pattern recognition via TCP/IP protocol.

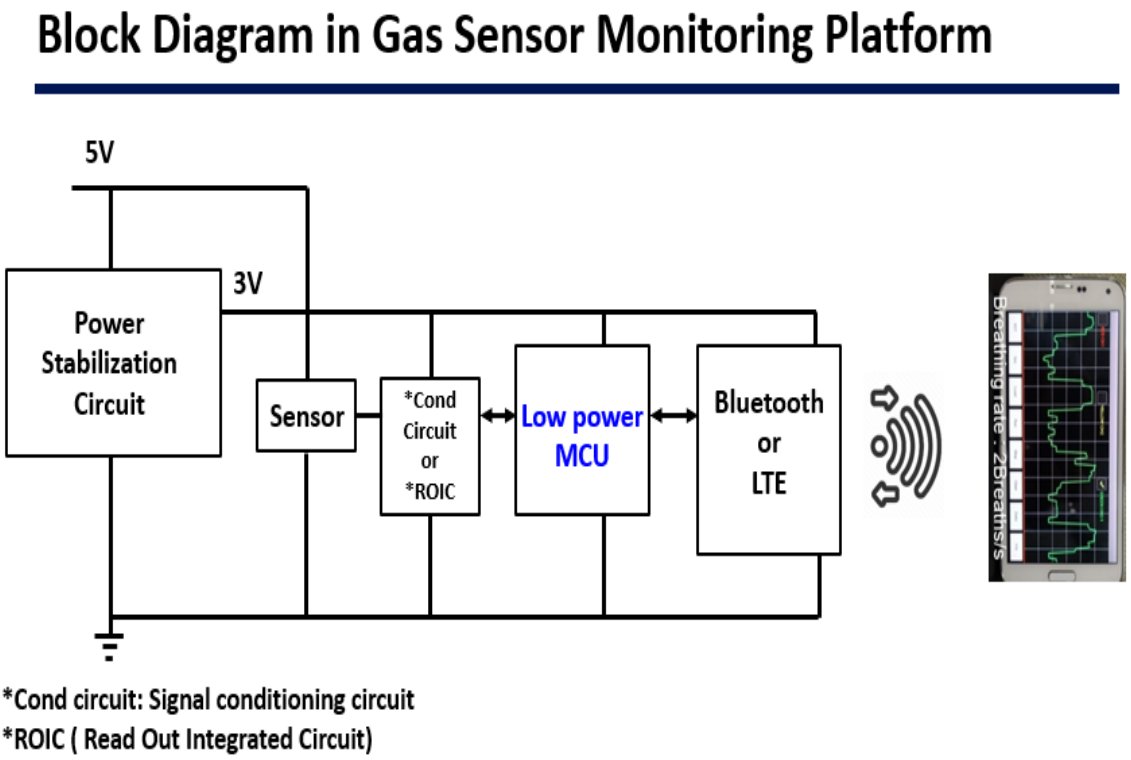

Figure 3.12. hardware implementation of gas sensor module.

Figure 3.12 presents how the gas sensor module is implemented in a hardware side. The hardware side is designed compactly with a gas sensor interfacing circuit implemented inside the ROIC. This ROIC has an additional calibration circuit implemented to reduce sensor sample variation of the gas sensor. Then, after acquiring gas sensor data, the data is sent via Bluetooth to monitor gas sensor data with

ULSAN NATIONAL INSTITUTE OF SCIENCE AND TECHNOLOGY

MATLAB or android application. The composition of the ROIC is presented in figure 3.13. The ROIC is composed at the front-end of the sensor to have a resistance to voltage converter because sensor express the gas concentration and in the ROIC before to be converted to the digital value, the resistance value of the sensor needs to be converted to the voltage. Before converting this sensor resistance value to the voltage, specific voltage can be set up in the resistance to voltage change block to manipulate the base line value when sensor has an offset. After converting and calibrating if needed, the voltage value can be amplified and at this step, if the slope of the gas reaction is not close to the ideal value this difference also can be calibrated before to be sent to the ADC. Finally, ADC convert this calibrated sensor data and send to the MCU via SPI communication protocol to process sensor data.

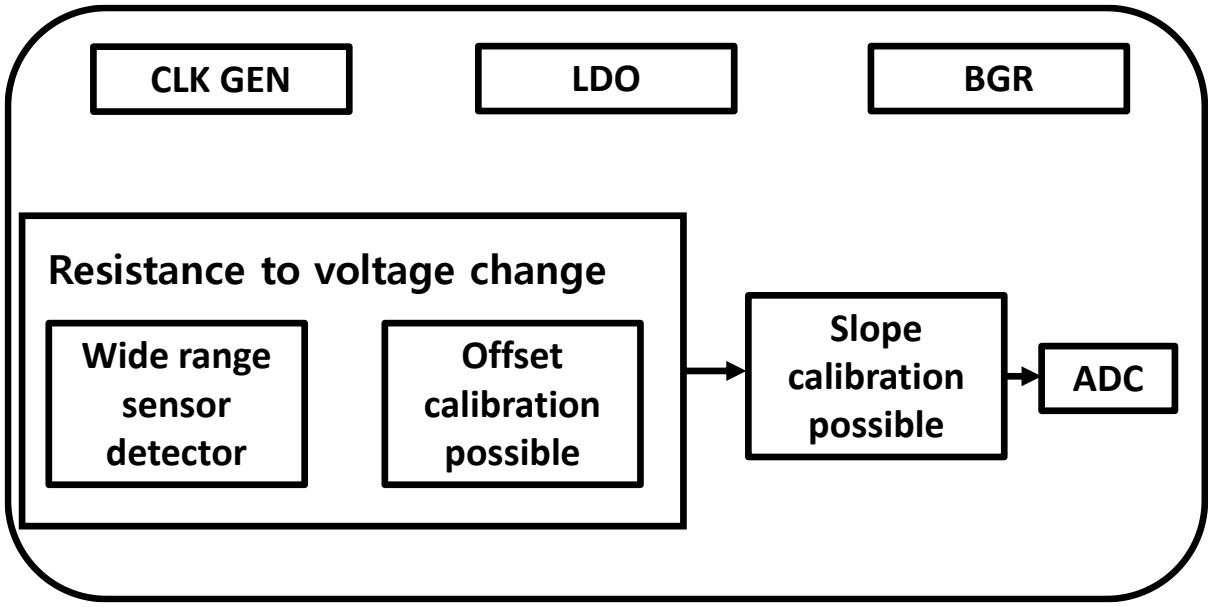

Figure 3.13. Multimode multichannel gas sensor interfacing ROIC structure.

After receiving, the data from the ROIC, the MCU send the data like previous preliminary research result, date are sent to the MATLAB in PC environment and data are analyzed. Figure 3.13 presents the software side which process the gas sensor data transmitted. Before operating in a real time data acquisition and processing mode, the AI model need to be pre-trained depending on the sensor type a preprocessing step is required. For the low-cost gas sensor platform, a PCA processing method was applied to reduce dimension and separate different gas type which were not separate correctly with the raw data. After applying PCA, useful feature can be extracted and with that feature training the AI for the gas pattern recognition. After pre-training the network, it is saved to be loaded in a real time data acquisition model.

ULSAN NATIONAL INSTITUTE OF
SCIENCE AND TECHNOLOGY

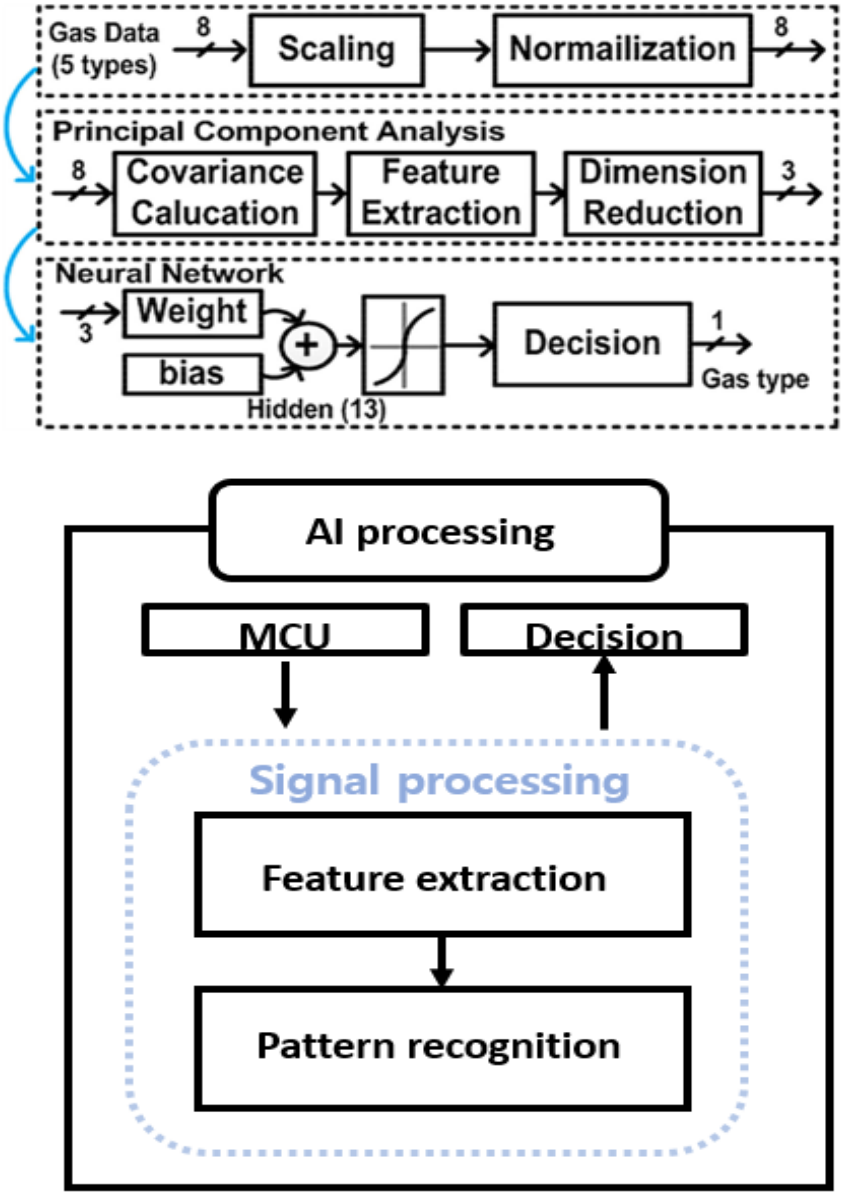

Figure 3.14. Signal processing structure

The final step is to monitor gas pattern and calibrate to a specific concentration. In this step first, the sensor module send data to the server (PC) and for one dataset 3 times communication is needed. Because of the 12 bits resolutions of the data, the limit of 1 transmission can only send 8bits of data. Receiving the second data, the total data is reconstructed and like the pre-training step, this reconstructed data is preprocessed and finally feed to the pretrained network. Conventional gas sensor module was verified and figure 3.14 represents the results of the platform. This platform still has several problems. First, to train the AI model, all the raw data need to be collected it consumes a lots of communication resources. Second, this training is done for a specific experiment condition it is not generalized. Feeding another similar dataset should have a big standard deviation. In order to reduce

ULSAN NATIONAL INSTITUTE OF
SCIENCE AND TECHNOLOGY

the standard deviation, other similar experimental data need to be collected and retrain the AI entirely to make new data in consideration. More this step is repeated more the training time increase. Thus the continual learning scheme presented in chapter 2 will be well suited to prevents such problems. Another, issue in this study exist it is about the efficiency about the processing structure. The Ai processing is performed in the server side. To augment the efficiency for the communication time and application time of the gas sensor pattern recognition monitoring system, the edge computing structure will be more efficient for gas monitoring system. Thus, the next preliminary research adopt this edge computing structure.

ULSAN NATIONAL INSTITUTE OF SCIENCE AND TECHNOLOGY

3.3. Gas sensor interfacing ROIC control and edge computing

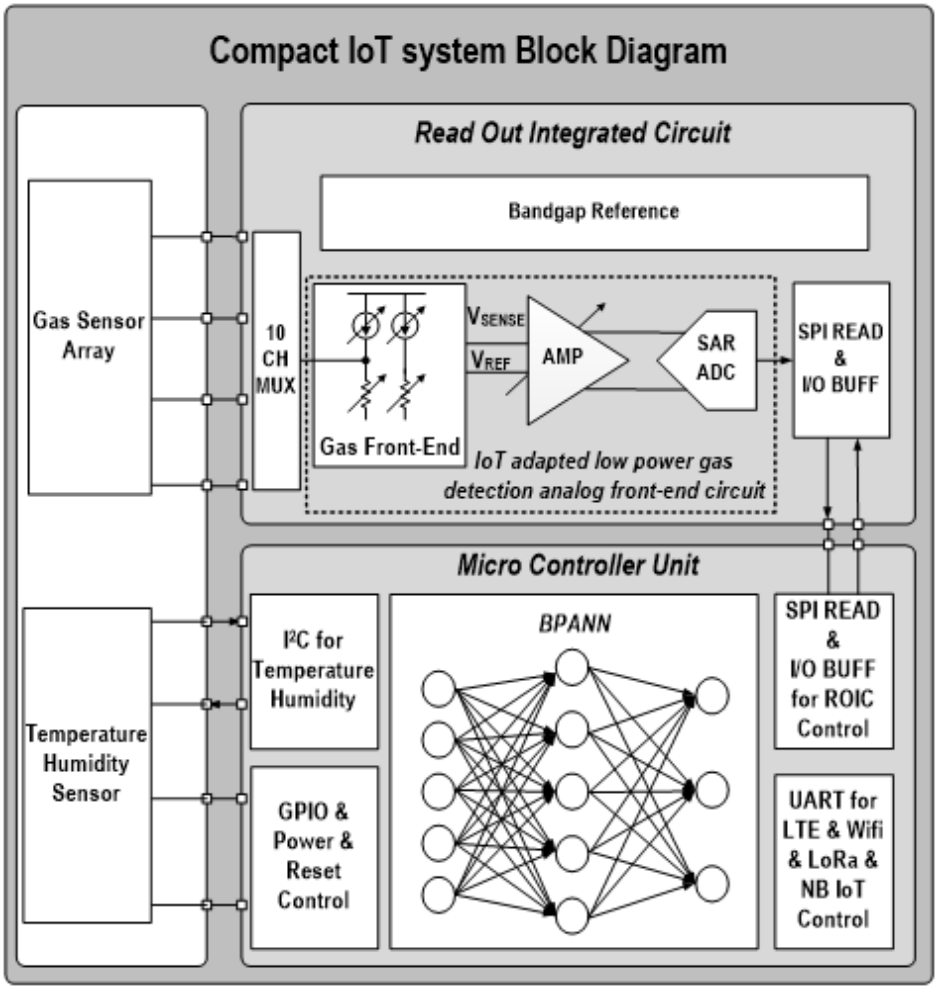

Figure 3.15 overall system architecture block diagram of edge IoT gas sensor system.

The IoT and edge computing technology has been strongly developed in the last decade to monitor and process sensor node information. Consequently, designing an IoT based gas sensor device is actively studied also to prevent severe accidents. On the other hand, for the efficient design of the gas sensor device, a ROIC development to process analogue signal, to reduce power consumption and to make device compact has proved its efficiency. Combining these two technologies can be a good strategy to design an efficient gas sensor device.

Previous study for the edge computing shows that using a small single board computer gives a good performance of pattern recognition. But the power consumption becomes important and designing a battery powered based device can be a challenge. Other edge processing is performed on the low power resource constraint device. It trains first the AI model in PC and transfer the weight result in a microcontroller unit due to their limited memory. In this case, if a situation when retraining the model

ULSAN NATIONAL INSTITUTE OF SCIENCE AND TECHNOLOGY

for the pattern recognition is needed, the device must be retrained in the desktop environment. Considering the aging factor of the low-cost gas sensor, the possibility of retraining the device need to be considered.

This preliminary research proposes an IoT edge processing device embedding a Back Propagation Artificial Neural Network model and a ROIC designed in a 180 nm CMOS process. The ROIC process and calibrates first analogue sensor's signal and Back Propagation Artificial Neural Network model is used to recognized pattern of gas leakage using 10 types of low-cost gas sensor. The performance of the pattern recognition reaches about 92% in the control environment. Also, with the monitoring system, the edge device has collected 14 months of gas data. The overall system architecture block diagram of IoT gas sensor system is presented in figure 3.15. Here, the sensor used to detect gas were the MQ series gas sensor. First, sensors signals are read by the ROIC and in the front end, a multiplexer is present to receive multiple channels of MOS type gas sensor selectively. When the gas sensor reacts to the target gas, the resistance of the sensor changes. This fact is considered inside the ROIC with an RDAC first. The role of the RDAC is to set an equal resistance to the sensor resistance and then read this resistance value.

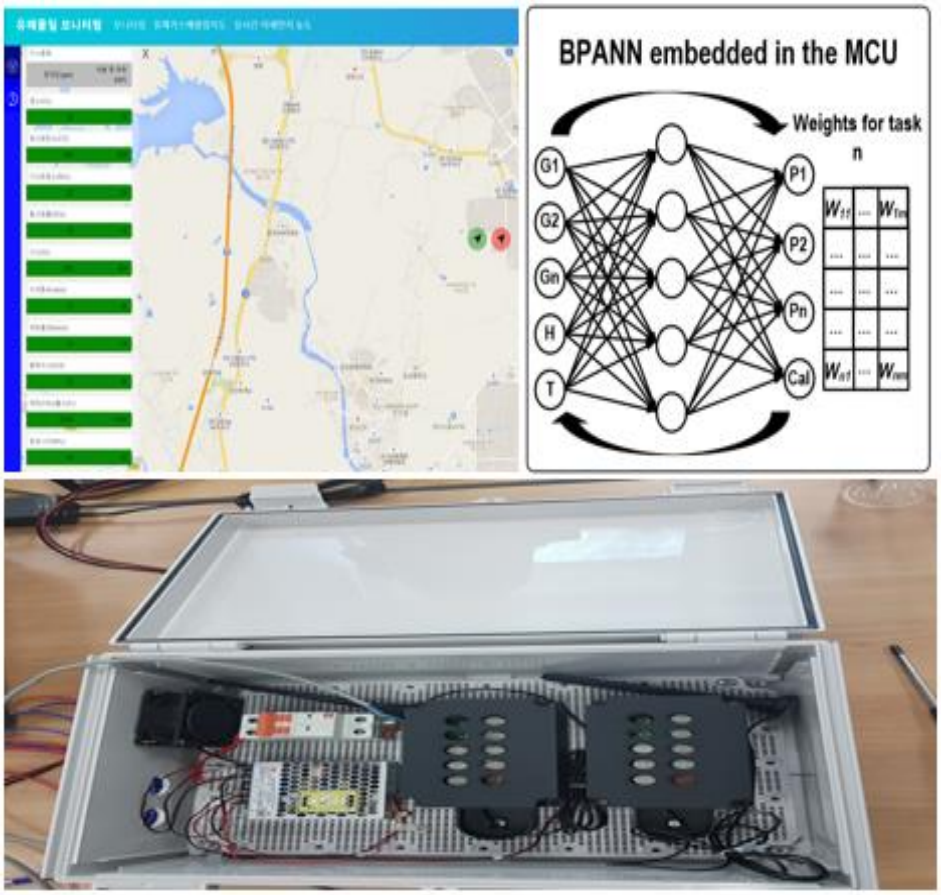

Figure 3.16 IoT based edge processing gas sensor device prototype and monitoring system.

ULSAN NATIONAL INSTITUTE OF SCIENCE AND TECHNOLOGY

After setting the resistance matched to the sensor, this value is sent to the Micro Controller Unit (MCU). To consider the error happening in this process, a correlate double sampling circuit is present at the back end to amplify error information and then send to the ADC. Finally, in the MCU both information about the resistance and the error is considered to get the sensor resistance value.

When collecting the information, sampling time is controlled by the MCU and if the MCU is in the training mode, with the general purpose of input output (GPIO), the target class are set for the supervised training mode. If the MCU is in the application mode, the result of the pattern recognition is sent with the sensor data to the server with the LTE module.

Figure 3.16 shows the developed prototype and the monitoring system of the IoT edge processing device for gas pattern recognition. The structure of the MLP implemented inside the device will be explained in detail. The input layer is composed with 12 nodes where 10 nodes are attributed to each gas sensor channel and 2 nodes are attributed for the temperature and humidity sensor. The hidden layer is composed with one layer and for the computational unity 20 nodes are attributed. Finally, the output is composed with 10 nodes which are the pattern of the gas to be determined.

The activation function is selected as a sigmoid function. A control logic is implemented to get the sensor signal from the ROIC chip. First, the device is placed in a chamber with a mass flow controller (MFC) to control the gas flow. Accurate concentration of gas is injected in the chamber and gas sensor react to the gas. The channel of the ROIC is selected successively to read all the sensor's value and then the sensor's resistance information is obtained. After that, the temperature and the humidity value are obtained from the commercial sensor. This information is organized in the matrix, and it is used to train the MLP. After training the MLP the model is pruned to save memory in the MCU, the pruning process is to suppress small value of weights. After suppressing small value of weights, the accuracy drops downs. To compensate this drop of accuracy important weights position are memorized and the network is retrained to compensate the loss of accuracy by pruning. Finally, an LTE module is controlled to send data wirelessly to the server and the gas data is display on the website.

These preliminary research result shows that the circuit and processing research for gas sensor system is becoming compact. Several proposed pre-calibrations with a circuit design for the analogue sensor signal augment the processing efficiency while the processing capability moved from the PC to the edge sensor node. This state of the art of the intelligent gas sensor system shows the future research direction which is a compact battery powered gas sensor device design need to be considered for a long life run after installation in the field. For this purpose, the power consumption of the processor needs to be considered because it consumes most of the power of the device. But generally low power DSP has a low memory.

Also, the signal processing capability of gas pattern recognition should cover as much as possible the irregularity of the gas sensor data. In this context, to overcome such challenges and limitation, this paper

ULSAN NATIONAL INSTITUTE OF
SCIENCE AND TECHNOLOGY

proposes a simple and efficient approach to be able to adapt to the irregularity of gas sensor data using a continual learning scheme with a low power Cortex-M4 DSP processor.

Recently, instead of collecting big data before training a classical AI model, Continual learning scheme which is able to accumulate new knowledge to the previous trained knowledge is receiving many attentions. It is well suited to the gas sensor system where data is strongly depending on the environmental factor and need to be learned for different situation consecutively.

Fitting this continual learning scheme specifically to the intelligent gas sensor system is a main proposition of this thesis.

ULSAN NATIONAL INSTITUTE OF SCIENCE AND TECHNOLOGY

Chapter IV

Implementation of Environment adaptable IoT Edge gas sensor device embedding analog supported continual learning scheme for pattern recognition

4.1. Background of proposed analog supported continual learning scheme

This section presents a background of the implementation of multi-gas sensor monitoring platform that has an optimized system structure for edge computing in internet of things (IoT) environments. Considering the environmental factors presented in previous sections that affect sensor device characteristics, a proposed analog-assisted continual learning scheme is embedded into the sensor edge device to enable a real-time sensor calibration and pattern recognition (PR). A designed readout integrated circuit (ROIC) for automatic calibration and analog-assisted normalization minimizes sample variations in sensor devices, which relieves the computational burden for PR to achieve the sensor selectivity. A mask-based continual learning (MBCL) structure is proposed to be compactly integrated into the edge device, providing environment-adaptable edge-computing functionality to the system. For functional feasibility, an edge-computing IoT device with a fabricated ROIC and a manufactured in-house semiconductor sensor array, supporting wireless on-site monitoring platform interfaces. The proposed environment-adaptable edge-computing capability is functionally verified through continually learned PR experiments on hazardous gases such as NO2 and CO under environmental factor variations in temperature and humidity. An average PR accuracy of 97% is achieved on several kinds of mixture gas patterns. The analog-assisted operation reduces the training cycles by 3 times, and the MBCL itself achieves an efficiency that is 25% better than conventional continual learning methods.

To address previous challenges and limitations presented in previous section with an optimized IoT system, this section proposes a simple and efficient novel edge-computing structure where a mask-based continual learning (MBCL) scheme is implemented in the micro-controller unit (MCU), that is, at the edge of the device. For its adaptive selectivity, masking weights connected to the specific nodes of the previously trained network is proposed. Thus, this method can prevent serious processing confusion when learning new patterns for its environment adaptability. For its reliability, a readout

ULSAN NATIONAL INSTITUTE OF SCIENCE AND TECHNOLOGY

integrated circuit (ROIC) with an analog-assisted calibration and normalization scheme is designed to reduce sensor sample variation and to enhance MBCL's training performance. The analog calibration and normalization ROIC pre-processes unstable gas sensor data. Then, these data are delivered to the MBCL model for training. Also, to provide wide range coverage, the ROIC is designed to be optimally controllable to interface with a wide range of sensors. Finally, for quantitative analysis, multiple linear regression is implemented to estimate the gas concentration. A wireless communication module is included to send data to a remote monitoring system, and the environmental gas PR system is functionally verified to recognize the pattern of individual NO2 and CO gases and their mixture patterns. In-house gas sensors composed of SnO2 to enhance selectivity performance are also manufactured in this work.

The motivation of the proposed work is to design a temperature and humidity robust IoT low-cost gas sensor device which can recognize gas pattern adaptively to the different environment. According to numerous previous studies [20], [21], [22], the temperature and the humidity effect are considered important when measuring a low-cost semiconductor type gas sensor signal.

Therefore, after acquiring gas sensor signal influenced by the temperature and humidity effect, processing for resolving the selectivity issue about the low-cost gas sensor can be performed only in the given temperature and humidity condition. This make the solution to the selectivity problem of the low-cost gas sensor in a narrow condition. Thus, for its adaptability to the environment condition, an adoption of a simple artificial intelligence (AI) based algorithm becomes more and more costly when retraining new coming gas sensor data influenced by new temperature and humidity condition. Other critical effects such as poisoning, aging effects are also important, but this proposed work concentrates to make robust the gas sensor system to the temperature and humidity effect when finding the gas type.

For the motivation to design a temperature and humidity robust adaptable gas sensor system, the first challenge comes from resolving the processing of a selectivity problem for a narrow condition. This challenge can be resolved adopting a continual learning based artificial intelligence (AI) method. The contribution is not about simply adopting a Compact Picking Growing (CPG) scheme which is well suited for an additional and adaptable learning capability. Its advantage is to learn additionally without forgetting. However, the fact that it doesn't forget previous learned pattern, this can bring a confusion in a gas sensor system. Adopting simply the CPG sharing the input node and increase only the hidden layer when new data is arrived can bring a processing confusion presented in the figure bellow.

ULSAN NATIONAL INSTITUTE OF SCIENCE AND TECHNOLOGY

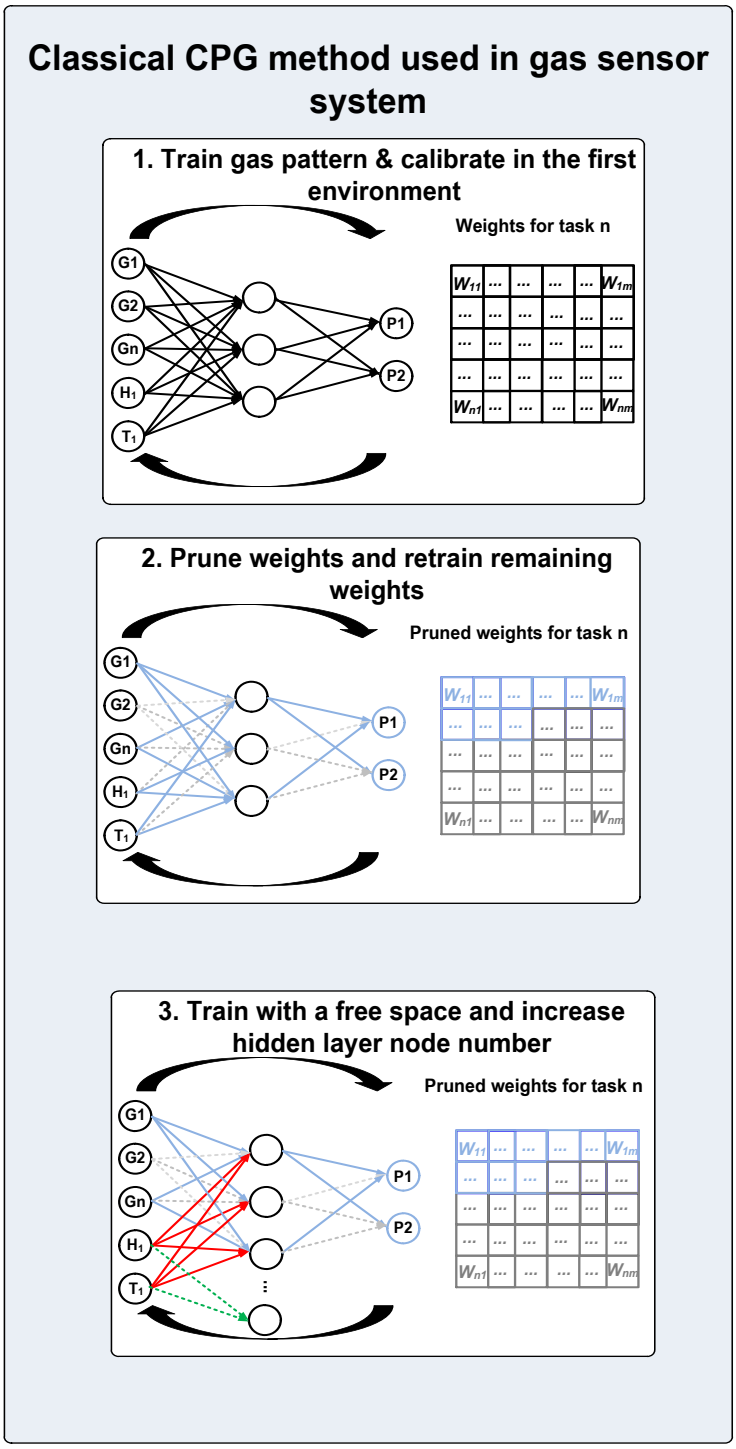

4.1 Possible confusion using classical mask based continual learning scheme

In this case, in the first step, weights connected to the temperature and humidity will be fitted to the first environment's temperature and humidity condition (red line). Thus, in the second and nth

ULSAN NATIONAL INSTITUTE OF SCIENCE AND TECHNOLOGY

environment (Green line), these weights will strongly constraint to learn a possible opposite gas sensor data with the same temperature and humidity condition. This can happen because of the presence of the different mixture of gas or other environment affectable issues. Thus, the growing network could not learn the opposite data with a wanted accuracy. Therefore, to cut this dependency, additional independent nodes is added and make the network self-organize to the changing environment. This simple method will:

- Make the sensor data system independent to the temperature and humidity influence in different environment.
- Consume less memory (increasement of hidden layer node numbers) to learn in a different environment compared to the classical approach.
- Achieve wanted accuracy in a different environment (without the dependency of previous environment).

In the gas sensor system, for its adaptability and additionally learning capability the consideration about these three factors when optimizing the growing and learning structure can be a contribution presented in the figure bellow.

To reinforce this contribution, other challenge comes when acquiring sensor data. The sample variation of the sensor combined with the environmental effect makes the sensor signal variation in a wide range. A calibration method is often adopted as a famous method to reduce this variety of the influence of the environmental factors. As presented before, an AI based processing method will be applied to determine the gas type further in the digital signal processor (DSP) side. Thus, reducing the processing while calibrating the gas sensor signal can provide an efficient result to make the sensor signal stable before processing the data. Previous work related to the calibration was presents in [6]. However, this presented calibration method has only a conceptual design. The optimization to combine with the ANN method is required and in this proposed work, a 2 steps calibration is proposed. Compared to the previous work, an optimization of the calibration block is applied. In the previous work [6] only one comparator is used to calibrate the sensor signal. Thus, the offset and the slope of the sensor reaction was performed at the same time. In this case for a multi-channel application, the control of multi sensor characteristics becomes difficult. The difference is presented in the figure bellow

The base resistance of the sensor is calibrated by programming RDAC with calibration data. And the sensitivity of the sensor is affected by the programmable Data of R-2R DAC with the least significant bit of it is $V_{CM.LSB}$.

The contribution of the proposed circuit part is as follow:

- Wide range of sensor interfacing capability including current and resistance type sensor interface circuit.
- 12 channels sensor interfacing circuit integrated in a 180 nm

ULSAN NATIONAL INSTITUTE OF SCIENCE AND TECHNOLOGY

- Calibrate the sensor sample variation without consuming computing power.
- Detailed 2 steps calibration method with an optimization of presented previous work.

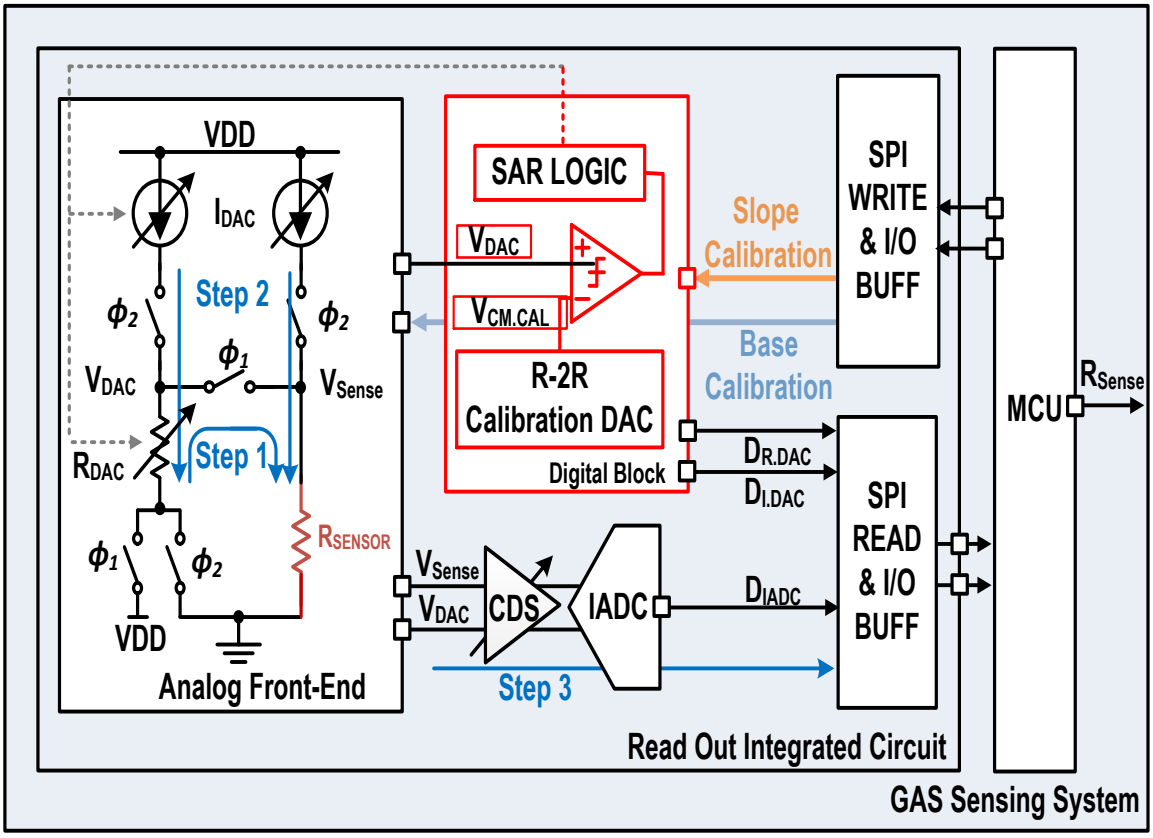

4.2 Calibration ROIC architecture

In order to analyze the mixture of gas qualitatively several backgrounds are needed to be studied. In this proposed work gazes used are a mix of reducing gas (CO) and oxidizing (NO2) gas type. Their chemical characteristic reacting to one sensor have an opposite direction. Thus, the difference in term of sensor signal becomes higher and using a smaller number of sensors can achieve higher accuracy such as presented in the figure bellow.

ULSAN NATIONAL INSTITUTE OF
SCIENCE AND TECHNOLOGY

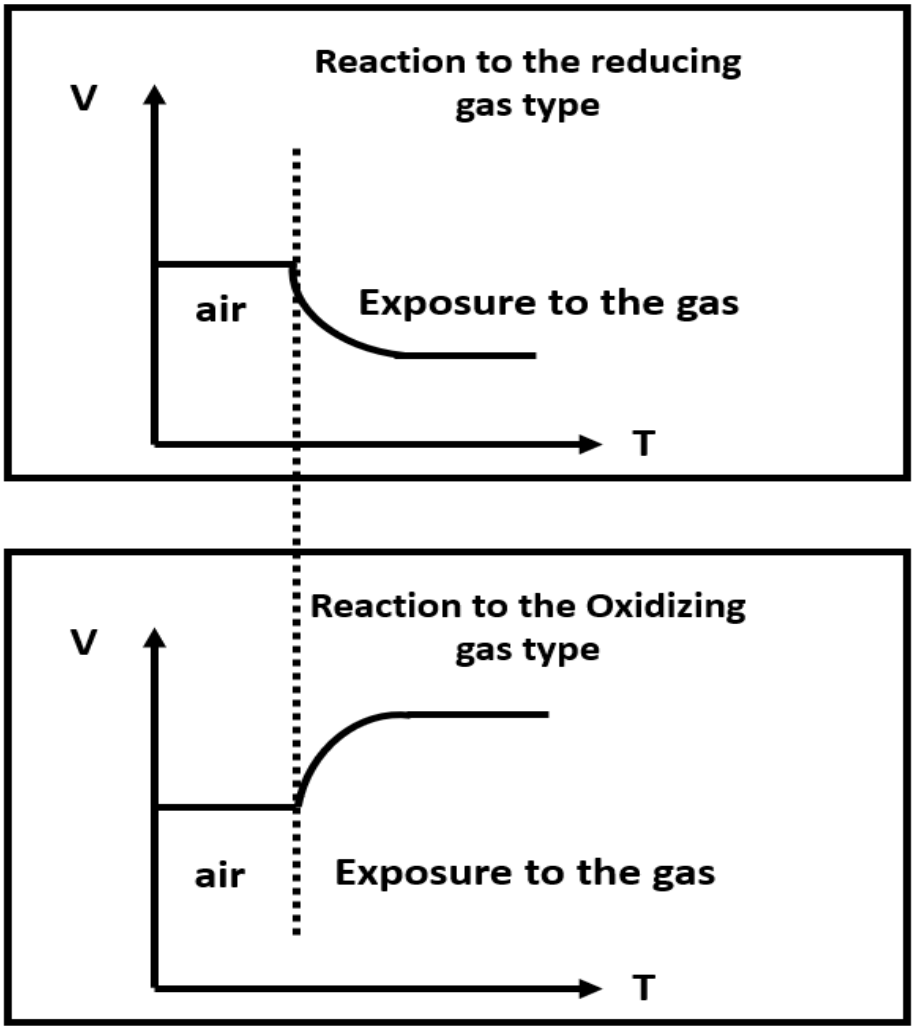

4.3 Sensor reaction direction depending on gas type

ULSAN NATIONAL INSTITUTE OF
SCIENCE AND TECHNOLOGY

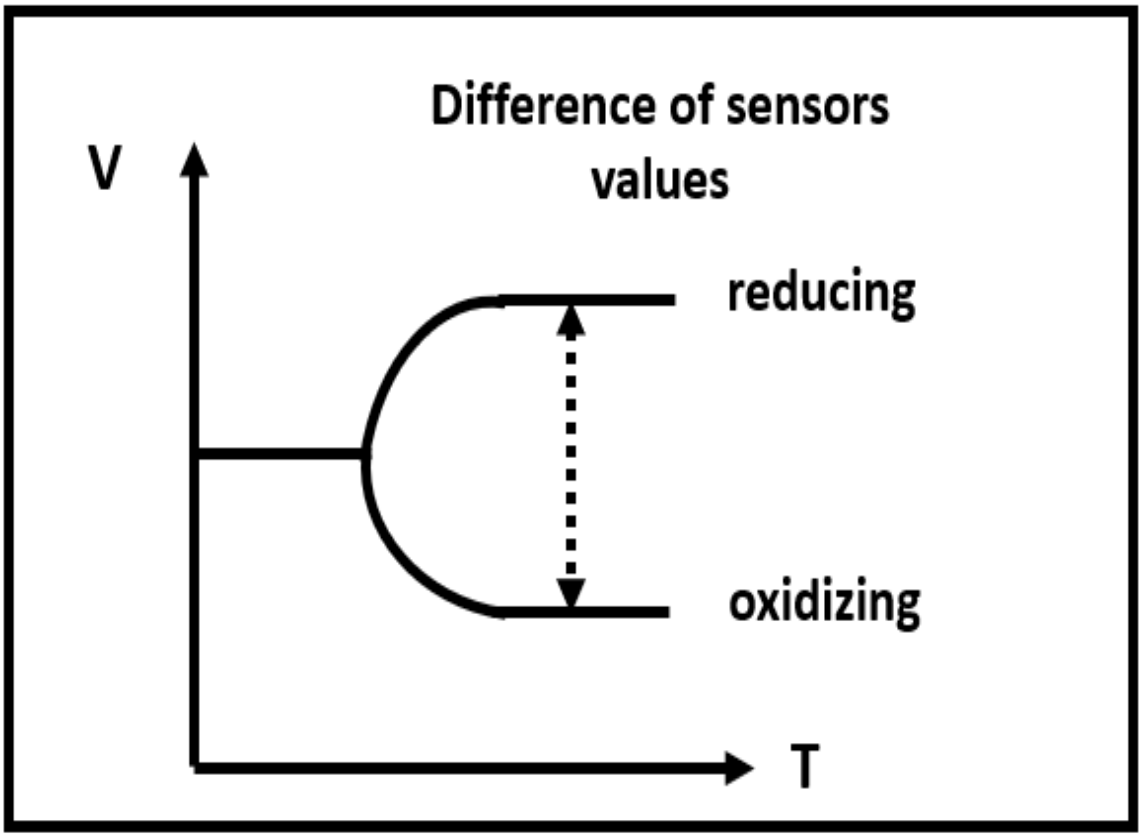

4.4 Sensor reaction direction depending on gas type

Thus, their signal difference enhanced with their opposite activation direction will make easier for any classifier to cluster the gas type or the mixed gas type. In the case of the mixed gas, the recognition accuracy will strongly depend to the ratio of the mixed gas. For example, if in the mixed ratio the dominant gas type is the reducing type, the signal will have a tendency to follow the signal form of the reducing type. Also, the amplitude of the mixed gas will be different from the dominant single gas. Thus, this own signal for each single or mixed gas ratio will make the recognition system to cluster each condition of gas experiment.

Also, using a same active direction gas type can also recognize gas pattern [23]. However, the recognition accuracy will depend on the developed sensing material characteristic. If the developed sensor can separate clearly the reaction between the same active direction gas type, without feature extraction step, the accuracy will stay high. However, if the difference doesn't have enough margin a confusion risk can happens presented in the figure bellow.

In this case, increasing the number of sensors to n+1 or applying feature extraction technic before delivering to the classifier could be a solution to achieve high accuracy [24]. Simple method such as window time slicing (WTS) feature extraction method can be applied to improve the pattern recognition

ULSAN NATIONAL INSTITUTE OF SCIENCE AND TECHNOLOGY

accuracy for the gas type with same active direction [25]. The WTS method can make the (S1-S2) difference to the (S12-S22). Thus, this higher difference can be considered in the classifier training performance.

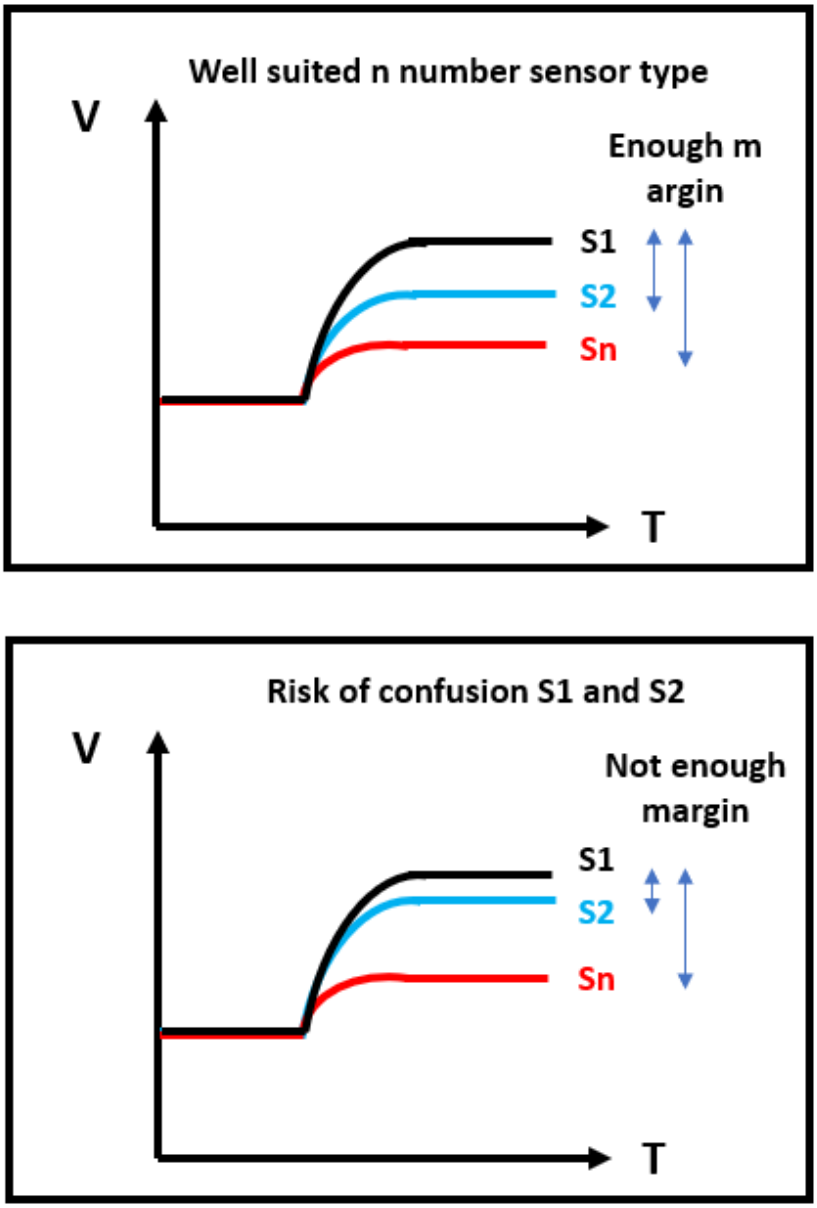

4.5 trade of between signal margin and sensor array numbers

ULSAN NATIONAL INSTITUTE OF
SCIENCE AND TECHNOLOGY

4.2. Overall architecture of Environment adaptable IoT Edge gas sensor device embedding analog supported continual learning scheme for pattern recognition

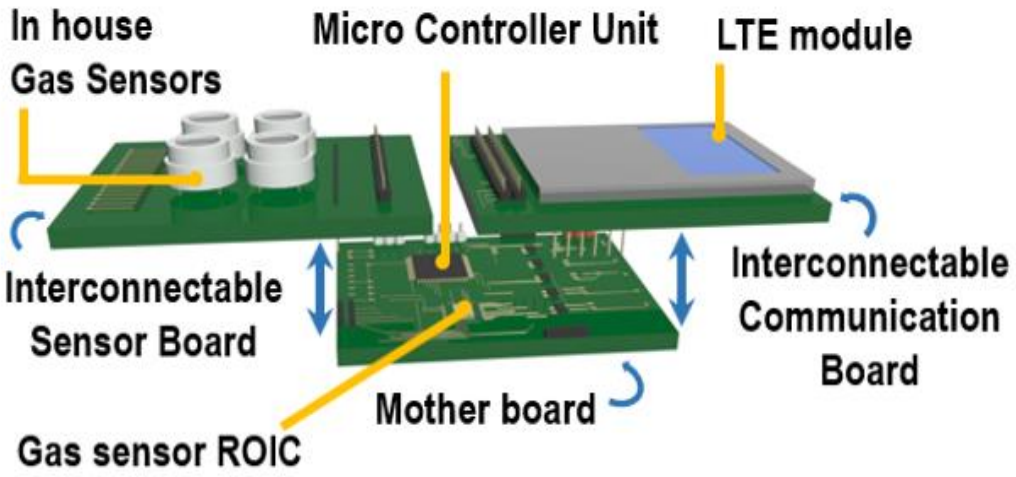

(a)

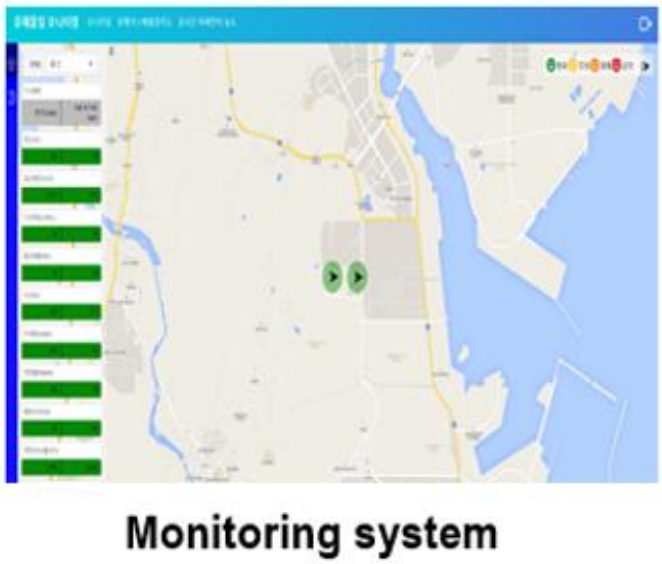

(b)

4.6 Overall composition of monitoring platform (a) device (b) monitoring system

ULSAN NATIONAL INSTITUTE OF SCIENCE AND TECHNOLOGY

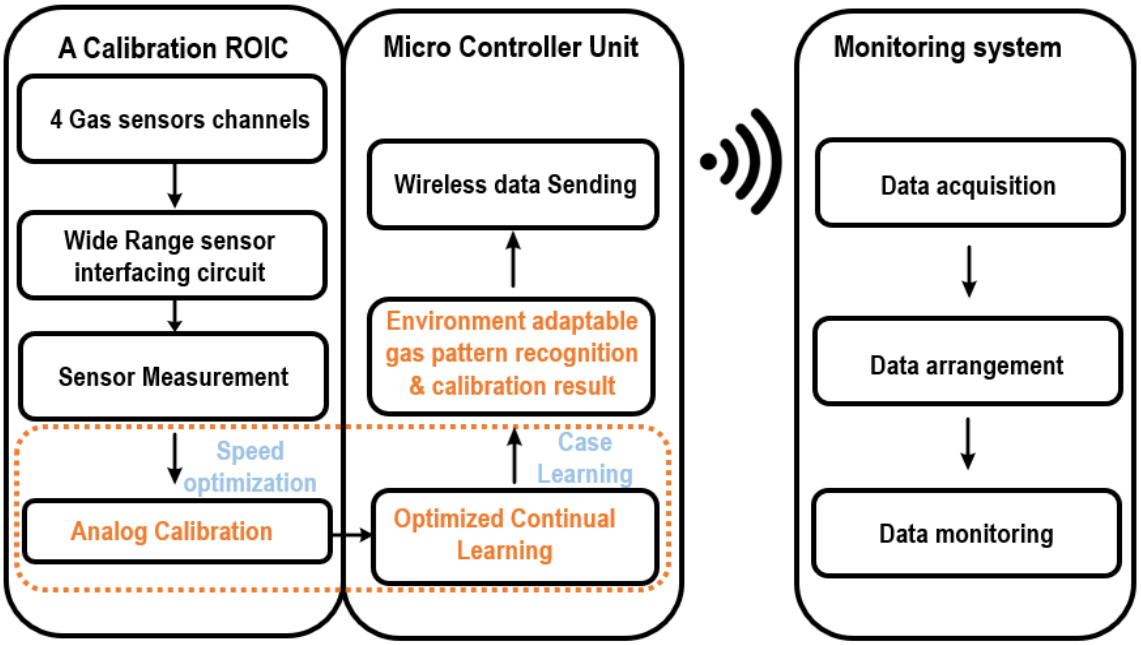

(c)

Figure 4.7 Conceptual architecture of the proposed IoT edge-computing system: (a) edge device structure, (b) remote monitoring system, and (c) component-based functional diagram.

Figure 4.1 presents a conceptual system architecture of a proposed IoT edge-computing device and its remote monitoring system. The edge device consists of an in-house sensor board, a wireless communication module, and a mother board with a designed ROIC and an MCU. For facile replacement of in- house sensors, the sensor board is designed to be detachable, and the communication module is also detachable to support various types of wireless communications, including long-term evolution (LTE), narrowband-IoT (NB-IoT), Wi-Fi, and Bluetooth. Figure 4.1 (c) presents a component-based functional diagram in the proposed IoT system. The ROIC performs a sensor readout operation and provides analog calibration and normalization for the proposed analog-assisted PR. Then, edge-optimized continual learning of the MBCL structure is performed inside the MCU. The corresponding environment-adaptable PR and sensing results are remotely displayed in the monitoring system.

ULSAN NATIONAL INSTITUTE OF SCIENCE AND TECHNOLOGY

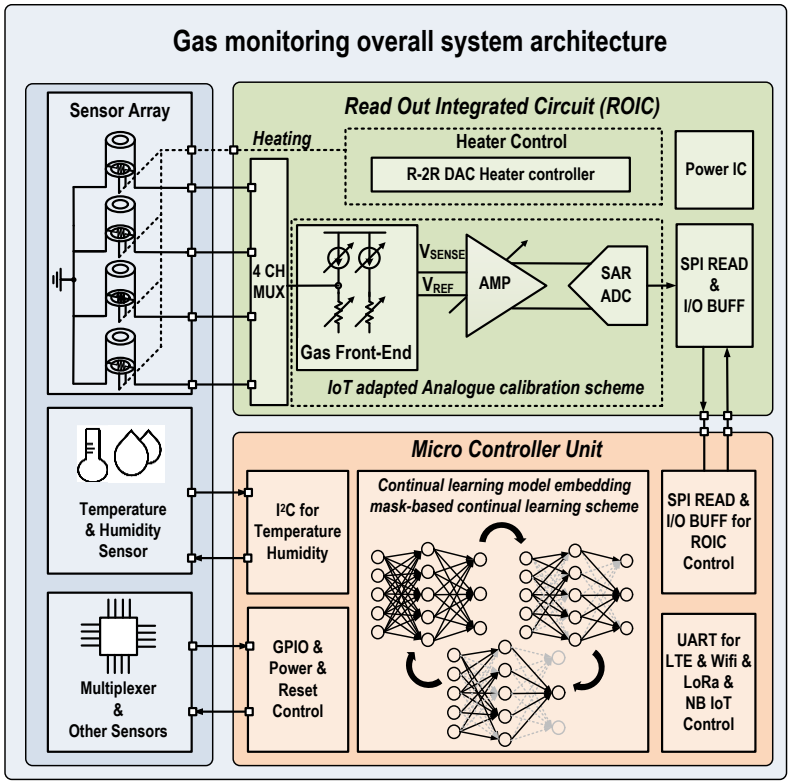

(a)

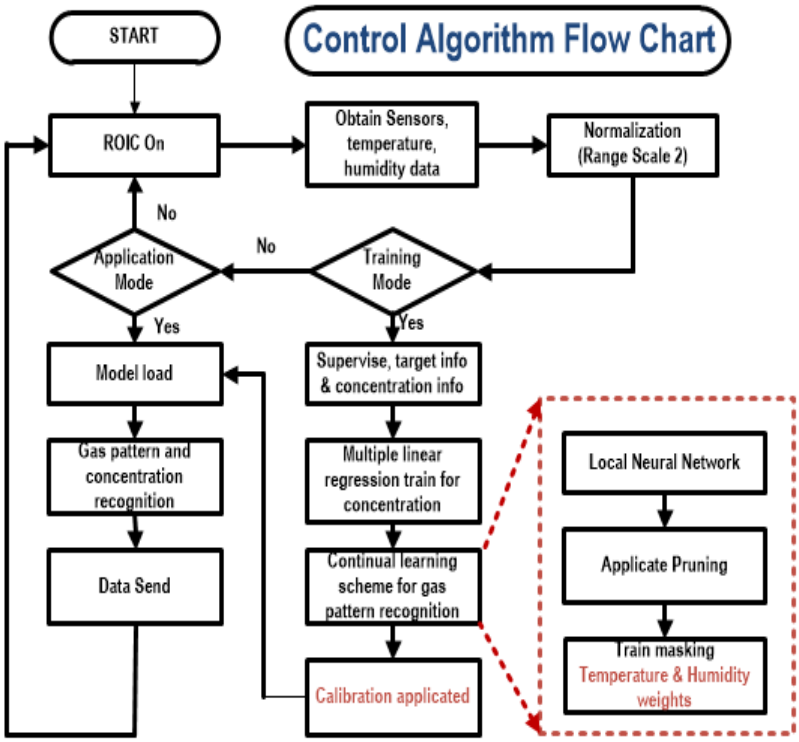

(b)

Figure 4.8 (a) Environment-adaptable IoT edge computing device block diagram. (b) IoT edge computing device control algorithm flow chart.

ULSAN NATIONAL INSTITUTE OF
SCIENCE AND TECHNOLOGY

Figure 4.2 shows a detailed implementation and control flow chart of the proposed edge device supporting environment-adaptable continual learning. This process starts from the acquisition of gas sensor data by activating the ROIC, where the four-channel gas sensor data are consecutively obtained through the multiplexing operation. In the analog front end of the ROIC, correlated double sampling (CDS) zooming [7] is performed to reduce low-frequency noises or offset effects. Then, digital conversion is performed by an internal incremental analog-to-digital converter (IADC), and the corresponding digitized data are transmitted to the MCU via the serial peripheral interface (SPI). For efficient edge-computing implementation inside the MCU, a proposed analog-assisted calibration and normalization scheme is also integrated into the ROIC to minimize the sample variation effects of the sensor devices. The implemented continual learning has two process modes of training and application.

For training-mode operation, temporary environmental information on temperature and humidity are included for the continual learning process. The MBCL is proposed for environmentally adaptable edge-based pattern recognition of gas types, and multilinear regression is utilized to determine the gas concentration. After this training period, the application-mode operation is performed based on the trained model, resulting in a kind of self-calibration under different environmental effects.

ULSAN NATIONAL INSTITUTE OF SCIENCE AND TECHNOLOGY

4.3. Design implementation

4.3.1 Proposed ROIC structure and control

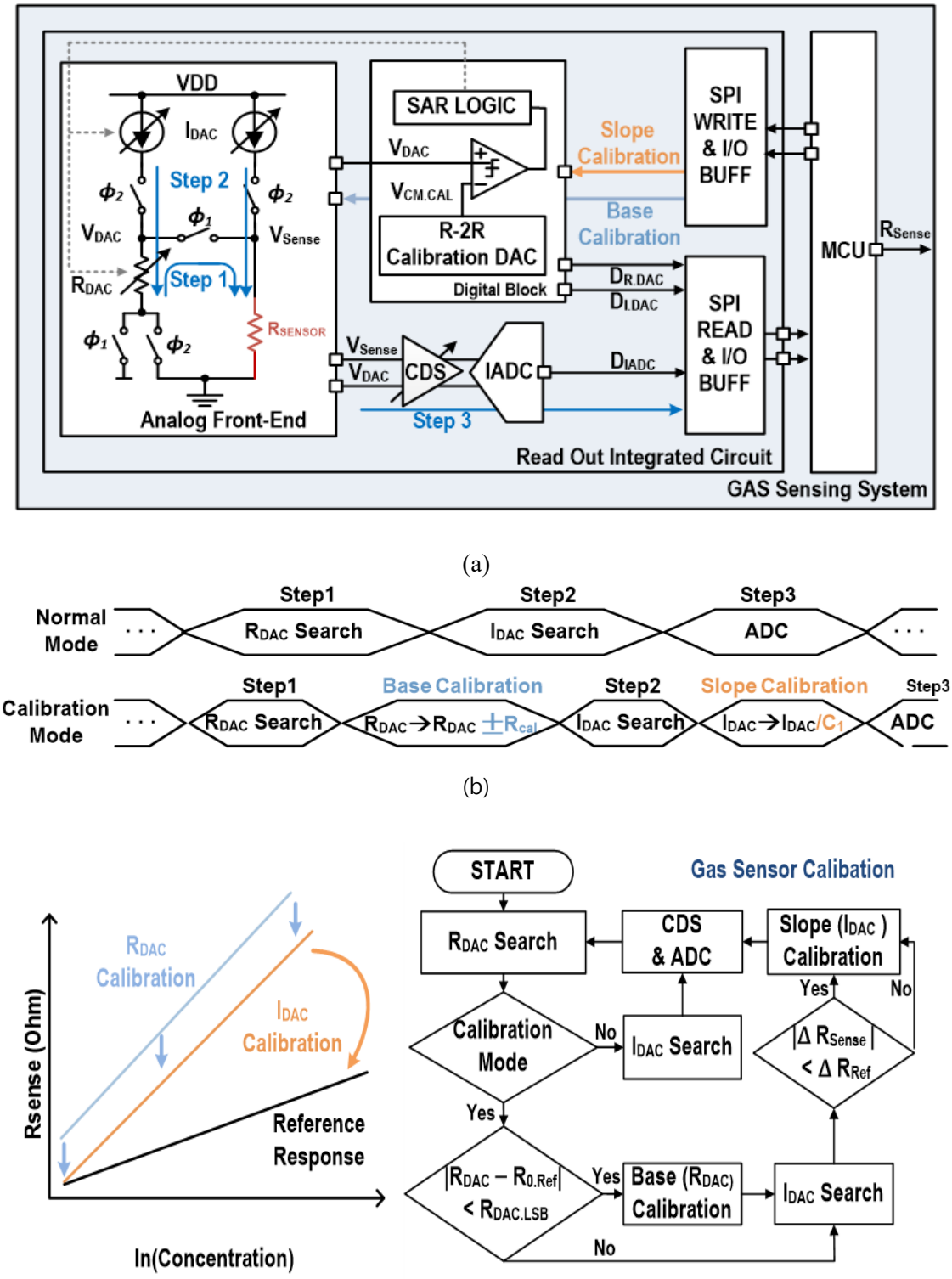

Figure 4.9 (a) Readout integrated circuit (ROIC): (a) simplified ROIC schematic, (b) operation timing diagram, (c) calibrations of base resistance and sensitivity, and (d) operational flow chart.

ULSAN NATIONAL INSTITUTE OF SCIENCE AND TECHNOLOGY

Figure 4.3(a) presents a simplified schematic of the designed ROIC, which consists of an analog front end and an 18-bit sigma-delta IADC. This ROIC includes an analog calibration capability for the base resistance and sensitivity of chemo-resistive sensors, which would contribute to the proposed analog-assisted continual learning operation. Based on the CDS zoom structure, the ROIC supports a wide range of sensor resistances from 40 Ω to 2 M Ω, and additive digital-to-analog converters (DACs) are utilized to reflect calibration and normalization feedbacks from the analog-assisted continual learning process.

The ROIC has two operation modes: normal and calibration modes. In the normal mode, the sensor resistance is detected by the CDS zooming structure in the following three steps. For the first step (Φ1), the bottom side of the resistive DAC (RDAC) is connected to the supply voltage (VDD), and the resistive sensor (RSENSOR) is connected to the RDAC in series, while the other side of the RDAC is tied to the ground (GND). This comprises a resistive divider circuit, and RDAC is controlled to be close to the RSENSOR value through the successive approximation register (SAR) operation, which is a kind of circuit-level binary search scheme. In the second step of normal mode (Φ2), two 8-bit current DACs (IDAC) are activated to enable more accurate detection and to generate a pseudodifferential signal that is more immune to noise, while the bottom node of RDAC is changed from VDD to GND. An optimal value of IDAC is programmed through the SAR operation or binary-searched to locate the output voltage (VDAC) in the middle of VDD and GND. Then, the pseudodifferential output (VOUT = VSENSE - VDAC) is generated, where VDAC is close to the VSENSE value due to the SAR-based binary search operations.

$$V\_Sense-V\_DAC=(R\_Sense-R\_DAC)*I\_DAC=V\_OUT \quad (8)$$

Then, the output VOUT is digitally converted through the following blocks of the CDS amplifier and the IADC. Finally, the sensor resistance is calculated as follows.

$$R\_Sense=V\_OUT/I\_DAC+R\_DAC=(D\_ADC*V\_LSB)/(D\_IDAC*I\_LSB)+D\_RDAC*R\_LSB \quad (9)$$

where DRDAC, DIDAC, and DADC are the digital outputs of RDAC, IDAC, and the IADC. RLSB, ILSB, and VADC are the minimum sensitivity of the target. For this purpose, RDAC needs to be adjusted for the base resistance calibration, and IDAC is adjusted for the sensitivity calibration of the sensor, as shown in figure 4.3(c). The operational flow chart is shown in figure 4.3(d). The base resistance calibration is performed by adjusting the RDAC. If the adjusted amount is less than the minimum adjustable resistance RDAC.LSB, it is bypassed. Then, IDAC is programmed as in step 2 of

ULSAN NATIONAL INSTITUTE OF
SCIENCE AND TECHNOLOGY

normal mode. Next, for the slope calibration, IDAC is adjusted to fit the reference response. The IDAC calibration is performed by programming an R-2R calibration DAC, the result of which is reflected in its SAR operation. In this way, the calibration mode ensures the consistency of each sensor against environmental variations.

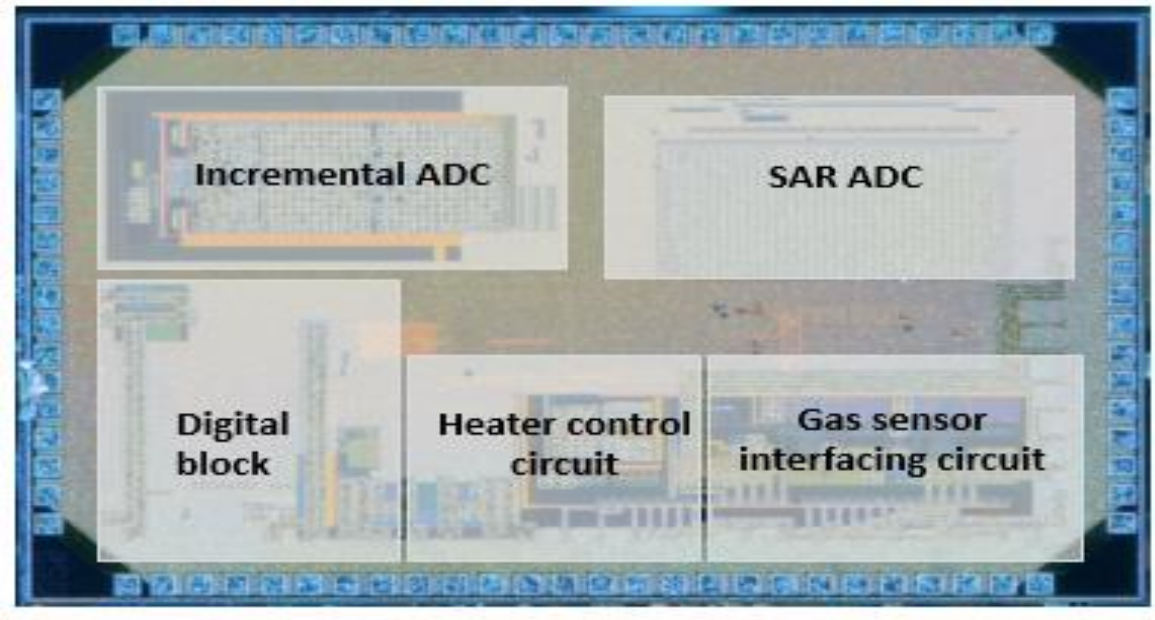

(a)

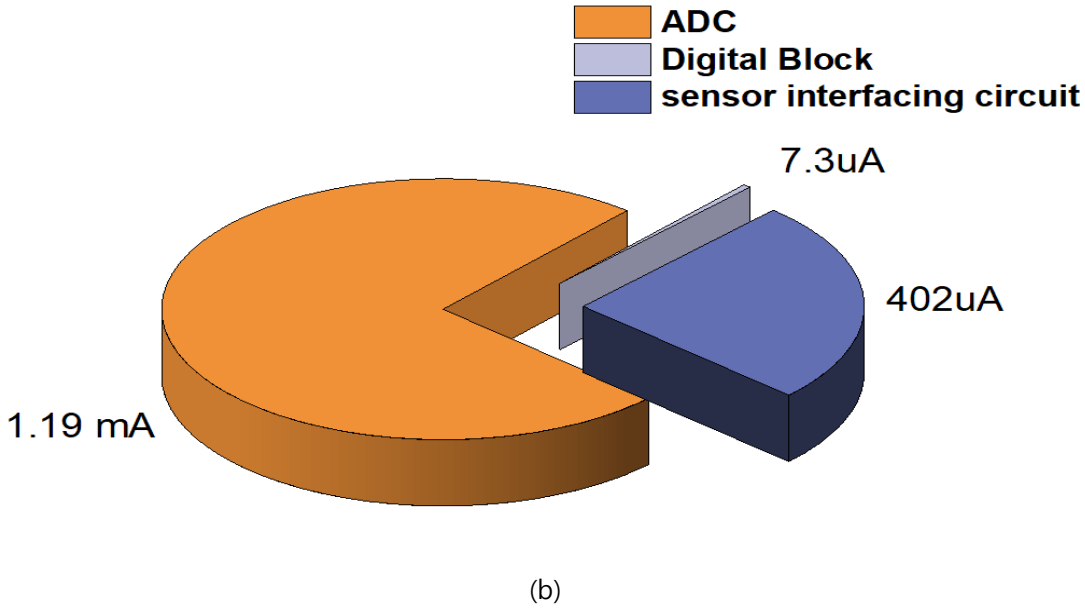

(b)

Figure 4.10 (a) ROIC microphotograph and (b) power consumption breakdown chart.

The designed ROIC was fabricated through a 0.18-μm complementary metal-oxide semiconductor

ULSAN NATIONAL INSTITUTE OF
SCIENCE AND TECHNOLOGY

(CMOS) process. Figure 4.4(a) shows the chip microphotograph, whose core area is 2 mm x 2 mm. The current consumption under a 3.3-V supply voltage is 3 mA, and its power breakdown is shown in Figure 4.4(b).

ULSAN NATIONAL INSTITUTE OF SCIENCE AND TECHNOLOGY

4.3.2 Proposed Mask based continual learning scheme design

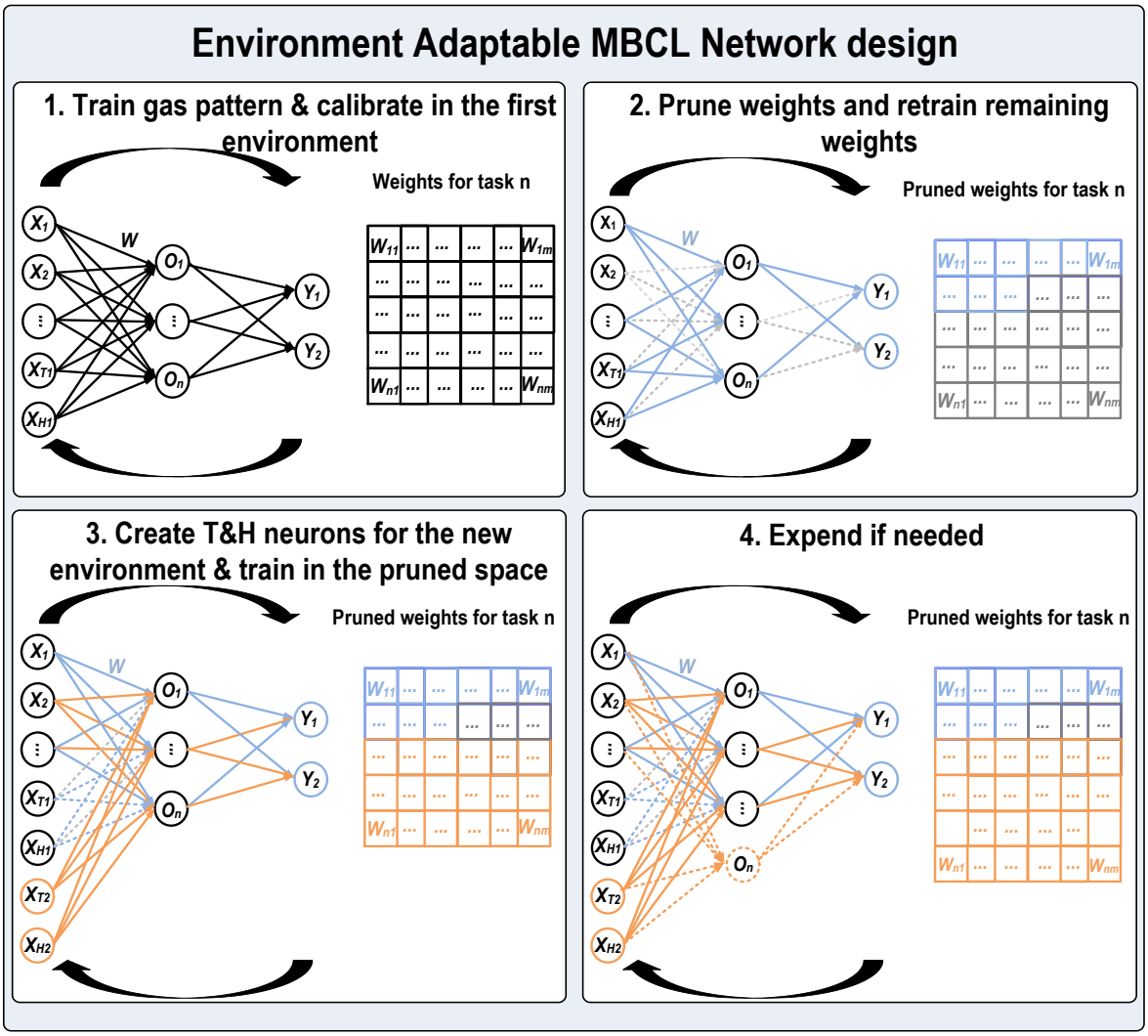

Figure 4.11 Illustration of the MBCL algorithm implemented in a resource constraint MCU.

Figure 4.5 shows the simplified MBCL algorithm implemented in the IoT edge-computing device. Classical approaches with the same training operation as the MBCL have included progressive neural networks, PackNet and Compact Picking and Growing networks CPG. These training methods start in common from step 1 presented in figure 4.5. The classical artificial neural network (ANN) is trained first. In the case of a progressive neural network, the second step to learn a new pattern is to expand the hidden-layer node number when a new pattern arrives. Thus, expanding the hidden-layer node number allows new weights to be created that can learn new patterns. However, the increased number of hidden-layer nodes is not incrementally performed, but a set of nodes is increased. In this case, the learning

ULSAN NATIONAL INSTITUTE OF
SCIENCE AND TECHNOLOGY

method becomes difficult to implement in an edge-computing device that has limited memory. In the case of PackNet, as in the second step presented in figure 4.5, a pruning step is applied to remove relatively small value weights.

After this step, the overall accuracy drops even if the removed weights are small because they participate in a multiplication operation. To compensate for this drop, the pruned single network is retrained with a remaining critical weight and the accuracy is recovered. Then, training a new pattern in the pruned space allows the single network to compactly learn multiple patterns. However, without the expansion of the hidden layer node, the learnable new patterns are limited. Merging these previously presented learning methods, CPG designed a compact pruned and growing network to continuously learn new patterns without forgetting previously trained patterns. However, the capability of not forgetting the previous pattern can disturb the new learning process for the scenario when opposite data reveal the same pattern learned in the previous network. In the case of the gas PR, the temperature and humidity influence often cause the same data to express other results. Thus, from step 3 presented in figure 4.5, a method for masking the previous trained weights connected to the temperature and humidity nodes and creating new temperature and humidity nodes to learn new patterns in different environments is proposed. Finally, in the last step, if the target accuracy is not achieved, the hidden-layer node number is incrementally increased. The Xn presented in the figure are the input data XT1, XH1 represents the temperature and humidity data in environment 1, On represents the transfer function applied result, Yn the result and Wi the weights. This MBCL is implemented in C language inside the MCU at the intelligent gas PR edge-computing IoT device to performs an environment adaptable learning capability.

ULSAN NATIONAL INSTITUTE OF SCIENCE AND TECHNOLOGY

4.4 Experimental result

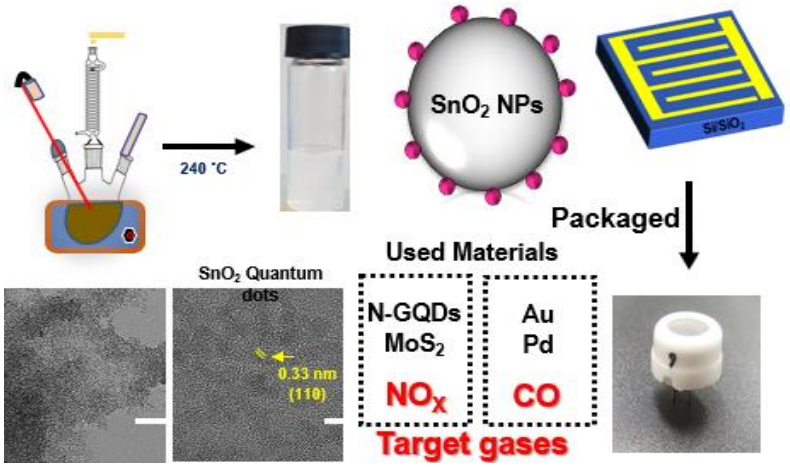

(a)

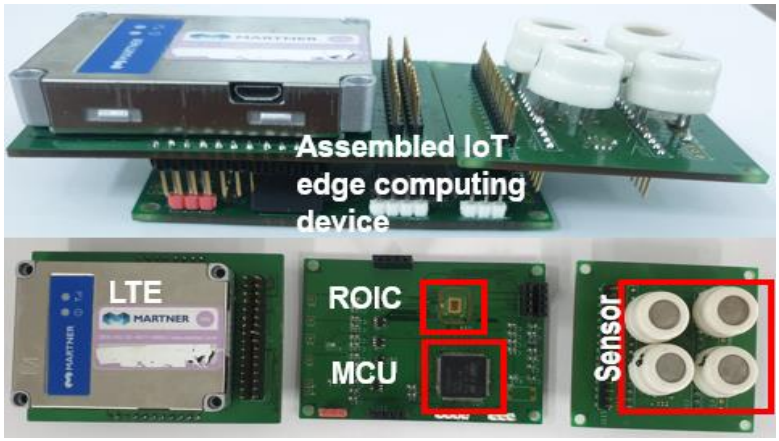

(b)

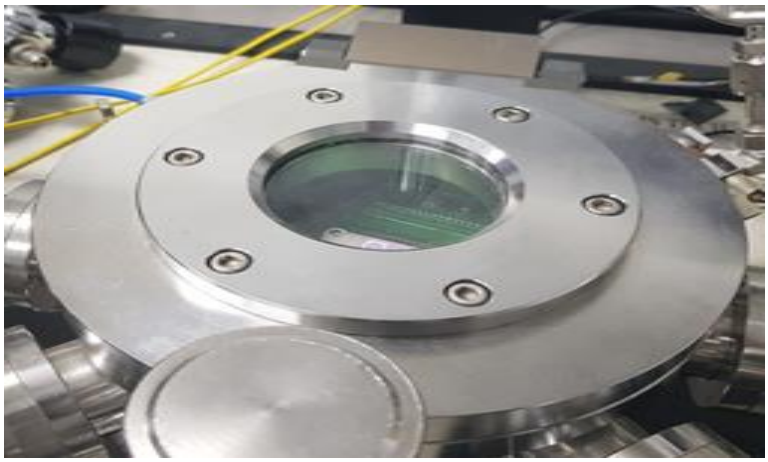

(c)

Figure 4.12 (a) Sensor development result. (b) Developed edge-computing IoT device. (c) experimental condition of controlled environment.

ULSAN NATIONAL INSTITUTE OF SCIENCE AND TECHNOLOGY

Figure 4.6(a) shows the sensor development result and its packaging before being mounted on the edge-computing IoT device. N-doped graphene quantum dots (N-GQDs) and MoS2 were selected as the materials used to react with NO2, and for the CO reaction, Au and Pd materials were used to detect the sensitivity in parts per billion (ppb). The developed edge-computing IoT device is presented in figure 4.6(b). Figure 4.6 (c) shows the experimental conditions in the controlled environment. For a controlled environment, a gas chamber is used for NO2 and CO exposure.

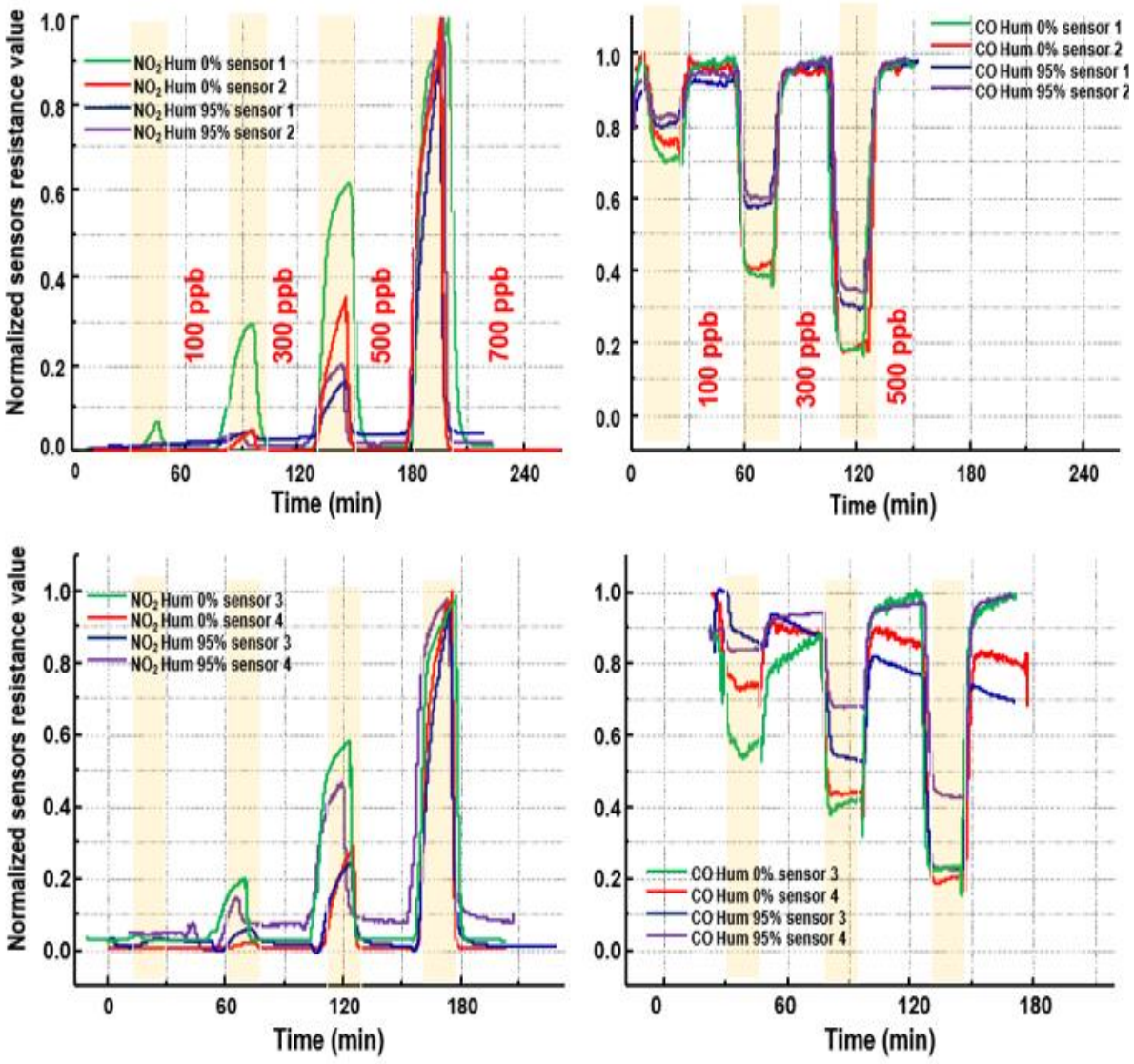

(a) (b)

ULSAN NATIONAL INSTITUTE OF SCIENCE AND TECHNOLOGY

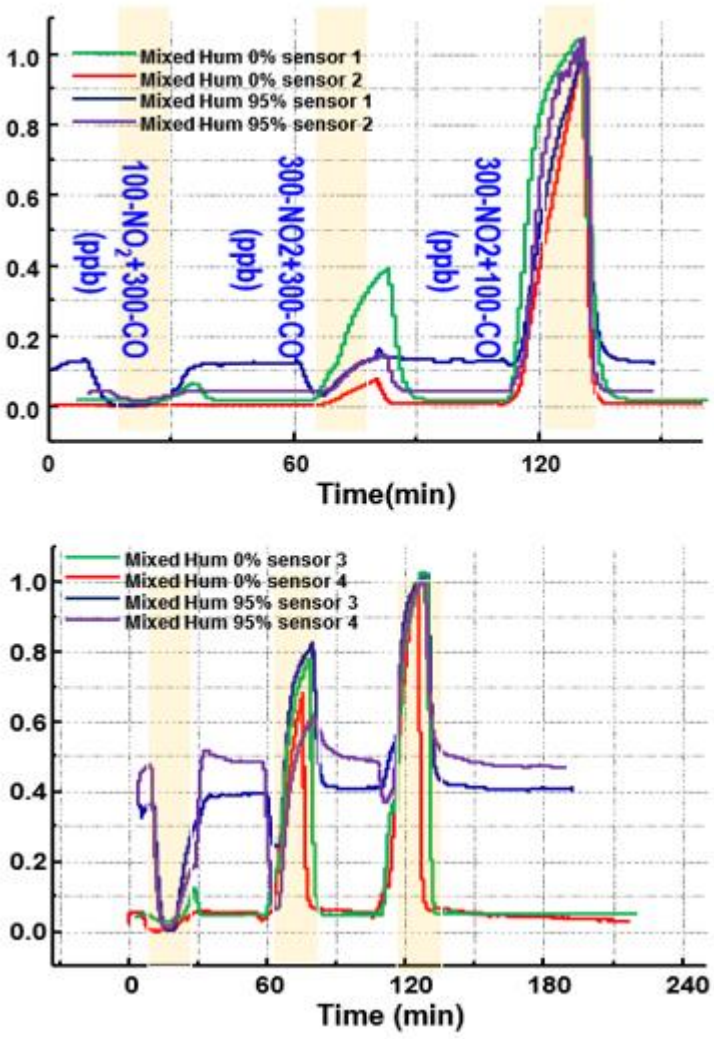

(c)

Figure 4.13 (a) Sensor array response to NO2, (b) sensor array response to CO and (c) sensor array response to CO and NO2.

The normalized sensing results of the developed in-house sensor are presented in figure 4.7 based on the difference in the data range. Figure 4.7(a) shows the sensor array data for different humidity values from 0% to 95%, and the exposed concentration is in the range of 100 to 700 ppb.

Figure 4.7(b) presents sensor array data upon reaction to CO with the variation in humidity. The condition of the humidity variation is the same as the NO2 exposure condition, and the concentration range is from 100 to 500 ppb. Finally, figure 4.7(c) shows the sensor array response reacting to the mixture of CO and NO2. First, 100 ppb of NO2 and 300 ppb of CO were exposed, 300 ppb of NO2 and CO were mixed, and finally, 300 ppb of NO2 and 100 ppb of CO were exposed

ULSAN NATIONAL INSTITUTE OF SCIENCE AND TECHNOLOGY

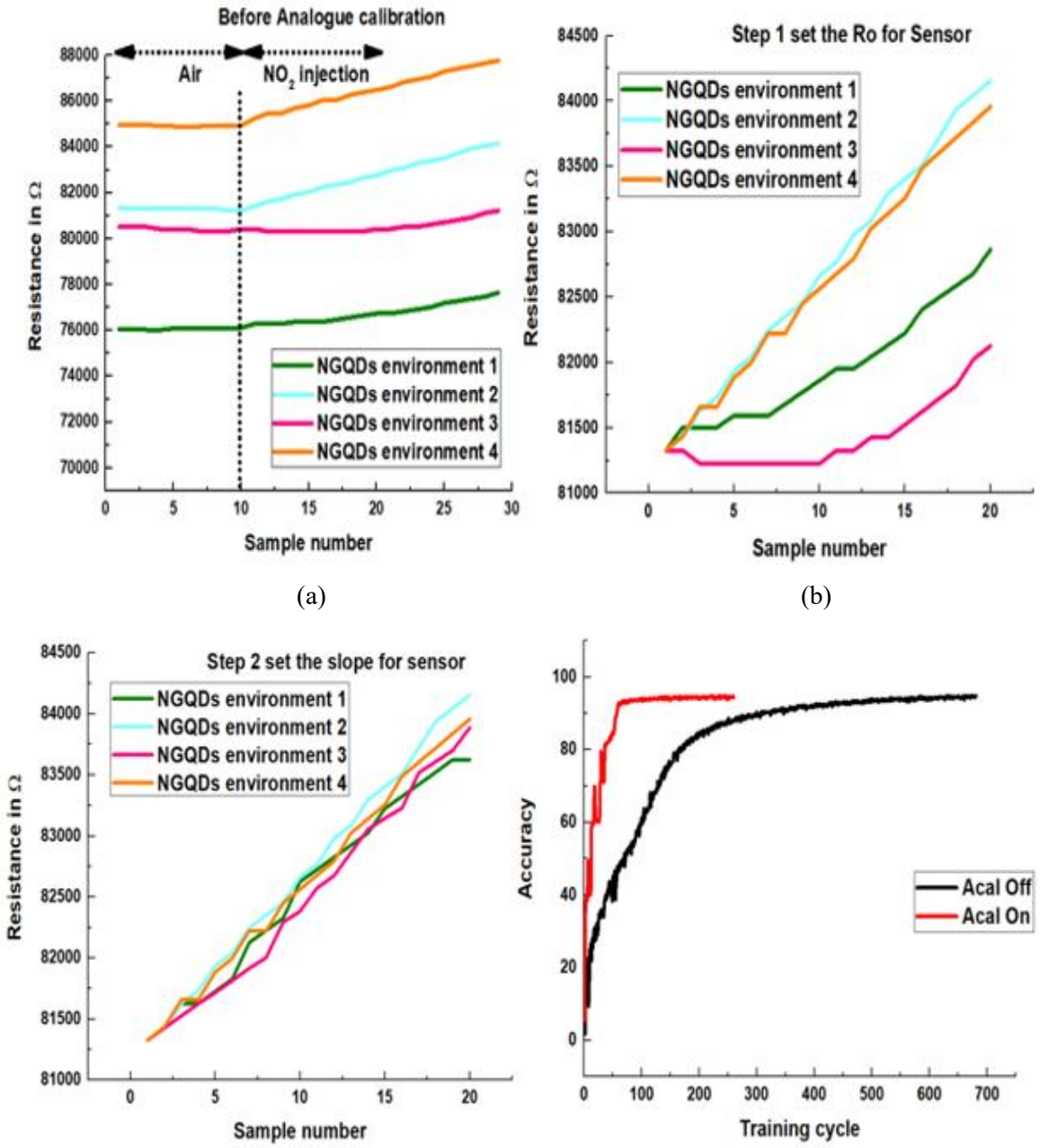

Figure 4.14 (a) Gas sensor response before calibration of the gas, (b) gas sensor response after calibrating R0 and (c) gas sensor response after calibrating the slope (d) training cycle reduction after analog calibration.

Figure 4.8 presents the result of the analog-assisted calibration and normalization scheme in figure 4.8(a). The sensor response in a transition state from the air exposure to the NO2 gas 300 ppb exposed state is presented. As shown in the figure, from the same air exposure state, the developed N-GQD sensor has different resistance values in different environments. Without analog-assisted calibration

ULSAN NATIONAL INSTITUTE OF SCIENCE AND TECHNOLOGY

normalization, the sensor's resistance value changes from 70 K to 85 K Ω. The result of the first analog calibration and normalization step is presented in figure 4.8(b). Different resistances expressing the same gas concentration are calibrated to a fixed resistance value. Then, figure 4.8(c) presents the final slope normalized result via analog calibration. Upon calibrating and normalizing over two steps, the analog gas sensor signal further provides an opportunity for the MBCL to learn less data for the same gas PR. As shown in figure 4.8(d), the target accuracy after analog calibration and normalization is met three times earlier when analog calibration is turned on compared to a classical prune and expend method. Better yet, the computation power to learn the gas pattern is reduced by three times.

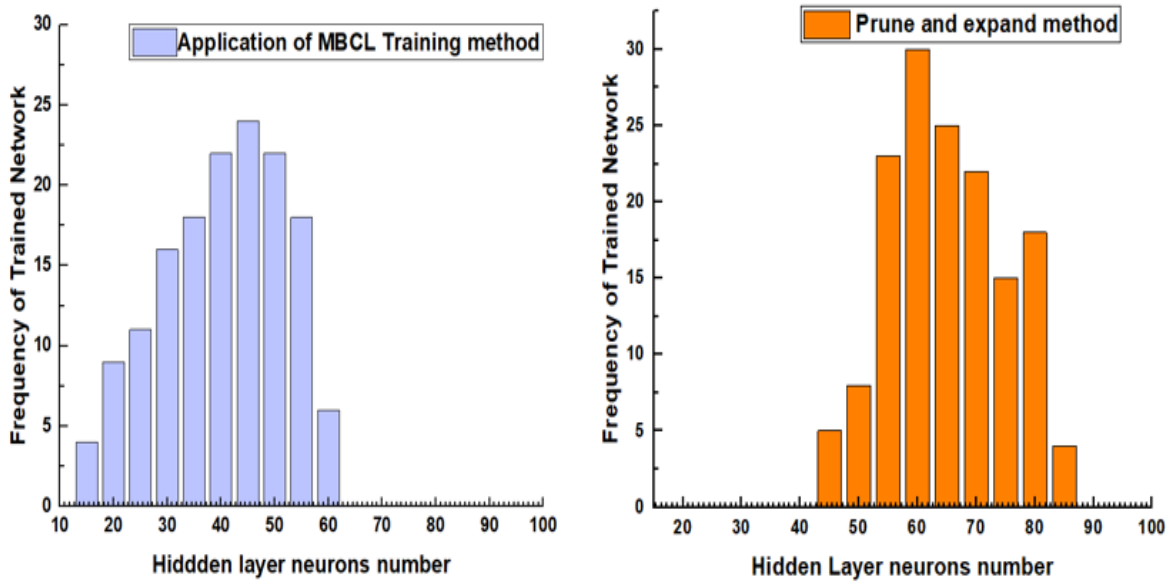

(a) (b)

# of Increased Hidden node	15	20	25	30	35	40	45	50	55	60	65	70	75	80	85	Average
Proposed MBCL	4	9	11	16	18	22	24	22	18	6	0					40.36
MBCL	0						5	8	23	30	25	22	15	18	4	65.1

(c)

Figure 4.15 (a) Hidden-layer nodes increased with the proposed algorithm. (b) Hidden-layer nodes increased with the classical approach. (c) Hidden-layer nodes increased value table.

ULSAN NATIONAL INSTITUTE OF SCIENCE AND TECHNOLOGY

Finally, figure 4.9 presents the comparison of the efficiency between the analog assisted MBCL algorithm and the classical prune and expend algorithm model. Figure 4.9(a) shows the histogram presenting the increased hidden node neuron number when the analog assisted MBCL algorithm learns gas PR in the new environment. The x-axis represents the number of hidden-layer neurons that are increased to learn the gas PR in the new environment. The y-axis represents the number of cases when the learning is finished with the increased number of neurons. Because of the random number distribution to the weights connected to newly created hidden-layer neurons, the performance for learning is different. Thus, statistical experimentation is performed to show the efficiency of the proposed analog assisted MBCL. Therefore, 150 training experiments of the MBCL model are performed from scratch. Among these 150 experiments, the smallest hidden-layer neuron number is increased to learn gas PR, with the proposed analog-assisted MBCL reaching 15.

On the other hand, for the classical MBCL model, the minimum hidden-layer neuron number increased to 45. For the worst case, the proposed MBCL shows 60, and the classical prune and expand method shows 85 augmentations of the hidden-layer neurons number.

Figure 4.9(c) presents the detailed value of the proposed algorithm to learn gas PR in the new environment. All the increased neuron numbers are rounded up to 5. As shown in figure 4.9(c), for the MBCL case, to learn a new gas PR with an average accuracy of 97%, for 150 training experiments from scratch, an average of 40.23 hidden-layer neurons is increased to learn gas PR remembering the previous trained pattern. For comparison to the proposed analog-assisted MBCL method, the classical prune and expend method need to add 65.1 hidden-layer neurons to learn gas PR in the new environment where the temperature and humidity are different. In this case also the training is performed after learned previously gas pattern in another environment.

Figure 4.10 presents the test confusion matrix of the gas PR performed by the proposed edge-computing IoT device. There are 100 data points that are used to test the performance. Three of the 100 data points are misclassified. Thus, the overall accuracy achieved is 97%. The recognition classes include NO2, CO, and 3 mixture gas patterns named MIX1, MIX2 and MIX3. The mixed gas ratio for MIX1 is 100 ppb of NO2 and 300 ppb of CO; for MIX2, 300 ppb of NO2 and 300 ppb of CO; and for MIX3, the ratio is 300 ppb of NO2 and 100 ppb of CO. As shown in the confusion matrix, confusion occurs between MIX1 and MIX2. Two MIX1 patterns are classified as MIX2, and 1 MIX2 pattern is classified as MIX1. Figure 4.11 presents the final installation of the IoT edge-computing device in the industrial field and its monitoring system. The development results are summarized in Table Ⅱ, which includes comparisons with other recent works. The developed edge-computing IoT device performs gas PR with 97% accuracy. Implemented analog assisted MBCL has the capability to learn new patterns for different environments in the MCU. Calibration is separately performed with classification to enhance the accuracy and training speed. Analog-assisted MBCL shows the adaptability and efficiency of

ULSAN NATIONAL INSTITUTE OF SCIENCE AND TECHNOLOGY

memory handling for intelligent edge-computing IoT devices performing classification in the MCU.

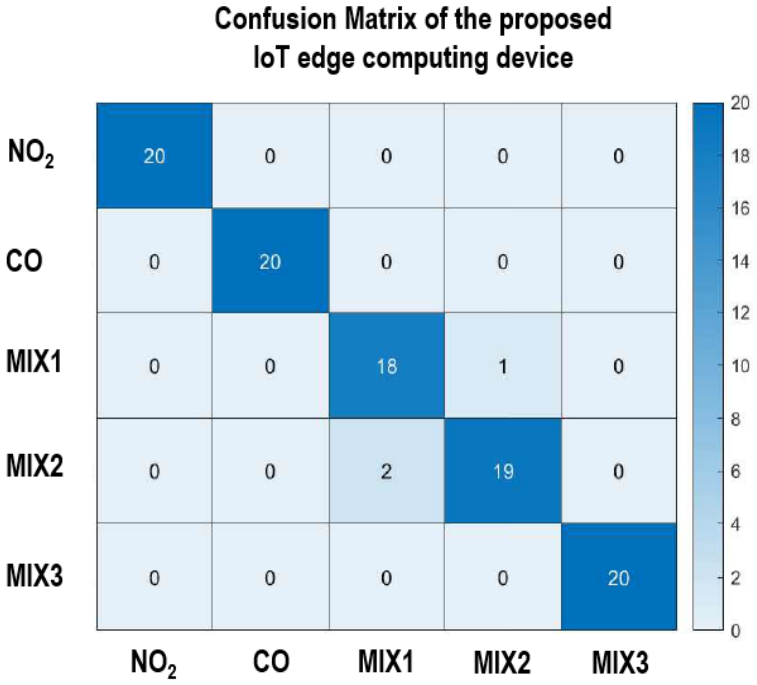

Figure 4.16 Confusion matrix of the edge-computing IoT device.

Figure 4.17 Industrial field installed IoT edge computing device and its monitoring result.

ULSAN NATIONAL INSTITUTE OF SCIENCE AND TECHNOLOGY

Table Ⅱ
GAS SENSOR SYSTEM SUMMARY AND COMPARISON WITH OTHER RECENT WORK

	TIM [7]	**TIE [6]**	**TIE [18]**	**TIE [19]**	**This work**
Classification accuracy (%)	91.8	99.4	96.1	90	**97%**
Pattern recognition performing DSP	CPU	CPU	CPU	MCU	**MCU**
IoT interface	-	Smart phone/PC	-	-	**Smart phone/PC**
Adaptivity of the learning model	Yes	No	No	Yes	**Yes**
Calibration and classification	T.L*	Analog assisted ANN	Wilks's lambda statistic LDA	ANN	Analog assisted MBCL
Memory optimiation	-	-	-	-	**25%**

ULSAN NATIONAL INSTITUTE OF
SCIENCE AND TECHNOLOGY

Chapter V

Conclusion

This doctoral thesis aims to design an environmentally adaptable IoT edge-computing device embedding an analog-supported MBCL scheme enhanced with analog calibration and normalization ROIC. Gas sensors are influenced to the environmental factor such as temperature and humidity and other effect. Thus, the instability of the sensor signal is always presents. To resolve such problem calibration method is adopted to resolve the reliability problem. On the other way, not only the reliability problem but also the selectivity problem exists. To resolve the selectivity problem classical approach is to combine a sensor array and ML method to find the gas type. This classical approach has a constraint to learn only the experimentally acquired data. Thus, continual learning method is adopted to learn additionally new gas pattern in different environment. Among different method of continual learning, a memory efficient method is adopted to give the gas sensor monitoring system the adaptability. But this method is designed to recognize image data. In the case of gas monitoring system, contradictory data is often present and applying simply the selected continual learning method can bring a processing confusion. To prevent such problem and adopt the continual learning scheme to the gas sensor monitoring system. the optimization of the classical prune and expend method is implemented as an MBCL to mask previously trained temperature and humidity nodes. This optimization allows the gas PR system to be independent of the pretrained information when learning a new pattern. In this way, learning an additional new pattern becomes memory efficient in the unusual environment, showing a 1.6-fold improvement with respect to the classical method learning. Additionally, an analog calibration and normalization ROIC is developed to resolve the sample variation in the sensor data to enhance the MBCL scheme, while the training cycle is reduced by 3 times. Furthermore, in-house gas sensors and monitoring systems are developed to optimize the sensing range and wirelessly monitor the gas PR data. This proposed novel approach is simple but efficient and provides an opportunity to design a large-scale deployable IoT edge-computing device system for a low-cost gas sensor.

ULSAN NATIONAL INSTITUTE OF SCIENCE AND TECHNOLOGY

References

1. M. Kampa and E. Castanas, “Human health effects of Air Pollution,” Environ. Pollution, vol. 151, no. 2, pp. 362–367, 2008.
2. J. Chatkin, L. Correa, and U. Santos, “External environmental pollution as a risk factor for asthma,” Clin. Rev. Allergy. Immunol., vol. 62, no. 1, pp. 72–89, 2021.
3. P. Mannucci and M. Franchini, “Health Effects of Ambient Air Pollution in Developing Countries,” Int. J. Environ. Res. Public Health., vol. 14, no. 9, p. 1048, Sep. 2017.
4. S.Dhingra, R. B. Madda, A. H. Gandomi, R. Patan and M. Daneshmand, "Internet of Things Mobile–Air Pollution Monitoring System (IoT-Mobair)," IEEE Internet. Things. J., vol. 6, no. 3, pp. 5577-5584, June 2019, doi: 10.1109/JIOT.2019.2903821.
5. R. Gutierrez-Osuna, “Pattern Analysis for Machine Olfaction: A Review,” IEEE Sensors J., vol. 2, no. 3, pp. 189–202, 2002.
6. Park, Kyeonghwan, et al. "An energy-efficient multimode multichannel gas-sensor system with learning-based optimization and self-calibration schemes." IEEE Transactions on Industrial Electronics 67.3 (2019): 2402-2410.
7. Lei Zhang and D. Zhang, “Domain adaptation extreme learning machines for drift compensation in E-Nose Systems,” IEEE Trans. Instrum. Meas., vol. 64, no. 7, pp. 1790–1801, 2015
8. J. Hodgkinson and R. P. Tatam, “Optical Gas Sensing: A Review,” Meas. Sci. Technol., vol. 24, no. 1, p. 012004, 2012.
9. H. Wan, H. Yin, L. Lin, X. Zeng, and A. J. Mason, “Miniaturized planar room temperature ionic liquid electrochemical gas sensor for rapid multiple gas pollutants monitoring,” Sen. Actuators B, Chem., vol. 255, pp. 638–646, 2018
10. Y. Lim, J.-I. Heo, M. Madou, and H. Shin, “Monolithic carbon structures including suspended single nanowires and nanomeshes as a sensor platform,” Nanoscale Res. Lett., vol. 8, no. 1, 2013.
11. X. Wang, M. Magno, L. Cavigelli, and L. Benini, “Fann-on-MCU: An open-source toolkit for energy-efficient neural network inference at the edge of the internet of things,” IEEE Internet. Things. J., vol. 7, no. 5, pp. 4403–4417, 2020.
12. Huerta, Ramon, et al. "Online decorrelation of humidity and temperature in chemical sensors for continuous monitoring." Chemometrics and Intelligent Laboratory Systems 157 (2016): 169-176.
13. Miskell, Georgia, Jennifer A. Salmond, and David E. Williams. "Solution to the problem of calibration of low-cost air quality measurement sensors in networks." ACS sensors 3.4 (2018): 832-843.

ULSAN NATIONAL INSTITUTE OF SCIENCE AND TECHNOLOGY

14. G. I. Parisi, R. Kemker, J. L. Part, C. Kanan, and S. Wermter, “Continual lifelong learning with neural networks: A Review,” Neural. Netw., vol. 113, pp. 54–71, 2019
15. Kirkpatrick, J., Pascanu, R., Rabinowitz, N., Veness, J., Desjardins, G., Rusu, A. A., ... & Hadsell, R. (2017). Overcoming catastrophic forgetting in neural networks. *Proceedings of the national academy of sciences*, *114*(13), 3521-3526.
16. Hung, S.C.Y., Tu, C.-H., Wu, C.-E., Chen, C.-H., Chan, Y.-M., Chen, C.-S.: Compacting, picking and growing for unforgetting continual learning.
17. Chae, Hee Young, et al. "A wearable sEMG pattern-recognition integrated interface embedding analog pseudo-wavelet preprocessing." IEEE Access 7 (2019): 151320-151328.
18. H. Sun, F. Tian, Z. Liang, T. Sun, B. Yu, S. X. Yang, Q. He, L. Zhang, and X. Liu, “Sensor array optimization of electronic nose for detection of bacteria in wound infection,” IEEE Trans. Ind. Electron., vol. 64, no. 9, pp. 7350–7358, 2017
19. L. Dutta, C. Talukdar, A. Hazarika, and M. Bhuyan, “A novel low-cost hand-held tea flavor estimation system,” IEEE Trans. Ind. Electron., vol. 65, no. 6, pp. 4983–4990, 2018
20. MASSON, N.; PIEDRAHITA, R.; HANNIGAN, M. Approach for quantification of metal oxide type semiconductor gas sensors used for ambient air quality monitoring. Sensors and Actuators B: Chemical, 2015, 208: 339-345.
21. MORRISON, S. Roy. Semiconductor gas sensors. Sensors and Actuators, 1981, 2: 329-341
22. YAMAZOE, Noboru. Toward innovations of gas sensor technology. Sensors and Actuators B: Chemical, 2005, 108.1-2: 2-14.
23. XU, Yonghui, et al. Research on a mixed gas recognition and concentration detection algorithm based on a metal oxide semiconductor olfactory system sensor array. Sensors, 2018, 18.10: 3264.
24. YAN, Jia, et al. Electronic nose feature extraction methods: A review. Sensors, 2015, 15.11: 27804-27831.
25. Ricardo, G.; Troy, N.H. A method for evaluating data-preprocessing techniques for odor classification with an array of gas sensors. IEEE Trans. Syst. Man. Cybern. B Cybern. 1999, 29, 626–632.

ULSAN NATIONAL INSTITUTE OF
SCIENCE AND TECHNOLOGY

ACKNOWLEDGEMENTS

I would like to thank my advisor Prof. Jae Joon Kim, who has given me a lot of advice and guidance. Thanks to these, I was able to conduct my research successfully during a period of my combined master's and PhD programs. Also, I would like to thank Prof. Yunsik Lee, Prof. Hungson Son, Prof. Hyunhyub Ko, and Prof. Jeong Min Baik for their advice and feedback about my doctoral thesis and defence presentation.

I would like to thank all the members and alumni of my laboratory who study and discuss about my research. Especially, thanks to Kyung Hwan, Subin, Kwangmuk, Chan Sam, Jeonghoon and Hyunjoong for helping and technical discussing a lot.

In particular, I thank my parents and my wife Hi jee for supporting and encouraging me.

ULSAN NATIONAL INSTITUTE OF SCIENCE AND TECHNOLOGY

Academic qualifications

PhD candidate in Electrical Computer Engineering, Ulsan National Institute of Science and Technology, Ulsan, South Korea

- Thesis title: Intelligent IoT edge platform embedding Transfer learning scheme for sensor calibration.
- Supervisor: Dr. Jae-Joon Kim

BS in Electrical Electronic Engineering, University of Pierre et Marie Curie (UPMC), Paris, France

Additional education

First and second year (passed) in Physics theory, University of Pierre et Marie Curie (UPMC), Paris, France

First year medical school, University of Orsay, Paris, France

Current research projects

*PCB (Printed Circuit Board)
*ROIC (Read Out Integrated Circuit)
*BLE (Bluetooth Low Energy)
*LoRa (Long Range communication module)
*NB IoT (Narrow Band-Internet of Things)
*LTE (Long Term Evolution)

Development of IoT sensors and plant-safety platform against hazardous substances, funded by UTP/Ulsan/MSIT

Role: Design customized board, Wireless Communication control (LoRa, NB IoT, LTE), Embedding machine learning in the Embedded system (Edge computing) for gas pattern recognition.

Biomimetic brain interface based minimal invasive B2X system applications, funded by KEIT/MOTIE

Role: Design customized board, Wireless Communication control, Embedding machine learning in the Embedded system (Edge computing) for EEG pattern recognition.

Completed research projects

Development of patch-type 7-modal multi-sensor devices and platform technology for wearable healthcare applications, funded by KEIT (Korea Evaluation institute of Industrial Technology)/MOTIE (Ministry of Trade, Industry and Energy)

Role: Designing Customized board (flexible PCB to be wearable), Control of communication module (Bluetooth), control of developed Bio signal acquisition sensor or electrode, control developed ROIC.

Development of suspended heterogeneous nanostructure-based hazardous gas microsensor systems funded by KEIT/MOTIE

Role: Designing customized board (Hand size PCB, portable wireless gas data sending Device), Control of developed and commercial gas sensor, control of communication (Bluetooth and BLE), application of signal processing (PCA, Neural Network in MATLAB), Monitoring (Android app design).

Development of non-conscious real-time wearable healthcare system for work-stress monitoring and management, funded by IITP (Institute for Information& communication Technology Planning & evaluation)/MSIT (Ministry of Science and ICT)

Role: Designing customized board, control ROIC, signal filtering processing (EMG, ECG), communication.

Current research works

- **H. Y. Chae*,** J. Cho *, J. Cho, R. Purbia, C. S., H. J. Kim, Y. Lee, J.M. Baik J. J. Kim, “Environment-Adaptable Edge Computing Multi-Gas Sensor Device with Analog-Assisted Continual Learning Schemes.” (in preparation).

Publication

- J. Park*****, D. Kang*, **H. Y. Chae** *, S. K. Ghosh, C. Jeong, Y. Park, S. Cho, Y. Lee, J. Kim, Yujung Ko, J. J. Kim, and H. Ko. “Hierarchical structured ferroelectric composite for dual human machine interfacing electronic skins” (**Science Advances Accepted 2022**)
- J. Jeon, C. S. Park, S. Lee, **H. Y. Chae**, J. J. Kim, H. Son, "Magnetic Induction Tomography Using Multi-Channel Phase-Domain Transceiver for Structural Health Monitoring," **IEEE Transactions on Instrumentation and Measurement, 2022. (Accepted)**
- K. Park, S. Choi, **H. Y. Chae**, C. S. Park, S. Lee, Y. Lim, H. Shin, J. J. Kim “An Energy-Efficient Multimode Multichannel Gas-Sensor System with Learning-Based Optimization and Self-Calibration Schemes," **IEEE Transactions on Industrial Electronics**, Vol. 67, Issue 3, pp. 2401-2410; doi:10.1109/TIE.2019.2905819, March 2020.
- S. Choi*, C.S. Park*, **H.Y. Chae**, B. Oh, J. Lee, Y. M. Kwon, J. M. Baik, H. Shin, J. J. Kim, “A Wide Dynamic Range Multi-Sensor ROIC for Portable Environmental Monitoring Systems with Two-Step Self-Optimization Schemes.” (Accepted in **IEEE TCAS 1** 2021/03/07).
- K. Lee, **H. Y. Chae**, K. Park, Y. Lee, S. Cho, H. Ko, J. J. Kim, "A Multi-Functional Physiological Hybrid-Sensing E-Skin Integrated Interface for Wearable IoT Applications," **IEEE Transactions on Biomedical Circuits and Systems**, Vol. 13, Issue 6, pp. 1535-1544; doi:10.1109/TBCAS.2019.2946875, December 2019.
- **H. Y. Chae**, K. Lee, J. Jang, K. Park, J. J. Kim, "A Wearable sEMG Pattern-Recognition Integrated Interface Embedding Analog Pseudo-Wavelet Preprocessing," **IEEE Access**, Vol. 7, pp. 151320-151328; doi:10.1109/ACCESS.2019.2948090, October 17th, 2019.
- J. W. Lee, S. Jung, T. W. Lee, J. Jo, **H. Y. Chae**, K. Choi, J. J. Kim, J. H. Lee, C. Yang, J. M. Baik, "High-output triboelectric nanogenerator based on dual inductive and resonance effects-controlled highly transparent polyimide for self-powered sensor network systems," **Advanced Energy Materials**, Vol. 9, Issue 36, doi:10.1002/aenm.201901987, September 26th, 2019**.**
- C. S. Park, J. Jeon, B. Oh, **H. Y. Chae**, K. Park, H. Son, J. J. Kim "A Portable Phase-Domain Magnetic Induction Tomography Transceiver with Phase-Band Auto-Tracking and Frequency-Sweep Capabilities," **Sensors**, 18(11), 3816; doi:10.3390/s18113816, November 2018**.**

ULSAN NATIONAL INSTITUTE OF SCIENCE AND TECHNOLOGY

- S. Choi, K. Park, S. Lee, Y. Lim, B. Oh, **H. Y. Chae**, C. S. Park, H. Shin, J. J. Kim, “A Three-Step Resolution-Reconfigurable Hazardous Multi-Gas Sensor Interface for Wireless Air-Quality Monitoring Applications,” **Sensors**, 18(3), 761; doi:10.3390/s18030761, March 2018.
- S.-W. Kim, Y. Lee, J. Park, S. Kim, **H. Chae**, H. Ko, J. J. Kim, "A Triple-Mode Flexible E-Skin Sensor Interface for Multi-Purpose Wearable Applications," **Sensors**, 18(1), 78; doi:10.3390/s18010078, January 2018.
- K. Lee, Y. Y. Choi, D. J. Kim, **H. Y. Chae**, K. Park, Y. M. Oh, S. H. Woo, J. J. Kim, "A Wireless ExG Interface for Patch-Type ECG Holter and EMG-Controlled Robot Hand," **Sensors**, 17(8), 1888; doi:10.3390/s17081888, August 2017.

Conference

- B. Oh, S. Choi, **H. Y. Chae**, J. J. Kim, "Multimode-based dual type gas sensor readout IC," 2020 IEIE Summer Conference, Aug. 19-21, 2020. (Poster).
- **H.Y Chae**, J. Jang, K. Lee, J. J. Kim, "Hybrid Hardware-Algorithm Platform for EMG Pattern Recognition," 26th Korean Conference on Semiconductor, Gangwon, Feb. 13-15, 2019. (Poster)
- J. Jang, K. Lee, **H. Chae**, J. J. Kim, "Sensor interface for electromyogram with wavelet filter," 18th RF/Analog Circuit Workshop, Jeju, Sept. 13-14, 2018. (Poster)
- S.-W. Kim, Y. Lee, J. Park, **H.Y Chae**, H. Ko, J. J. Kim, "A Wireless Multi-Functional E-skin Sensor System," International SoC Conference, Seoul, Nov. 6-7, 2017. (Special Session)

Skills & accomplishment

- **Linguistic skills: Korean (native), French(native), English(intermediate)**
- **Computer linguistic skills: C, Java, Python**
- **Used Tools: Matlab, Tensorflow, Android Studio, Keil uvision, Cadence PCB**